Indoor Hygrothermal Environment of Naturally Ventilated Residential Buildings in Tropical Climate Regions in Indonesia

ムハッマド, イクバル

出版情報：Kyushu University, 2023, 博士（工学）, 課程博士
バージョン：
権利関係：

Doctoral Thesis
博 士 論 文

Indoor Hygrothermal Environment of Naturally Ventilated Residential Buildings in Tropical Climate Regions in Indonesia

熱帯気候に属するインドネシアの住宅において室内熱環境へ及ぼす自然換気の影響

2023 年

Muhammad IQBAL
ムハッマド　イクバル

Contents

Chapter 3 Development of simulation model of louver openings

Appendix A contains a paper describing a simulation called THERB for HAM, which is capable of estimating the hygrothermal environment and heat load of an entire building using a physical model.

Appendix B consists of a questionnaire that was utilized for surveying and assessing the indoor thermal comfort in naturally ventilated houses in Indonesia (English and Indonesia version).

Acknowledgments

Chapter 1. Introduction

1.1. Research background and purpose

1.1.1. Hygrothermal environment of naturally ventilated house in tropical regions Indonesia

Indonesia, with a population of over 270 million people, holds the distinction of being the world's fourth most populous country. Its geographical expanse encompasses more than 17,000 islands that stretch over 5,110 km from east to west and 1,900 km from North to South, making it the largest archipelago globally. Positioned along the equator, Indonesia experiences a tropical rainforest climate and savanna climate, characterized by distinct dry and rainy seasons. However, these seasonal variations have become less pronounced due to the impact of global warming, further blurring the line between the two seasons. Since the economic crisis in 1997, the Indonesian government has implemented poverty alleviation policies. Despite these efforts, there are still population groups residing just above the poverty line who are vulnerable to economic and social factors.

The indoor environment of naturally ventilated residential buildings is significantly influenced by the local climate and the utilization of environmental controls. The impact of outdoor climate can be mitigated by employing various controls. Common controls, such as openable windows, blinds, louvers, lights, and fans, provide occupants with the means to adjust the thermal environment and seek comfort. These controls offer individuals the opportunity to modify their immediate surroundings to align with their preferred thermal conditions [1]. Indonesia is considered the most extensive tropical country globally and is located in the heart of the equator line, with 6° - 11° North Latitude and 95° - 141º East Longitude. Climate conditions depend on the monsoon, creating hot and humid conditions throughout the year. There is no temperature and relative humidity difference between the rainy and dry seasons. The daily air temperature observed ranges between 20 and 35 ℃, and the relative humidity fluctuates from 60% at noon to almost 95% in the morning until late.

Especially in recent years, many countries have been facing more extreme weather events due to climate change, and Indonesia has also experienced an increase in outdoor temperature. The increase in external temperatures is driving greater demand for air conditioning, as well as increasing energy poverty. Moreover, with the majority of the population in Indonesia living in naturally ventilated houses due to economic issues, the hot and humid outdoor conditions in Indonesia can significantly affect the occupants' thermal comfort. The study of thermal comfort in the tropics started 70 years ago. Webb observed and analysed thermal comfort in equatorial climates and examined thermal discomfort in tropical climates by developing a nomogram for the equatorial comfort index [2]. Ellis concluded that race, age, or gender differences do not affect thermal comfort [3]. Additionally, subsequent research reveals that the occupants' response to a naturally ventilated room is three degrees warmer than the perceived ISO thermal comfort standard [4]. Moreover, other studies on thermal comfort

focused on testing neutral temperatures based on gender, age, body mass index level, and ethnic background [5].

Furthermore, studies on thermal comfort for naturally ventilated houses were conducted to determine the neutral temperature in naturally ventilated houses in Yogyakarta, Indonesia [6], and to assess the comfort of houses in Banda Aceh, Indonesia, to determine the comfort range [7]. However, research on naturally ventilated houses and thermal comfort in tropical climates regarding window opening ratios is overlooked, especially in Indonesia. This chapter will focus on the impact of window opening ratios on indoor environmental conditions and occupant comfort as an initial step to provide an improved design plan for residential buildings in the tropical climate of Indonesia.

Therefore, the study aims to address this research gap by examining the influence of window opening ratios on indoor environmental conditions and occupant comfort. The ultimate goal is to provide an initial step towards improving the design of residential buildings in the tropical climate of Indonesia. The research focuses on optimizing window openings in Indonesian dwellings to enhance indoor thermal comfort. Specifically, the objectives are to investigate the thermal comfort performance of two types of naturally ventilated houses, identify airflow scale votes and air freshness scale votes, explore thermal preferences and body responses in the indoor environment, and study occupants' adaptive behaviors in modifying indoor conditions for greater comfort.

1.1.2. Naturally ventilated house

1.1.2.1. Discharge coefficient of louver openings in naturally ventilated buildings

Natural ventilation (NV) benefits the environment by lowering operating costs, improving indoor air quality (IAQ), and increasing occupant satisfaction with their thermal comfort [8, 9]. In addition, NV can provide adequate ventilation [10, 11]. However, accurately determining the ventilation rate of a naturally ventilated building remains a challenge [12, 13]. It is crucial in building design to control ventilation openings and monitoring gas and dust emissions from NV housing [14]. Natural ventilation has been investigated in buildings for more than 50 years. Despite many descriptive experimental and numerical studies conducted for airflow estimation paired with heat transfer to aid such an understanding, the mechanics of such a physical problem remains unclear. Many factors influence the proper implementation of natural ventilation systems to meet the comfort needs of occupants, thereby affecting a building's energy usage. Natural ventilation has attracted interest because of its vent and cooling benefits. Such benefits can significantly reduce building energy consumption with respect to location (latitude). In tropical latitudes with high humidity and temperatures with weak day-night fluctuations, ventilation, appropriate thermal mass, and insulation significantly improve thermal comfort [15, 16].

This is particularly true for vernacular and low-cost houses in tropical regions. In tropical regions, households mainly rely on natural ventilation for cooling, rather than operating an air conditioner for

the entire year. In addition, louver opening is a natural ventilation method used to achieve human thermal comfort in an indoor housing environment throughout the year. Nevertheless, studies on the discharge coefficient of louver openings are lacking despite the common use of this opening in residential buildings at tropical regions. Therefore, this study deals with the development of on-site ventilation rate measurements, pressure difference, wind velocity, and temperature difference, and evaluates the discharge coefficient for various louver openings with installed sash angles. The discharge coefficient (Cd) accounts for the effects of the flow contraction and frictional losses through an opening. A value of Cd = 0.6 is typically used and can be derived analytically for a sharp-edged orifice opening [17, 18]. The flow rate and pressure difference when a fluid passes through an aperture is measured to determine the discharge coefficient of the opening [18, 19]. Iqbal et al. [20] stated that the discharge coefficient of a window decreases as the opening angle increases in the absence of wind. The discharge coefficient decreases with increasing louvre opening angles in a fully formed turbulent flow, and the sash installed in the openings could improve the natural ventilation rate. According to Heiselberg et al. [18], the Cd value of side-hung window ranges from 0.65 to 0.77 and that of a bottom-hung window ranges from 0.78 to 1.0. When the pressure differential increases, the Cd value for the bottom-hung window decreases; beyond 10 Pa, a nearly constant value is attained. It is important to emphasize that the Cd values for bottom-hung windows are always higher than 0.82, and the pressure difference for the natural ventilation process is often below 10 Pa. In addition, Chiu et al. [21] discovered a relationship between the Cd value and external wind activity, in which values as low as 0.25 were found to be possible. Depending on the shape of the aperture (orifice or long opening) and the flow direction, the wind's impact on the flow changes (exposed inlet or exposed outlet). When the outlet is exposed to external flow, the effect of wind on the Cd value for a lengthy opening is insignificant. Awbi et al. [22] noted that the discharge coefficient value varies depending on the geometry of the opening and the pressure differential owing to external factors. Moreover, the variance in Cd indicated that this value varied for several variables; hence, there could be significant inaccuracies in calculating this coefficient. Therefore, it is essential to establish methods for carrying out on-site measurements as accurately and efficiently as possible to reduce such inaccuracies. In addition, the discharge coefficient value also calculated by CFD simulation for naturally ventilated house in Indonesia.

According to the natural ventilation principle, air is propelled by the pressure difference across the openings created by thermal buoyancy and wind forces [23]. Bernoulli's theory states that the pressure difference can be transformed into kinetic energy by assuming a steady incompressible flow, as shown in the equation below:

$$V_{th} = \sqrt{\left(\frac{2\,.\,\Delta P}{\rho}\right)} \quad (1.1),$$

where Vth is the theoretical air velocity through the opening (m/s), ΔP is the pressure difference across the opening (Pa), and ρ is the air density (kg/m^3). Given the pressure difference, the volume airflow rate (Q) through an opening can be calculated by combining Bernoulli's equation and the conservation of mass, as follows:

$$Q = C_d\,.\,A\,.\,\sqrt{\left(\frac{2\,.\,\Delta P}{\rho}\right)} \quad (1.2),$$

where Cd is the dimensionless discharge coefficient of the opening, which is introduced to account for the effects of flow contraction and friction due to viscous forces [24]. The discharge coefficient can be determined by rearranging Eq. (1.2) to give:

$$C_d = \frac{Q}{A}\,.\,\sqrt{\left(\frac{\rho}{2\,.\,\Delta P}\right)} \quad (1.3)$$

Therefore, the primary objective of this chapter is to ascertain the discharge coefficient value for different sash angles. Additionally, it investigates the influence of the louver geometric parameter on the discharge coefficient value, as well as the impact of wind velocity and pressure difference on the discharge coefficient value.

1.1.2.2. Wind pressure coefficients

The wind pressure coefficient (Cp) is a dimensionless parameter that represents the difference between the static pressure of the wind and the static reference pressure at a particular point on a structure or surface due to the action of the wind. The wind pressure coefficient is commonly used in engineering to calculate wind loads on buildings, structures, or other surfaces. In addition, the wind pressure coefficient describes the pressure distribution on the building surfaces. According to Cóstola et al. [25], there are two main sources of Cp data. The primary sources consist of full-scale measurements, wind-tunnel measurements, and Computational Fluid Dynamics (CFD) simulations. The secondary sources, on the other hand, include databases and analytical models.

In this study, computational fluid dynamics (CFD) is employed for numerical simulations in order to assess wind pressure coefficients. Additionally, wind pressure coefficients are derived from a reference value using CPX. Subsequently, a comparison is made between the wind pressure coefficients obtained from the CFD simulations and the reference value, with the aim of evaluating the

accuracy of the numerical simulation. This validation process involves comparing the results to measurement data using THERB for HAM with NAF.

1.1.3. Passive design on naturally ventilated houses in tropical regions Indonesia

Approximately 40% of the energy consumption worldwide is attributed to buildings, indicating their crucial role in the energy market. Moreover, the demand for building energy is expected to persistently increase in the forthcoming decades [26]. Tropical regions such as Indonesia have similar weather patterns of high temperature and humidity annually, thus triggering higher energy demands for cooling indoors.

Energy poverty has emerged as a critical issue in global development, particularly in Indonesia. Many small islands in Indonesia do not have electricity, and most Indonesians are in deep energy poverty [27], which describes a condition whereby a household spends more than 10% of its total income on energy services [28]. Furthermore, providing access to energy in Indonesia is still challenging because many people live in remote areas and are spread on approximately 16.056 islands. The Papua and East Nusa Tenggara provinces have electrification ratios of approximately 61.4% and 59.8% [27], respectively. This implies that most Indonesians experiencing energy poverty may be unable to afford air conditioning or electricity, increasing the risk of heat-related diseases. Because of the thermal discomfort experienced by individuals living in energy poverty, their physical and mental health are adversely affected [29–34]. Moreover, this may result in underlying medical conditions such as respiratory [35] and cardiovascular diseases [33, 36, 37].

Furthermore, Indonesia still lacks building codes to reduce building thermal loads. In 2005, national standards related to building envelopes, air conditioning, lighting, and building energy auditing were established for the first time but were not mandated. In 2012, the capital city of DKI Jakarta issued the first and only mandatory green building regulation. However, most neighbouring and remote cities lack attention. This implies that the mandatory regulation energy standard for building design in Indonesia needs to be complied with and upgraded according to climate zones.

In addition, Indonesia is rich in mineral resources, energy resources and plant resources. Economic growth is expected from the peak of the demographic bonus period. Demand for energy is expected to increase rapidly due to improvements in the living environment such as indoor air conditioning. Since the consumption of energy derived from daily life is certain to increase in the near future, we aim to save energy in buildings. It is necessary to formulate building thermal performance standards corresponding to environmental design such as passive and active cooling.

To address the abovementioned issues, a passive design plan for naturally ventilated Indonesian houses should be developed as an initial step to comply with the existing standards according to the climate zones. Therefore, this study developed a passive design for a naturally ventilated house by investigating the effects of various passive design improvements on indoor environmental conditions.

We simulated the developed improvement plans' cooling loads and compared them to existing general Indonesian households. Additionally, considering various climate conditions, we examined the annual cooling loads of the performance improvement plan in various cities in Indonesia according to their respective climate zones.

1.2. Thesis organization

Chapter 1 describes the previous studies and issues, the study's purpose, and the dissertation's structure.

Chapter 2 survey and investigate a standard low-cost house that adopts natural ventilation in Indonesia. The detail of construction is captured in order to provide building simulation data. The main focus of this chapter is to study and evaluate indoor thermal comfort among occupants during the daytime through a questionnaire. The questionnaire is related to occupants' sensation vote based on thermal sensation vote (TSV) and thermal comfort vote (TCV). In addition, airflow and air freshness, thermal preferences, and behavioural adaptation are also captured as an initial step to understanding indoor condition performance.

Chapter 3 develops a simulation model of louver openings in the naturally ventilated building through experimental studies conducted in an environmental testing laboratory and by simulation of computer fluid dynamics (CFD). The performance characteristic of ventilation rate, indoor and outdoor weather, outdoor wind velocity, inlet wind speed, and pressure difference was investigated and analyzed. The discharge coefficient of several louver opening types based on different sash angles is determined to provide simulation data for the network airflow model. In addition, CFD was performed to determine the wind pressure coefficient of the case study building. Finally, the model is validated by the numerical software THERB for HAM with NAF.

Chapter 4, a plan for enhancing the performance of energy-efficient naturally ventilated houses in tropical regions of Indonesia is presented. Initially, on-site measurements are carried out to gather data such as indoor/outdoor temperature and relative humidity in Lhokseumawe, an Indonesian city. These experimental data are then used to verify a numerical simulation model. The next step involves using the numerical simulation to develop energy-efficient design solutions for homes in 14 different locations in Indonesia. The study also investigates the annual cooling loads for the entire simulated regions. This research has the potential to serve as a foundation for achieving zero-energy housing and ensuring adequate thermal comfort for occupants in unconditioned and naturally ventilated homes in Indonesia.

Chapter 5 summarizes the observations obtained in each previous chapter and organizes future issues in a structured manner.

References

[1] M. Indraganti, “Adaptive use of natural ventilation for thermal comfort in Indian apartments,” Build Environ, vol. 45, no. 6, pp. 1490–1507, 2010.

[2] C. G. WEBB, “An analysis of some observations of thermal comfort in an equatorial climate.,” Br J Ind Med, vol. 16, no. 4, pp. 297–310, 1959.

[3] F. P. Ellis, “Thermal comfort in warm and humid atmospheres: Observations on groups and individuals in Singapore,” Journal of Hygiene, vol. 51, no. 3, pp. 386–404, 1953.

[4] R. J. de Dear, K. G. Leow, and S. C. Foo, “Thermal comfort in the humid tropics: Field experiments in air conditioned and naturally ventilated buildings in Singapore,” Int J Biometeorol, vol. 34, no. 4, pp. 259–265, 1991.

[5] T. H. Karyono, “Report on thermal comfort and building energy studies in Jakarta - Indonesia,” Build Environ, vol. 35, no. 1, pp. 77–90, 2000.

[6] H. Feriadi and N. H. Wong, “Thermal comfort for naturally ventilated houses in Indonesia,” Energy Build, vol. 36, no. 7, pp. 614–626, 2004.

[7] L. H. Sari, D. J. Harris, and M. Gormley, “Indoor thermal assessment of post-tsunami housing in Banda Aceh, Indonesia,” International Journal for Housing Science and Its Applications, vol. 37, no. 3, pp. 161–173, 2013.

[8] G. S. Brager and R. J. de Dear, “Thermal adaptation in the built environment: A literature review,” Energy Build, vol. 27, no. 1, pp. 83–96, 1998.

[9] P. Heiselberg and M. Perino, “Short-term airing by natural ventilation - implication on IAQ and thermal comfort,” Indoor Air, vol. 20, no. 2, pp. 126–140, 2010.

[10] N. Monghasemi and A. Vadiee, “A review of solar chimney integrated systems for space heating and cooling application,” Renewable and Sustainable Energy Reviews, vol. 81, no. June 2017, pp. 2714–2730, 2018.

[11] F. Jomehzadeh et al., “A review on windcatcher for passive cooling and natural ventilation in buildings, Part 1: Indoor air quality and thermal comfort assessment,” Renewable and Sustainable Energy Reviews, vol. 70, no. November 2016, pp. 736–756, 2017.

[12] Y. Choi and D. Song, “How to quantify natural ventilation rate of single-sided ventilation with trickle ventilator?,” Build Environ, vol. 181, no. April, p. 107119, 2020.

[13] X. Shen, C. Zong, and G. Zhang, “Optimization of sampling positions for measuring ventilation rates in naturally ventilated buildings using tracer gas,” Sensors (Switzerland), vol. 12, no. 9, pp. 11966–11988, 2012.

[14] X. Shen, R. Su, G. K. Ntinas, and G. Zhang, “Influence of sidewall openings on air change rate and airflow conditions inside and outside low-rise naturally ventilated buildings,” Energy Build, vol. 130, pp. 453–464, Oct. 2016.

[15] J. Araúz, D. Mora, and M. C. Austin, “Impact of the envelope layout in the thermal behavior of buildings in Panama: A numerical study,” Proceedings - 2019 7th International Engineering, Sciences and Technology Conference, IESTEC 2019, pp. 209–214, 2019.

[16] M. Zune, L. Rodrigues, and M. Gillott, “Vernacular passive design in Myanmar housing for thermal comfort,” Sustain Cities Soc, vol. 54, p. 101992, Mar. 2020.

[17] D. Etheridge, Natural Ventilation of Buildings: Theory, Measurement and Design. 2011.

[18] P. Heiselberg, K. Svidt, and P. V. Nielsen, “Characteristics of airflow from open windows,” Build Environ, vol. 36, no. 7, pp. 859–869, Aug. 2001.

[19] H. Cruz and J. C. Viegas, “On-site assessment of the discharge coefficient of open windows,” Energy Build, vol. 126, pp. 463–476, Aug. 2016.

[20] A. Iqbal, A. Afshari, H. Wigö, and P. Heiselberg, “Discharge coefficient of centre-pivot roof windows,” Build Environ, vol. 92, pp. 635–643, 2015.

[21] Y. H. Chiu and D. W. Etheridge, “External flow effects on the discharge coefficients of two types of ventilation opening,” Journal of Wind Engineering and Industrial Aerodynamics, vol. 95, no. 4, pp. 225–252, Apr. 2007.

[22] H.B. Awbi, Ventilation in Buildings. Taylor and Francis, London and New York, 2005.

[23] Evola G and Popov V, “Computational analysis of wind driven natural ventilation in buildings,” Energy Build, vol. 38, pp. 491–501, 2006.

[24] K. T. Andersen, “Inlet and ouflet coefficients. A theoretical analysis,” 5th International Conference on Air Distribution in Rooms ROOMVENT’96, pp. 379–390., 1996.

[25] D. Cóstola, B. Blocken, and J. L. M. Hensen, “Overview of pressure coefficient data in building energy simulation and airflow network programs,” Build Environ, vol. 44, no. 10, pp. 2027–2036, 2009.

[26] Y. Xing, N. Hewitt, and P. Griffiths, “Zero carbon buildings refurbishment - A Hierarchical pathway,” Renewable and Sustainable Energy Reviews, vol. 15, no. 6, pp. 3229–3236, 2011.

[27] M. T. Sambodo and R. Novandra, “The state of energy poverty in Indonesia and its impact on welfare,” Energy Policy, vol. 132, no. October 2018, pp. 113–121, 2019.

[28] Y. Choi, D. Song, A. Ozaki, H. Lee, and S. Park, “Do energy subsidies affect the indoor temperature and heating energy consumption in low-income households?,” Energy Build, vol. 256, p. 111678, 2022.

[29] C. N. B. Grey, T. Schmieder-Gaite, S. Jiang, C. Nascimento, and W. Poortinga, “Cold homes, fuel poverty and energy efficiency improvements: A longitudinal focus group approach,” Indoor and Built Environment, vol. 26, no. 7, pp. 902–913, 2017.

[30] C. Liddell and C. Morris, “Fuel poverty and human health: A review of recent evidence,” Energy Policy, vol. 38, no. 6, pp. 2987–2997, 2010.

[31] T. Oreszczyn, S. H. Hong, I. Ridley, and P. Wilkinson, “Determinants of winter indoor temperatures in low income households in England,” Energy Build, vol. 38, no. 3, pp. 245–252, 2006.

[32] J. A. Paravantis and M. Santamouris, “An analysis of indoor temperature measurements in low- and very-low-income housing in Athens, Greece,” Advances in Building Energy Research, vol. 10, no. 1, pp. 20–45, 2016.

[33] J. Rudge and R. Gilchrist, “Measuring the health impact of temperatures in dwellings: Investigating excess winter morbidity and cold homes in the London Borough of Newham,” Energy Build, vol. 39, no. 7, pp. 847–858, 2007.

[34] M. Santamouris et al., “Freezing the poor - Indoor environmental quality in low and very low income households during the winter period in Athens,” Energy Build, vol. 70, pp. 61–70, 2014.

[35] R. Bardhan, R. Debnath, A. Jana, and L. K. Norford, “Investigating the association of healthcare-seeking behavior with the freshness of indoor spaces in low-income tenement housing in Mumbai,” Habitat Int, vol. 71, no. September 2017, pp. 156–168, 2018.

[36] R. Jevons, C. Carmichael, A. Crossley, and A. Bone, “Minimum indoor temperature threshold recommendations for English homes in winter – A systematic review,” Public Health, vol. 136, pp. 4–12, 2016.

[37] E. Webb, D. Blane, and R. De Vries, “Housing and respiratory health at older ages,” J Epidemiol Community Health (1978), vol. 67, no. 3, pp. 280–285, 2013.

Chapter 2. Assessment of indoor thermal comfort in tropical regions

2.1. Overview of approach

Thermal comfort studies employ three common approaches: model-based, human-based, and space-based. The first approach, the model-based approach, focuses on simulating the physical conditions of the indoor environment and assessing occupants' thermal comfort levels based on certain assumptions and standards. Accurate prediction results in this approach require proper simulation and measurable, proportional data collection. The second approach, the human-based approach, involves direct investigation of building occupants to evaluate thermal comfort. Data and information collected through systematic experiments in specific rooms or field settings must be carefully controlled. This approach is suitable for conducting a comprehensive evaluation of thermal comfort and developing appropriate standards to obtain precise and accurate results. The third approach, the space-based approach, is used to study thermal comfort on a larger scale, particularly in specific spaces. It is applied in building design and building service system studies, such as exploring passive cooling strategies through architectural layout, building form, and wall insulation.

It is important to note that field surveys may be influenced by factors that are not considered in laboratory settings. For instance, when comparing field survey results from different socioeconomic areas, it is crucial to consider the impact of local conditions and behavioural norms that are unique to each location and not replicated in the laboratory [1]. Hence, for this study focusing on naturally ventilated houses, a human-based approach will be employed to investigate human perception of indoor environmental conditions as an initial step for further research.

2.2. Climatic conditions

Outdoor climatic condition is essential for the naturally ventilated house in the tropical climate because it will affect indoor condition due to window opening in the house. Therefore, the climatic conditions of the study area during the on-site survey were demonstrated [2] in Figure 2.1 - Figure 2.3. The average solar radiation recorded is 156.15 W/m² with a maximum value at 01.00 p.m. of 674.99 W/m². The relative humidity demonstrates a high value with a maximum of 98.29%, which tends to occur at night, and the minimum and average relative humidity are 57.04% and 82.65%, respectively. In addition, the average air temperature value is 27.48 ℃, where the minimum and maximum values are classified at 23.20 ℃ and 32.50 ℃, respectively. Furthermore, the wind direction flows to the building dominated from the south. Wind speed shows a maximum of 11 m/s and an average of 4.18 m/s, respectively.

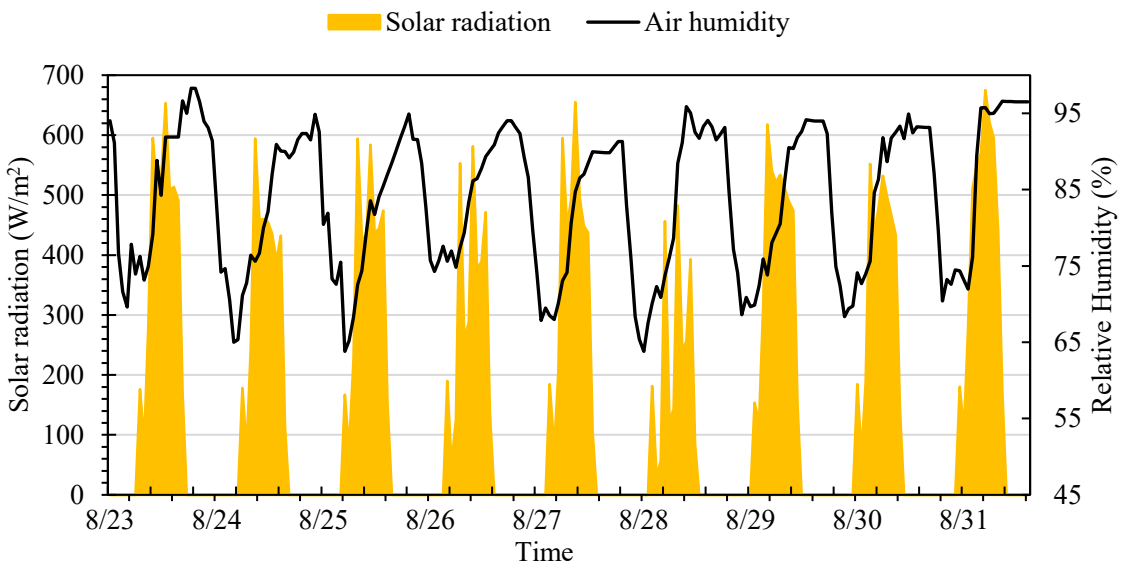

Figure 2.1 Solar radiation and air humidity

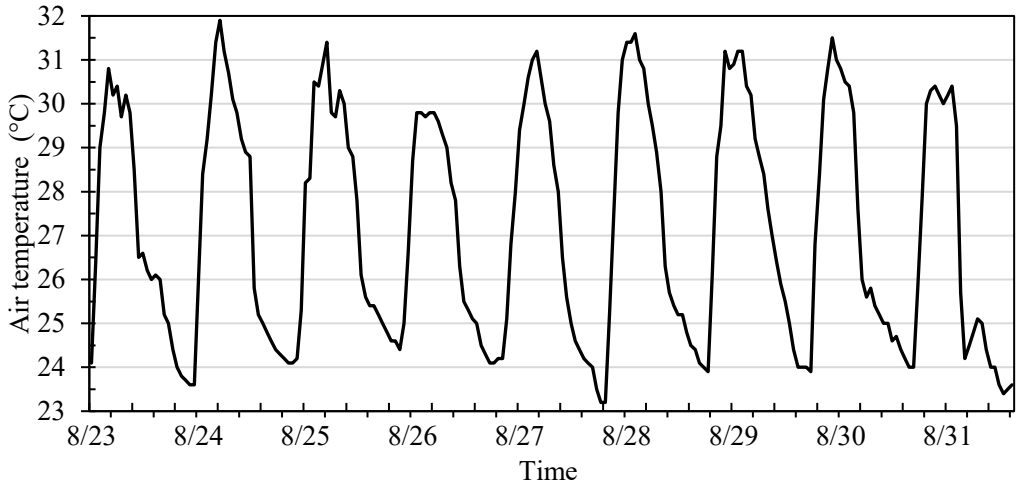

Figure 2.2. Air temperature

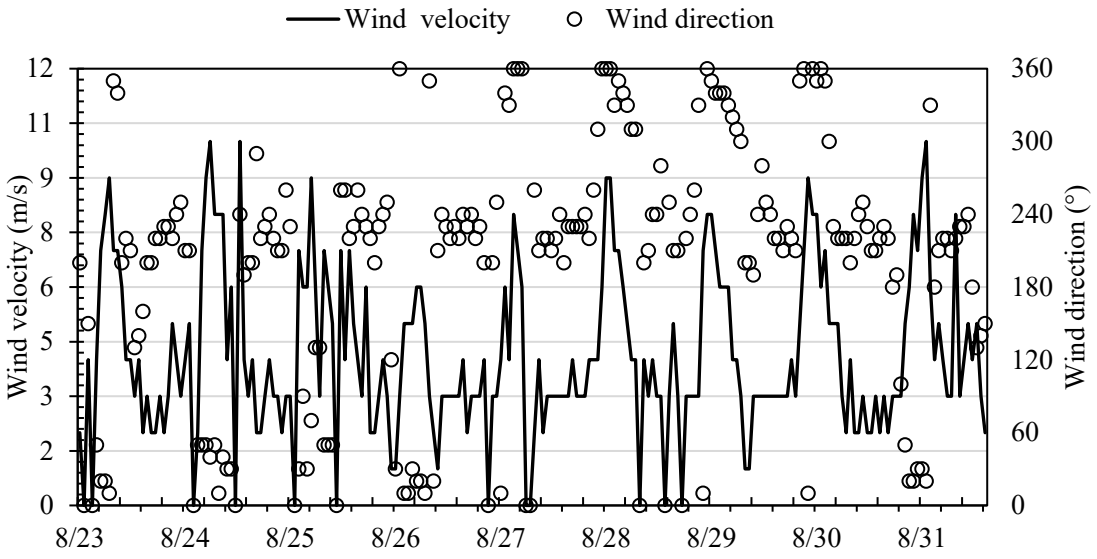

Figure 2.3. Wind velocity and wind direction

2.3. Research object and method

2.3.1. Research object

Most of the houses in this study are low-cost houses and meet the standards recommended by the Indonesian government. The houses consist of two types, located in Aceh Province, Indonesia. The locations both of types are different. Type 1 is situated on a hill, and type 2 is close to the sea, as shown in Figure 2.4. However, the two regions' outdoor temperature and absolute humidity were almost similar during the measurements. Therefore, the impact of microclimate on thermal comfort is excluded in this study because it has no significant effect on indoor performance for comparison among the house types.

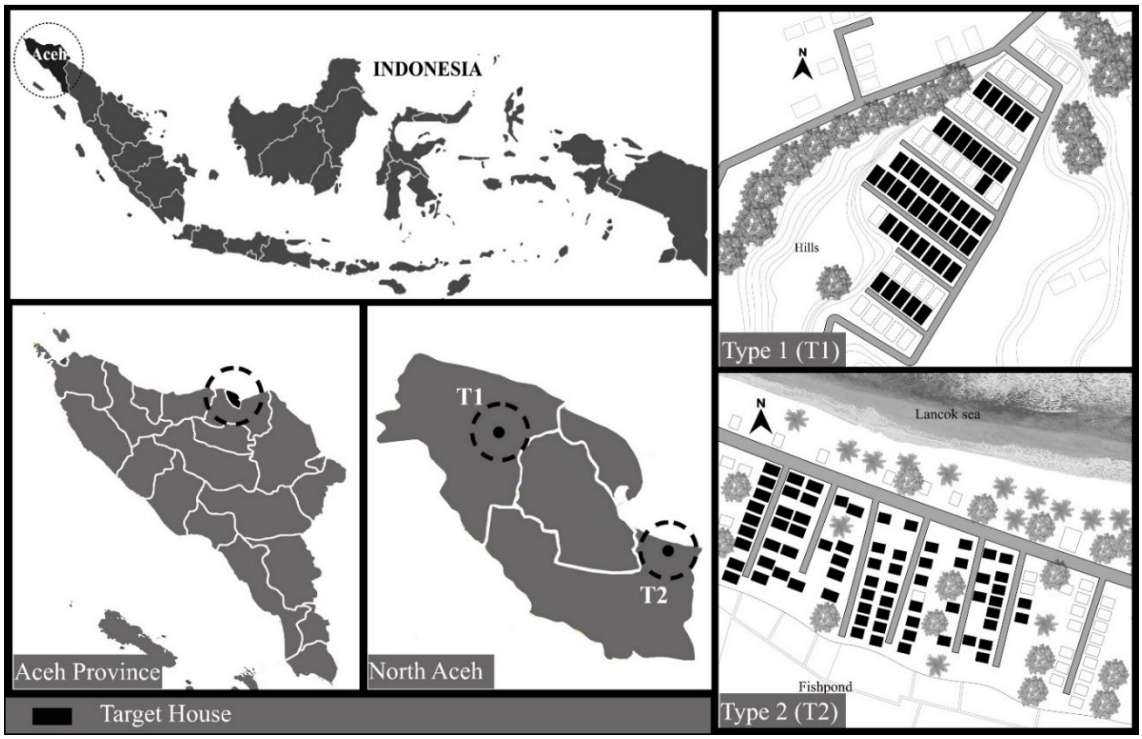

Figure 2.4. Site location of the houses

2.3.1.1. Type 1 (Developer House)

The developer house is one of the residential types built by a local private company. It is the most common house found in North Aceh, Indonesia. More than one hundred houses had been built by a local company. The house is a grounded permanent house built in heavyweight construction such as plastered brickwork and concrete structures. Figure 2.5 and Figure 2.6 illustrate the floor plan and the exterior and interior appearance of type 1. The house has two bedrooms, a living room and a kitchen, with an area of 33 m^2. Window to wall ratio (WWR) and window to floor area (WFR) are 7.39% and 16.48%, respectively.

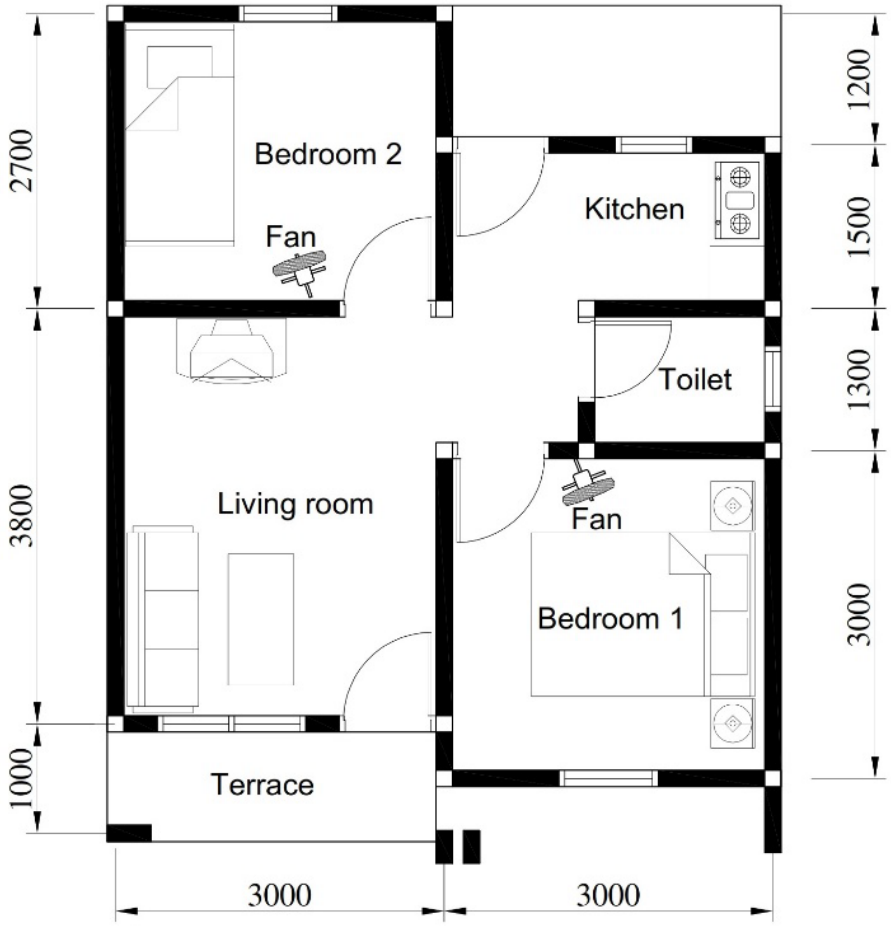

Figure 2.5. Floor plan of type 1

Figure 2.6 Exterior and interior appearance of type 1

2.3.1.2. Type 2 (NGO house)

NGO house is a non-government organization house. After Indonesia's earthquake and tsunami disaster in December 2004, over 100,000 houses were built in Aceh Province, Indonesia [3]. The

houses are similar to the typical house found in Aceh Province. Most of the type has the same size and shapes due to the houses being built simultaneously by an NGO (non-government organization). The floorplan, exterior, and interior appearance are demonstrated in Figure 2.7 and Figure 2.8. The type 2 house is more extensive than type 1 with a uniform room configuration. It has two bedrooms, a living room and a kitchen, with an area of 39.75 m2. However, the window to wall ratio (WWR) and window to floor ratio (WFR) is 5.58 % and 9.06 %, respectively. Therefore, compared to type 1, type 2 is less than type 1.

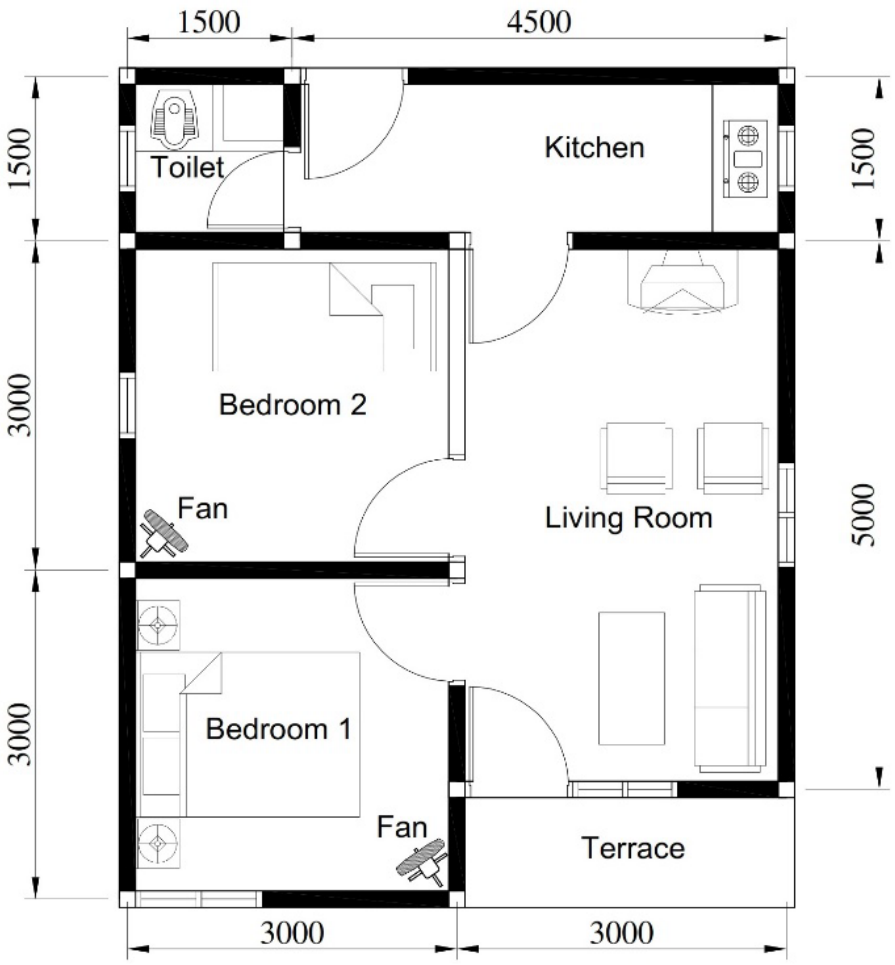

Figure 2.7. Floor plan of type 2

Figure 2.8. Exterior and interior appearance of type 2

2.3.2. Methods

2.3.2.1. Households selection

The on-site survey is conducted to obtain data on the perception of building users, indoor environment preferences, and user responses due to uncomfortable situations during daily life. More than 200 occupants have been selected that represent a population with a low standard of living. The houses selected and the number of the subject are divided into two types. The on-site survey and questionnaire distribution were carried out from August 23, 2020, to August 31, 2020. However, due to limited access to the case study locations, questionnaires were only conducted in the morning - evening (06:00 - 18:00).

Even though the data is not available on the percentage of air conditioning use in households, it believes that Indonesian commonly performs in non-air-conditioned environments and has a passive regulation in achieving thermal comfort in houses.

For example, the whole subject was initially 90 and 160 respondents for type 1 and typed 2. However, about two respondents on type 1 and six on type 2 were not included because they operate the air conditioner daily. As a result, the subjects surveyed are 88 respondents for type 1 and 154 respondents for type 2. Moreover, in order to measure relevant data from field surveys, some criteria for housing and respondent selection are proposed as follows:

- The housing relies on passive cooling strategies to create a relaxed indoor environment.
- Respondents currently occupy the housing in order to catch the real attitude improvement.
- Residents are willing to fill out the questionnaire simultaneously without any reward.

2.3.2.2. Questionnaire

Recording the response occupants is the most vital aspect of this study. This research used a paper-based questionnaire, and the occupants responded only once in this survey. Therefore, some common questions to investigate thermal sensation and thermal comfort votes have been used. In order to evaluate the whole thermal perception, using both of the seven scales of ASHRAE thermal

sensation and the Bedford scale are proposed. It also examines the consistency of response between thermal sensation and perception. Table 2.1. present the two-scale used for this study.

Table 2.1. Rating scale used for thermal comfort survey

ASHRAE Scale	Bedford Scale
-3 cold	-3 much too cool
-2 cool	-2 too cool
-1 slightly cool	-1 comfortably cool
0 neutral	0 comfortable
+1 slightly warm	+1 comfortably warm
+2 warm	+2 too warm
+3 hot	+3 much too warm

In addition, the other questions will ask about the occupant's preference, airflow and freshness scale sensation, thermal preference and body response. These questions are required to classify whether the occupant's feelings corresponded well with the perception of the indoor environment. Moreover, it also gathers information about occupants' control and behavioural adaptation in daily life for a whole day. All questionnaires filled by respondents who stayed in naturally ventilated houses have been evaluated except for households with air conditioners.

2.4. Result and Discussion

2.4.1. Respondent Information

The respondents' gender and age of dwelling types are evenly distributed. The comparison of distribution between gender and age is commonly similar among the surveyed types. Table 2.2 presents the respondent information of this study.

Table 2.2. Respondent

	Type 1	**Type 2**
Gender		
Male	49 (55.68%)	74 (48.05%)
Female	39 (44.32%)	80 (51.95%)
Age (Years)		
<20	1 (1.14%)	4 (2.6%)
21 - 30	24 (27.27%)	29 (18.83%)
31 - 40	46 (52.27%)	48 (31.17%)
41 - 50	9 (10.23%)	41 (26.62%)
>50	8 (9.09%)	32 (20.78%)

2.4.2. Thermal comfort between two types of house

The study investigates the window opening area and room area against thermal sensation vote in order to understand the effect of the window openings ratio and room area to thermal sensation vote (TSV) and thermal comfort vote (TCV). In this case, the occupants are requested to sit in the living room and relax before filling out the questionnaire.

Moreover, all of the windows in the house are asked to open during this survey. Table 2.3 presents TSV (ASHRAE scale) and TCV (Bedford scale) between two types of houses. The mean vote for the whole subject of two different house types is 0.58 and 0.48 ASHRAE scale and 1.70 and 1.47 on the Bedford scale. This result also presents the consistency of comfort vote between TSV and TCV, respectively. Moreover, the standard ASHRAE stated that the acceptability of thermal comfort should be defined as the condition where 80% of residents vote for the central three categories (-1,0,1).

Therefore, Figure 2.9 demonstrates the three main categories of the thermal sensation vote (TSV). The occupants of type 1 houses prefer comfort vote for both scales, where the ASHRAE scale and the Bedford scale were 79.55 % and 86.36 %, followed by warm and hot sensations 17.05 % and 10.23 %, respectively. However, most occupants on type 2 felt warm and hot at 53.90 %, followed by a neutral vote of 46.10 %. On the other hand, the Bedford scale shows that the occupants vote dominated by too warm and much too warm at 54.55 %, followed by comfortable warm at 45.45%.

Table 2.3. Comparison of TSV and TCV on two types of house

Scale	Type 1				Type 2			
	TSV	%	TCV	%	TSV	%	TCV	%
-3	0	0.00	0	0.00	0	0	0	0
-2	3	3.41	3	3.41	0	0	0	0
-1	5	5.68	3	3.41	8	5	2	1
0	36	40.91	42	47.73	30	19	47	31
1	29	32.95	31	35.23	33	21	21	14
2	12	13.64	7	7.95	12	8	44	29
3	3	3.41	2	2.27	71	46	40	26
Total	88	100%	88	100%	154	100%	154	100%
Mean	0.58		0.48		1.70		1.47	

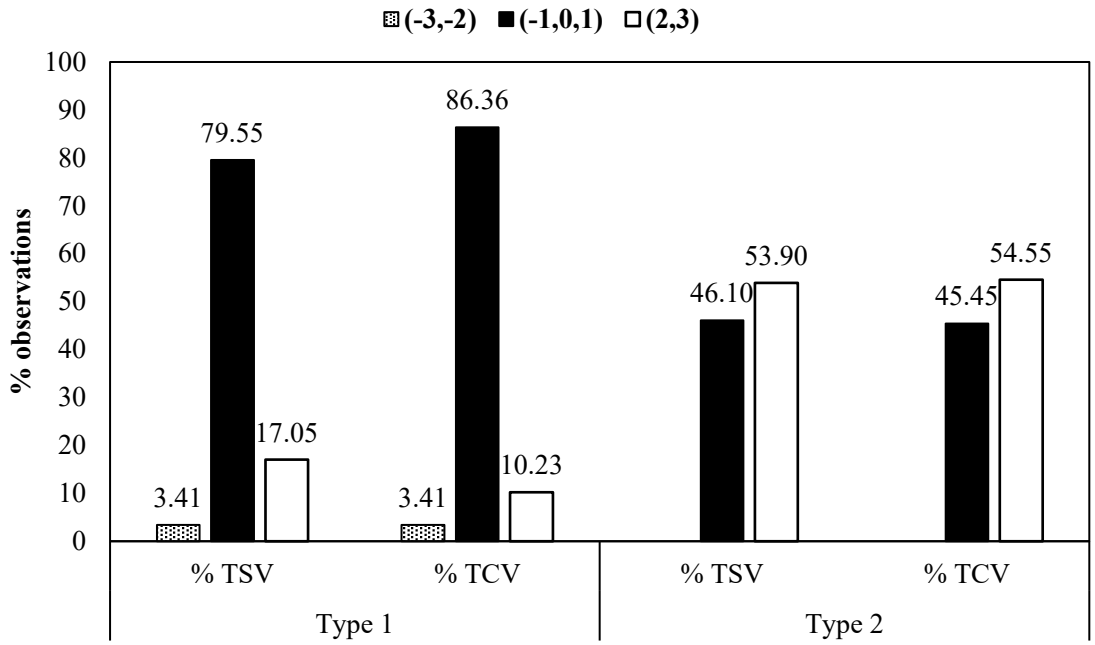

Figure 2.9. TSV and TCV on the central three categories

2.4.3. Airflow and air freshness

The airflow of whole subjects was identified in this study. The occupants were asking," how do you feel about airflow in this room at this moment?". The chosen answer is much too still, too still, slightly still, just right, slightly breezy, too breezy, and much too breezy. Figure 2.10 demonstrates the airflow scale vote. Most of the occupants on type 1 voted "just right" with 37.50%, followed by "slightly breezy" and "too breezy" at 23.86% and 11.36%, respectively. In addition, 2.27% voted "much too breezy". However, some occupants also voted "much too stuffy" and "too stuffy". Meanwhile, the vote distribution type 2 was dominated by "too still" 30,52%, followed by "just right" and "much too still" 26.62% and 20.13%. The occupants also vote "slightly breezy" and "too breezy", with 5.84% and 2.6%, respectively.

Moreover, the comparison vote for three central categories related to thermal sensation vote (TSV) shows that the occupants of type 1 vote 70.45% as a comfortable sensation, as shown in Figure 2.11. On the other hand, the occupants of type 2 vote 46.10% as a comfortable sensation. Therefore, we can conclude that type 1 performs better airflow in this survey.

This study reveals that the larger of opening area, the more significant the air movement in an indoor environment. It has been proved that the value of WFR and WWR affects indoor environment conditions, where the large of WWR and WFR is better than a small one.

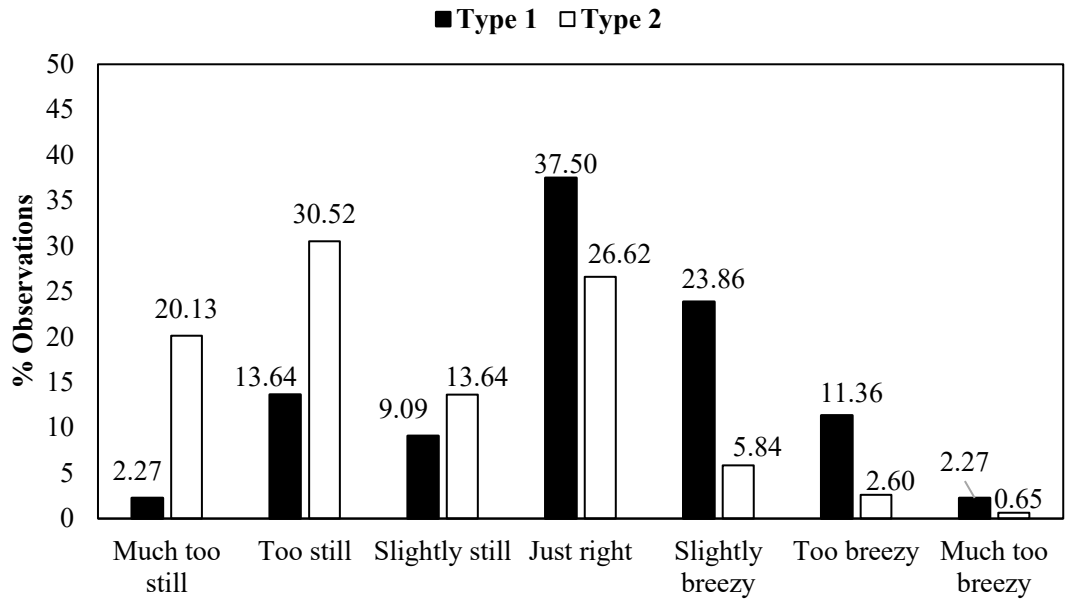

Figure 2.10. Airflow scale vote

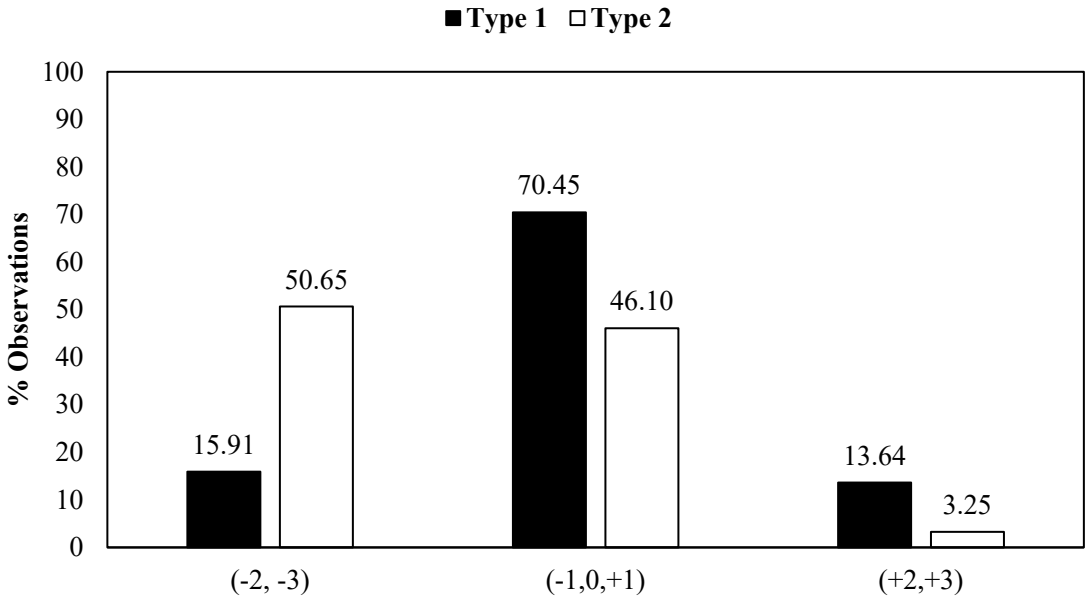

Figure 2.11 Airflow scale on the central three categories

Furthermore, using the Bedford scale, the question for the air freshness scale is: "how do you feel about air freshness in this room now?". Generally, the air freshness vote is similar to the airflow vote, as shown in Figure 2.12 and Figure 2.13. Most occupants on type 1 voted "neutral" at 40.91%, followed by "slightly fresh" at 19.32% and "too fresh" at 11.36%, respectively. In addition, the respondent also votes "much too fresh" at 6.82%. On the other hand, the air freshness vote on house

type 2 was dominated by "too stuffy" of 30.52%, followed by "much too stuffy" and "slightly stuffy" of 20.78% and 14.29%, respectively.

However, some occupants also vote "neutral", "slightly fresh", and "too fresh", with 22.08%, 11.04% and 1.30%. Moreover, the comparison vote for three central categories related to ASHRAE Scale shows that the occupants on type 1 vote 68.18 as a comfortable sensation. On the other hand, the occupants on type 2 just voted 47.40% as a comfortable sensation. Therefore, we can conclude that type 1 performs better air freshness than type 2 in this study.

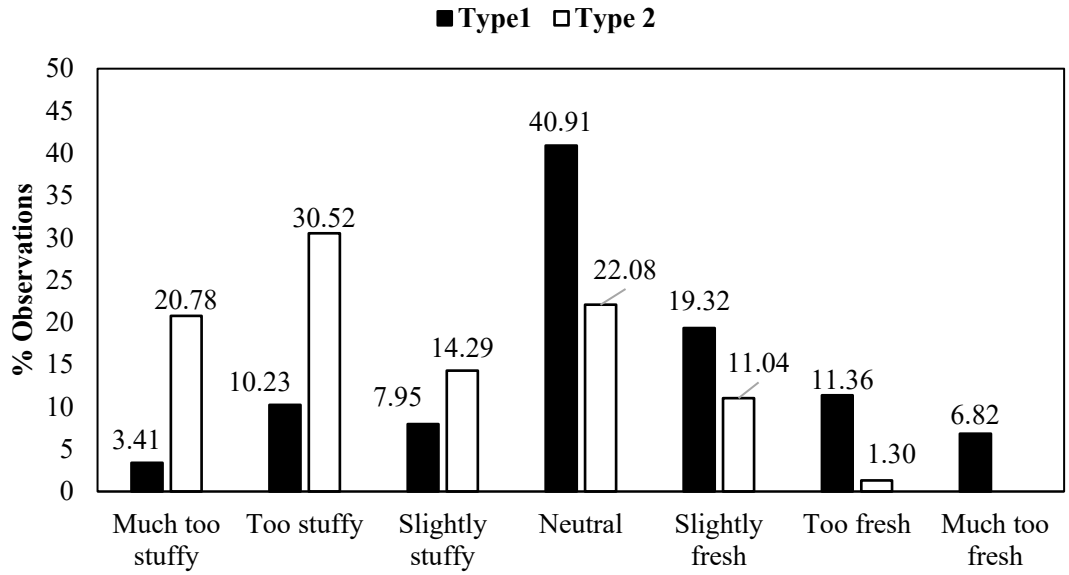

Figure 2.12 Air freshness scale vote

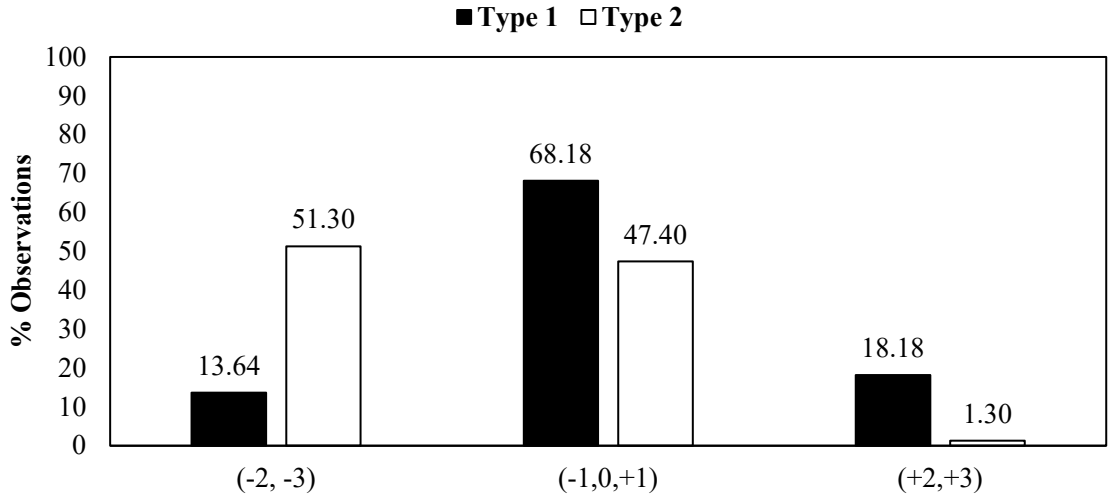

Figure 2.13 Air freshness scale on the central three categories

2.4.4. Thermal preference

The study used the "McIntyre scale" to investigate thermal preference by asking: "How would you prefer the current environment?". There are highly different answers between respondents on type 1 and type 2, where type 1 is better than type 2. Figure 2.14 shows the thermal preference vote for both types of houses. More than 79% of occupants on type 1 voted "just right". Based on three central categories related to TSV, the survey reported that 2.27% of occupants who vote between warm and hot on the ASHRAE scale also choose "just right" as a thermal preference. The other, 3.41% of the respondents who vote cool and cold want to be warmer in this survey. It is contrary to the occupants on type 2, where most of them want to be cooler 66.23 %, followed by just right 33.77%, and no one votes want to be warmer.

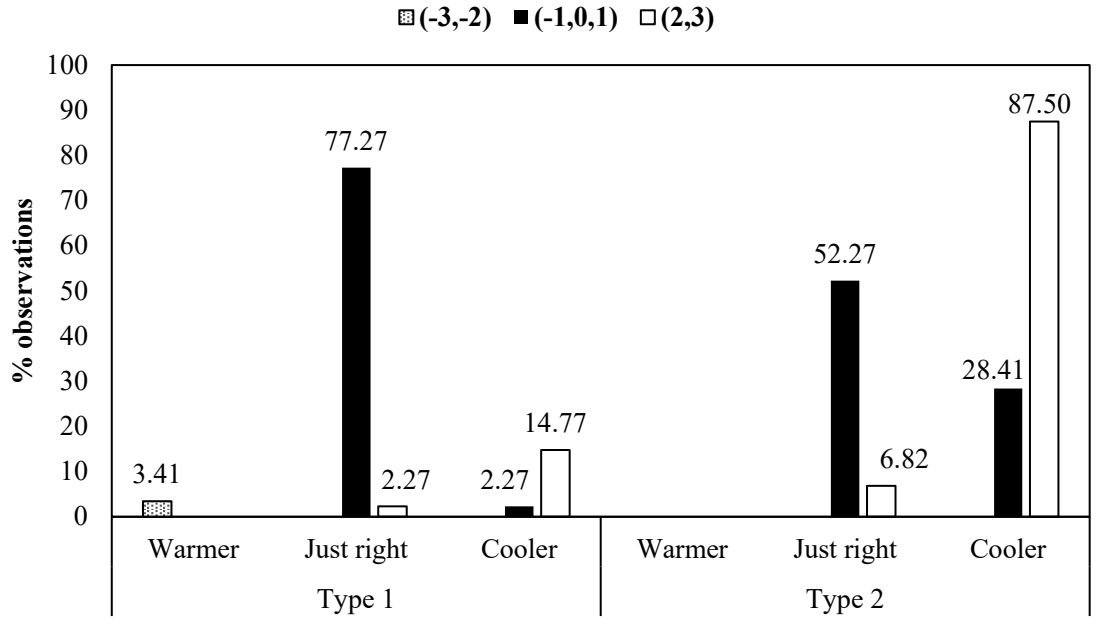

Figure 2.14 Thermal preference vote

2.4.5. Body response

This study also investigated the body response during the survey. This question is essential to understand the current indoor condition's effect on human body response. The body response scale was measured during the on-site survey by asking, "are you sweating now?". It reports that most occupants of type 1 are not sweating, followed by slightly and moderate. Contrary to another type, they chose "moderate" as a higher response, followed by slightly, no sweating and profusely. The distribution of body response votes is illustrated in Figure 2.15.

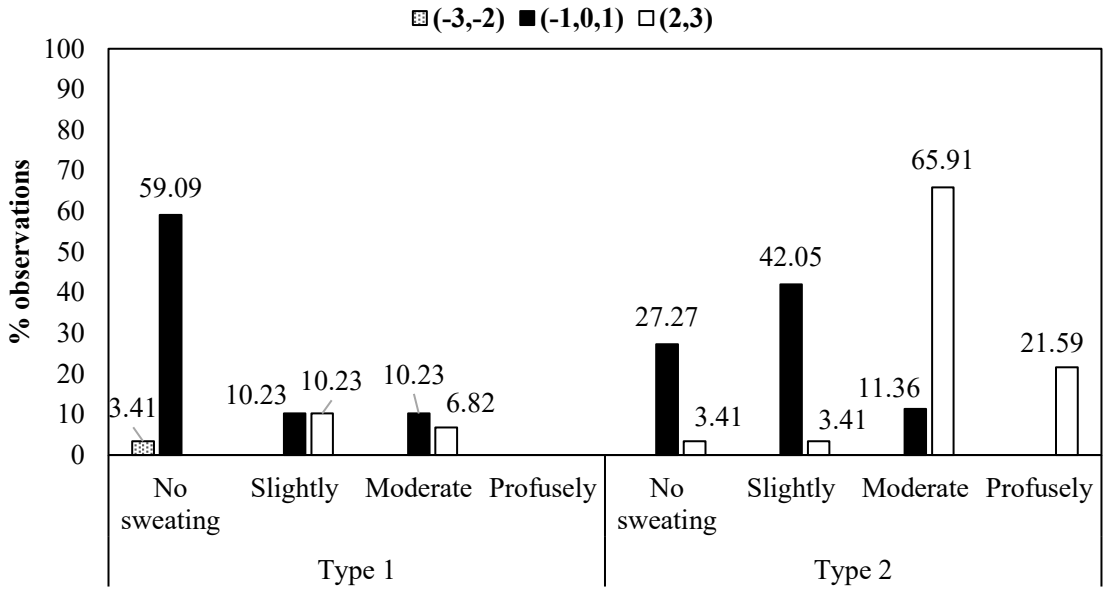

Figure 2.15 Body response vote

2.4.6. Behavioral adaptation

The study identifies the respondent's adaptive actions while staying in the living room. For example, it is commonly changing from just regulating the body by taking a bath more frequently, switching on a fan, opening the window, drinking the water, or changing the clothing. Regarding this concern, the question addressed to the respondent is how likely action is to be taken when the indoor condition is uncomfortable for a whole day. This result indicated that most occupants prefer to open the window, switch on the fan, and take a bath before employing other options to achieve thermal comfort.

Furthermore, another analysis that has been carried out is the detailed window openings and switching on the fans in the bedroom. The specification of action time is divided into four different times there are morning (7-12 a.m), afternoon (1-6 a.m), evening (7-12 p.m), and night (1-6 a.m). Generally, the comparison of body action due to uncomfortable conditions between turning on the fan and usage of bedroom windows are 55.74 % and 44.26 %, respectively. The fan usage mainly occurred at noon and night at 23.83 % and 14.47 %. Besides, the evening and morning time is rare, with frequent 7.94 % and 9.50 %. Furthermore, the usage of window bedrooms reported at noon and morning of 20.99 % and 19.72 %, respectively.

Therefore, it can be said that most of the occupants prefer to operate the fan together with opening the window at noon. We assume that the indoor environment during noon is slightly warm to warm. Meanwhile, most occupants permanently close the window and switch on the fan during the night to control the indoor environment more relaxed.

2.4.7. Regression of thermal sensation vote (TSV) and thermal comfort vote (TCV)

The occupant's vote data is used to derive a comfort range by analysing regression TSV (ASHRAE scale) against TCV (Bedford scale). Figure 2.16 and Figure 2.17 present the linear regression between the ASHRAE thermal sensation scale and the Bedford sensation scale for the types surveyed. Based on the correlation value, type 1 performs better in occupant's vote than type 2. The following linear regression equation for type 1 ($r^2 = 0.7804$) and type 2 ($r^2 = 0.6818$) are obtained:

$$TCV = 0.7836\ TSV + 0.0231 \quad (2.1)$$

$$TCV = 0.9261\ TSV + 0.3363 \quad (2.2)$$

Moreover, we can calculate the range of neutral in the ASHRAE scale and comfortable in the Bedford scale for the type of house. For example, we calculate the comfort range for type 1. As mentioned earlier, the Bedford scale state that the comfortable range is at TCV = 0. The equation shows that the comfortable range (TCV = 0) on the Bedford scale is at a TSV vote (ASHRAE scale) of -0.0294.

Therefore, the value of the TSV result is close to neutral. In addition, another report for TSV that occupants votes for the comfortably cool (TCV = -1) and comfortably warm (TCV = +1) on the Bedford scale are at -1.2466 and 1.3056 on the ASHRAE scale, respectively. Meanwhile, type 2 performs slightly differently between thermal sensation and thermal comfort votes in the comfort range. Therefore, using equation 2, the comfortable range of type 2 is found. While TCV = 0 on the Bedford scale, the TSV is at -0.3631. Therefore, the result shows comfortable range is close to slightly cool. In addition, when the occupants of type 2 vote comfortably cool (-1) and comfortably warm (+1), the TSV is at -1.4429 and 0.7166, respectively.

Furthermore, we can conclude that the comfortable range is at the three central votes in the ASHRAE scale for both types. This result reveals that the respondents feel comfortable in the slightly cool environment (ASHRAE scale) and comfortably warm at slightly warm votes (the Bedford scale).

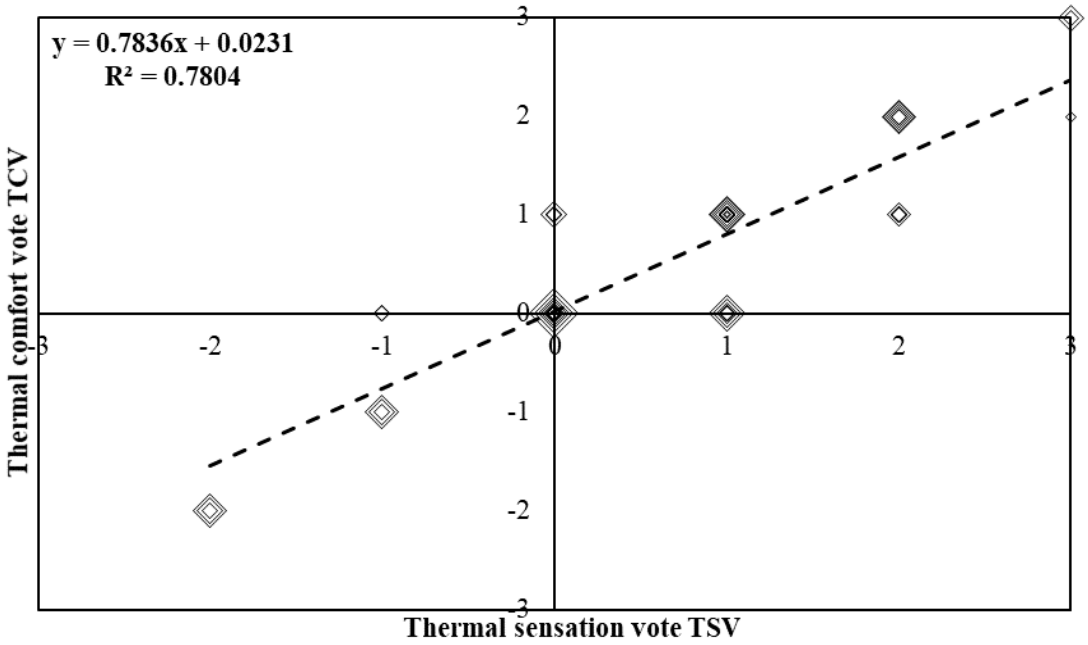

Figure 2.16. Regression linear of TSV against TCV for type 1

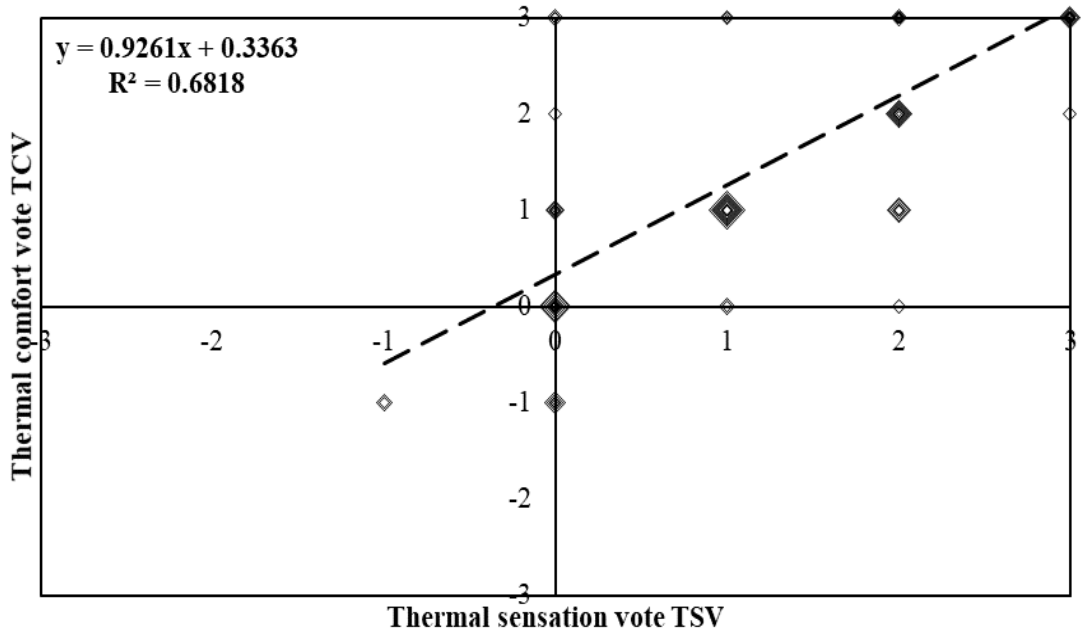

Figure 2.17. Regression linear of TSV against TCV for type 2

2.5. Conclusion

The questionnaire's analysis obtains user responses to thermal comfort assessment and their adaptations in an actual indoor environment. Some of the conclusions are as follows:

- Type 1 performs better thermal comfort than type 2 based on some questions related to airflow, air freshness, thermal preference, and body response.
- The openings ratio affects thermal comfort where the larger openings area is more comfortable than the other.
- This study confirmed the consistency of votes between TSV (ASHRAE) and TCV (Bedford).
- The occupants prefer opening the windows, switching on fans, and taking baths to modify indoor environmental conditions.
- It is necessary to study natural ventilation design factors, especially the effect of opening ratio on ventilation flowrate and thermal comfort for naturally ventilated houses in tropical climates, as further research.

References

[1] Cena, K. (1993). Thermal and Non-Thermal Aspects of Comfort Surveys in Homes and Offices. In Oseland, N.A., and Humphreys, M.A (Eds). Thermal Comfort: Past, Present, and Future. BRE–Garston.

[2] BMKG, (2020), Weather data of North Aceh, Badan Meteorologi, Klimatologi dan Geofisika, Malikussaleh, Indonesia.

[3] BRR. (2008). Monthly Report, Pusdatin BRR, Indonesia (Issue February).

Chapter 3. Development of simulation model of louver openings

3.1. Overview the measurement

3.1.1. Target building

The measurements were conducted in a naturally ventilated building during summer at various pressure differences, external/internal wind velocities, wind directions, air temperature, and relative humidity. In addition, field measurements were collected in a full-scale experimental building to initiate natural ventilation conditions in an actual building at the environmental laboratory of Kyushu University (Ito Campus), Fukuoka City, Japan. The experimental room was placed on the third floor facing east. The photo appearance, floor plan, and elevation are demonstrated in Figure 3.1.

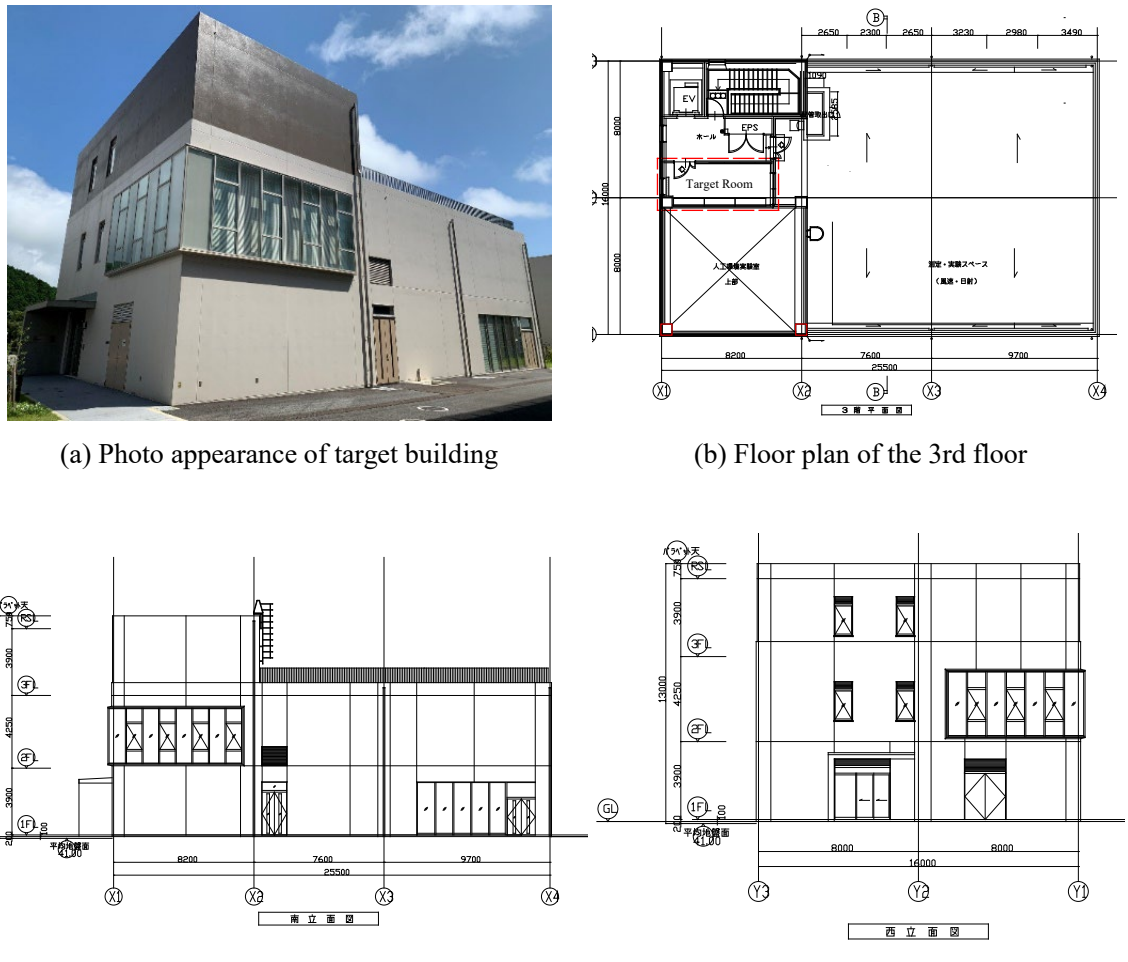

(a) Photo appearance of target building

(b) Floor plan of the 3rd floor

(c) North Elevation

(d) West Elevation

Figure 3.1. Photo appearance, floor plan and elevation of experimental building, Kyushu University, Fukuoka City, Japan.

3.1.2. Measurement setup

The internal dimensions of the chamber were 6500 mm × 4000 mm × 2600 mm, and the measurement configuration in the test room was set up, as shown in Figure 3.2. The entrance and windows were closed, except for the opening of the louvres. The opening of the louvre was linked to the window frame in the measurement chamber. The measurement periods for the three cases were completed during summer. In addition, cooling or heating were not used during the measurements. Instead, the indoor temperature, relative humidity, and CO_2 concentration were recorded at the center of the room. Louvre openings were opened to assess variations in the interior concentration of the tracer gas. In addition, the average inlet air velocity was determined by measuring the airflow at the center of the louvre ventilation. Because the air velocity fluctuates depending on the position of the inlet, a preliminary experiment was conducted to identify the representative location, and the results demonstrated the typical inlet air velocity of the louvre ventilation. To measure the pressure difference, one of the wind pressure sensors was placed near the opening shape (outer wall surface on west side), while another was placed in the center of the room. The outdoor environment was measured, and the devices were positioned on the rooftop of the target building. In addition, the measurement specifications are listed in Table 3.1. Every measurement section was captured using a data logger at intervals of 5 min.

Figure 3.2. Measurement configuration in the target room.

Table 3.1. Measurement specification

Items	**Instrument**	**Specification**
CO_2 concentration	Multi-chamber ventilator, SK-001	Range of measurement : 0 - 5000 ppm, accuracy of ±50 ppm, res. =1 ppm.
Inlet air velocity	KANOMAX 6501-00	Range of measurement : 0.01 - 30 m/s, accuracy of 0.02 m/s, res. = 0.01 m/s.
Pressure difference	TESTO 400	Range of measurement : 100 - 200 hPa, accuracy of 0.001hPa, res. = 0.1°C.
Indoor temperature	Ondotori (ESPEC-RS14)	Range of measurement : 0 - 55°C, accuracy of ±0.5°C, res. = 0.1°C.
Indoor RH		Range of measurement : 10 - 95% RH, accuracy of ±5% RH, res. = 1%.
Outdoor wind velocity	Hideko seiki WS 502 (weather station)	Range of measurement : 0 - 75 m/s, accuracy of ±0.3 m/s, res. = 0.1 m/s
Outdoor wind direction		Range of measurement : 0 - 359.9°, accuracy of 3°, res. = 0.1°
Outdoor temperature		Range of measurement : 50 - 60°C, accuracy of ±0.2°C
Outdoor RH		Range of measurement : 0 - 100%, accuracy of ±0.2%.

3.1.3. Cases configuration

The cases configuration of this study is based on the actual louver openings of Indonesia house. In tropical buildings, window openings can be effective to reduce heat build-up, which in turn can lower indoor air temperatures and night time cooling loads [1]. Notably, Indonesia house attach the louver above the window/door with various sash degree. It is one of the traditional design factors of Indonesian housing which can partly improve the comfort level by increase air velocity [2, 3]. The louvers are typically arranged in a pattern, either horizontally or vertically, and it is usually made from wood, although modern homes may also use metal or plastic materials.

Therefore, to determine the effect of the geometrical louvre on the ventilation rate and discharge coefficient value, the measurement cases were divided into three categories: louvres with a sash of 0°, louvres with a sash of 15°, and louvres with a sash of 30°, as depicted in Figure 3.3.

Photo 1

Photo 2

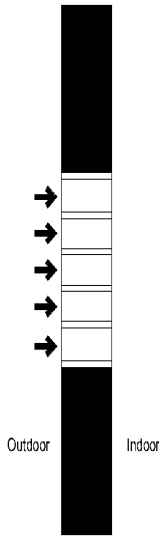

Louver with sash 0°

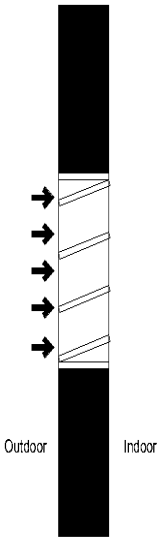

Louver with sash 15°

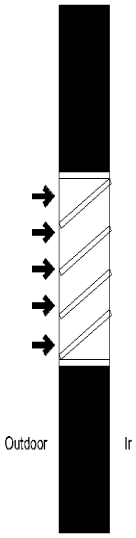

Louver with sash 30°

Figure 3.3. Cases of measurement.

3.1.4. Natural ventilation rate estimation

Tracer gases are utilized in various diagnostic procedures such as leakage detection, environmental tracing, and building ventilation monitoring [4]. The tracer gas approach can be classified into three types: the constant injection, concentration decay, and constant concentration methods. The concentration approach is extensively used because it requires only the smallest amount of gas and reasonably straightforward equipment. The study utilizes constant concentration method to investigate ventilation rate. The measurement range of the devices used was 5000 ppm, and the accuracy of the devices was approximately 50 ppm. In this study, we used a CO_2 concentration of 3500 ppm [5]. The relationship between the concentration of CO_2 produced by natural processes and ventilation rate can be expressed as follows:

$$Q_w = \frac{k}{(Pi - Po)} \tag{3.1}$$

where Q_w denotes the ventilation rate, k denotes the generated volume of outgassing, Pi denotes the indoor carbon dioxide concentration, and Po denotes the outdoor carbon dioxide concentration.

3.2. Result and discussion

3.2.1. Outdoor weather conditions

Figure 3.4 present the outdoor temperature and relative humidity during the summer. The average of outdoor temperature and relative humidity during the measurement periods are of 25.84 °C and 72.33 %, respectively. The maximum and minimum of temperature were 36.10 °C and 25.84 °C while the relative humidity were recorded at 100 % and 72.33 %, respectively.

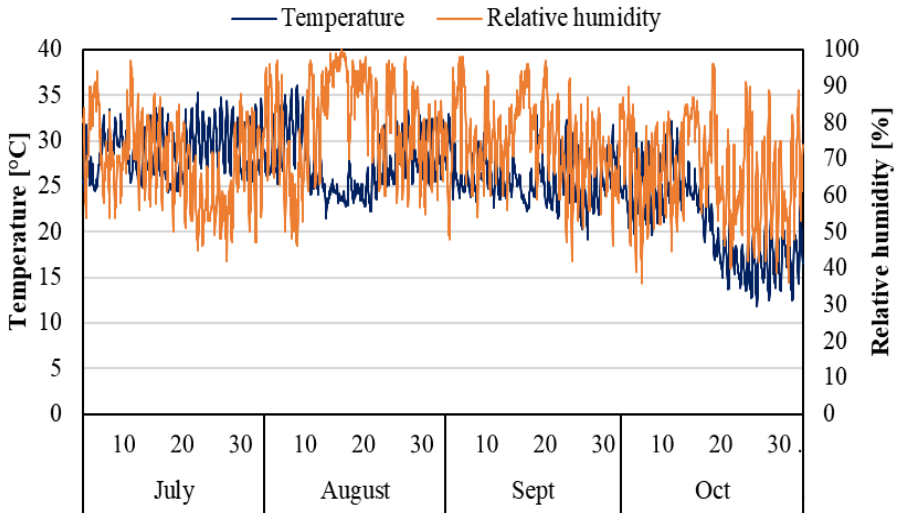

Figure 3.4. Outdoor temperature and relative condition.

The average outdoor wind velocity for the whole summer was 3.54 m/s, with maximum and minimum values of 13.20 m/s and 0 m/s, respectively. Figure 3.5 shows the changes in outdoor wind velocity during the summer. In addition, the frequencies of the outdoor wind velocity during the summer were analysed and are shown in Figure 3.6. Approximately 66 % of the measured outdoor wind velocity in the summer was less than 4.0 m/s. This can be explained by the fact that the external wind speed conditions in all cases represented the general summer conditions in the measurement area.

As a result, we concluded that the outdoor conditions for the entire summer were similar to those during the measurement periods for each case tested, and the results of this study can be used for the entire summer conditions of naturally ventilated buildings in Fukuoka City, Japan.

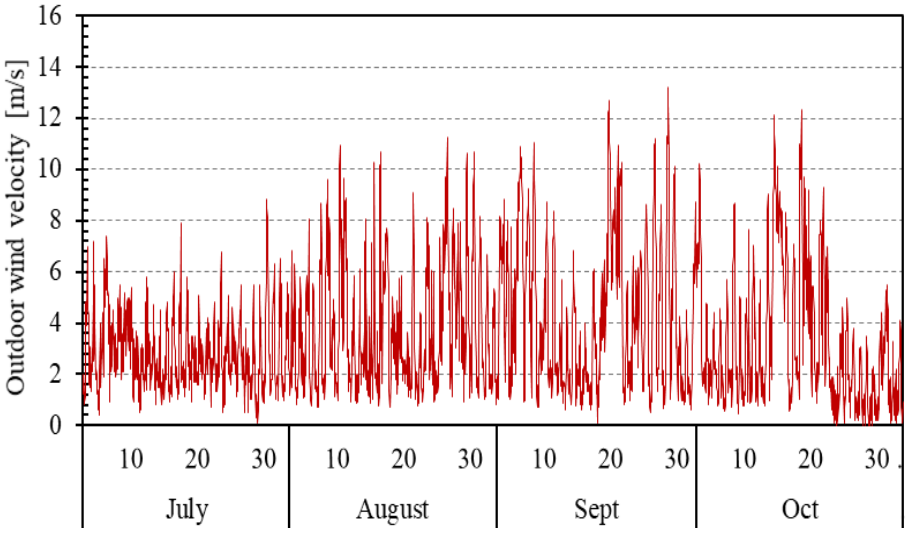

Figure 3.5. Outdoor wind velocity condition.

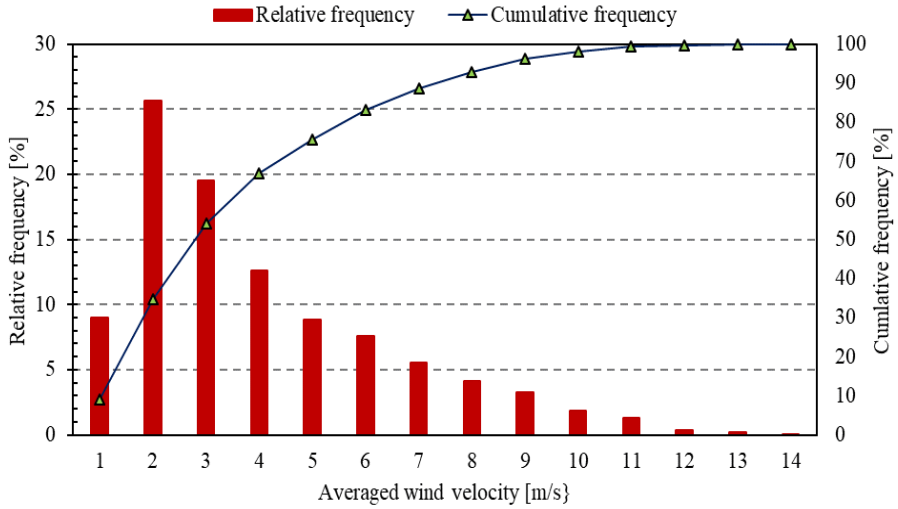

Figure 3.6. Frequency of outdoor wind velocity.

Moreover, the average outdoor weather conditions were similar among the tested cases, as shown in Table 3.2. The outdoor wind velocity ranged from 2.19 m/s to 3.87 m/s, while the average pressure difference was 1.16 Pa for all cases. The mean temperature difference was 3.37°C.

As a result, the temperature difference for all measurement cases was insignificant [6, 7]. This means that the thermal buoyancy effect was not dominant in this study; therefore, the effect of the temperature difference was excluded from the analysis.

Table 3.2. The average outdoor weather conditions.

Measurement	**Case 1**	**Case 2**	**Case 3**
Outdoor wind velocity	2.87	3.87	2.19
Temperature difference	3.50	2.76	3.87
Pressure difference	0.81	1.54	1.12

Figure 3.7 illustrates the wind direction recorded throughout the summer seasons, and Figure 3.8 demonstrates the frequency of seasonal wind direction. Although the predominant wind direction can be inferred, the actual wind direction exhibited constant fluctuations. Notably, there were no discernible patterns in the seasonal wind direction during the entire study period. The wind direction remained the maximum constant value only of 7.69 % at 10 min. This indicates that determining the impact of wind direction on naturally ventilated is challenging due to the continuous changes in wind direction, and therefore the wind direction in this study is excluded from the analysis.

Furthermore, the turbulence intensity which measures wind speed fluctuations is defined as the ratio of standard deviation of velocity fluctuations to mean wind velocity. Figure 3.9 presents the calculated turbulence intensity for different wind speeds based on an average outdoor wind velocity measured over a 5-minute period.

The results revealed that turbulence intensity was higher and the range of turbulence intensity was larger during low wind speed conditions, indicating increased variation in wind velocity during the summer. This implies that lower wind speed conditions in the summer experienced more variability in wind speeds, potentially leading to gusty or erratic wind patterns. Proper consideration of turbulence intensity in assessing outdoor wind conditions, especially during low wind speed conditions, is crucial for designing outdoor spaces and buildings to ensure optimal wind comfort and performance.

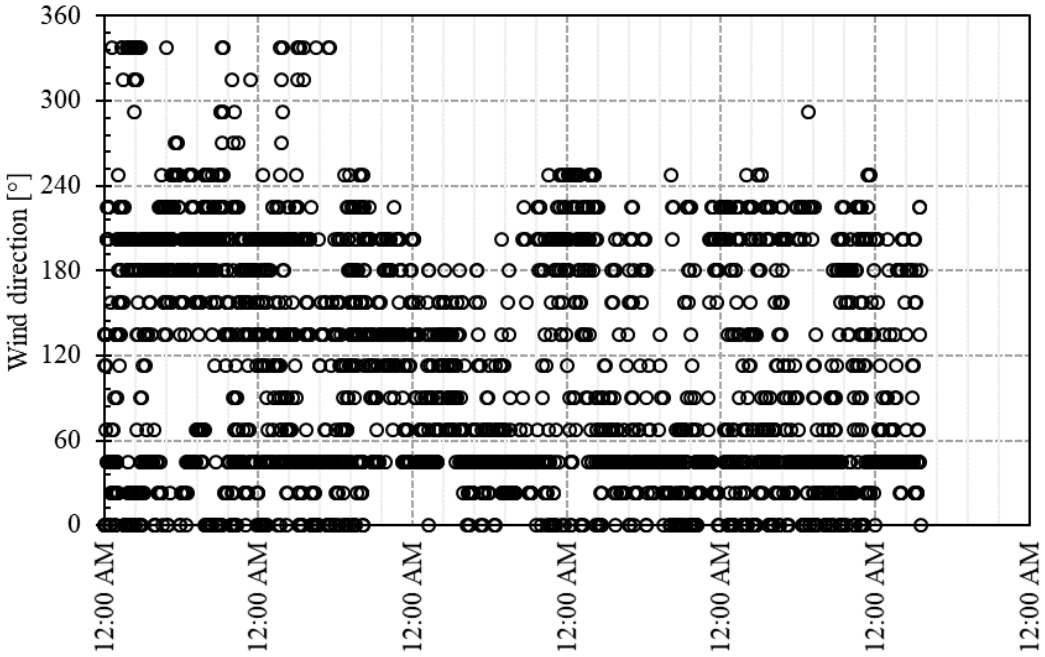

Figure 3.7. Seasonal wind direction changes.

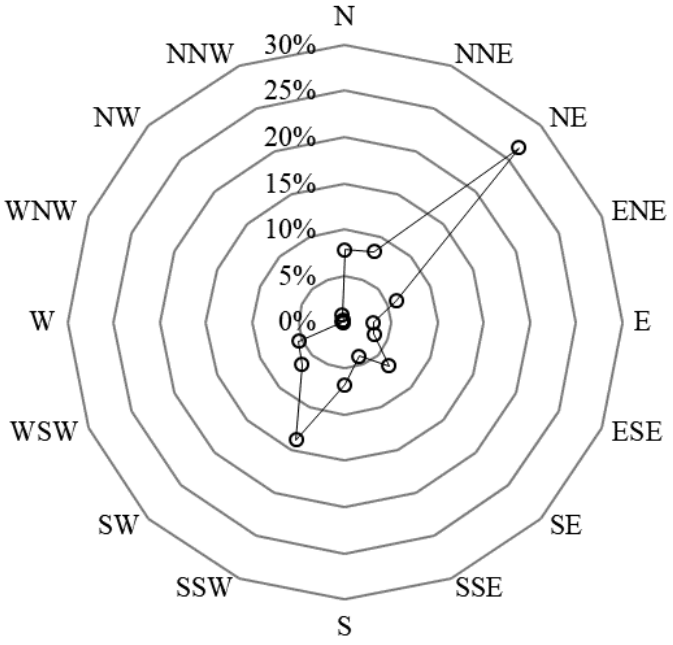

Figure 3.8. Frequency of seasonal wind direction.

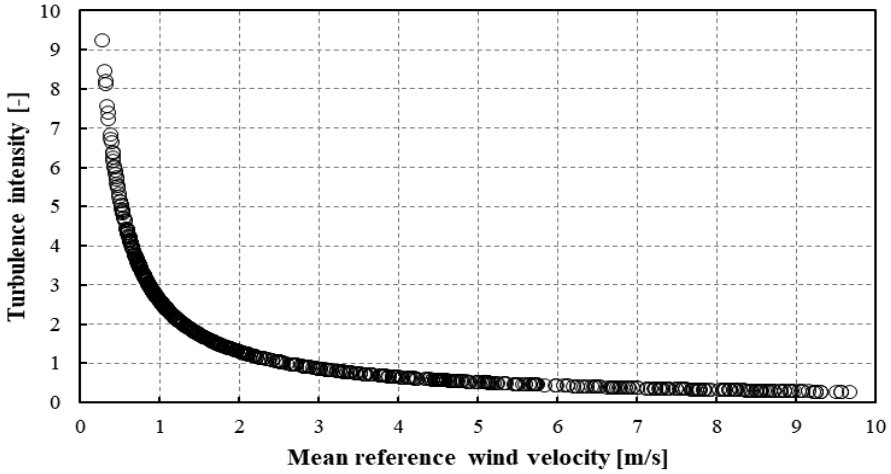

(a)

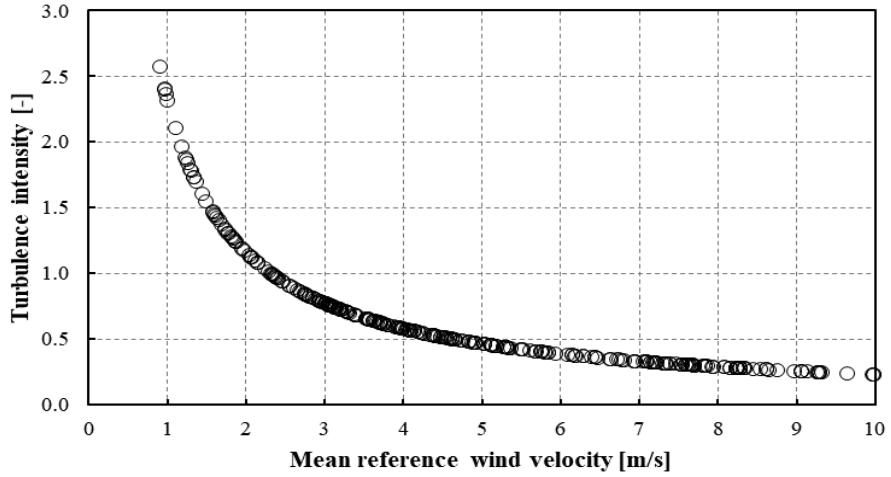

(b)

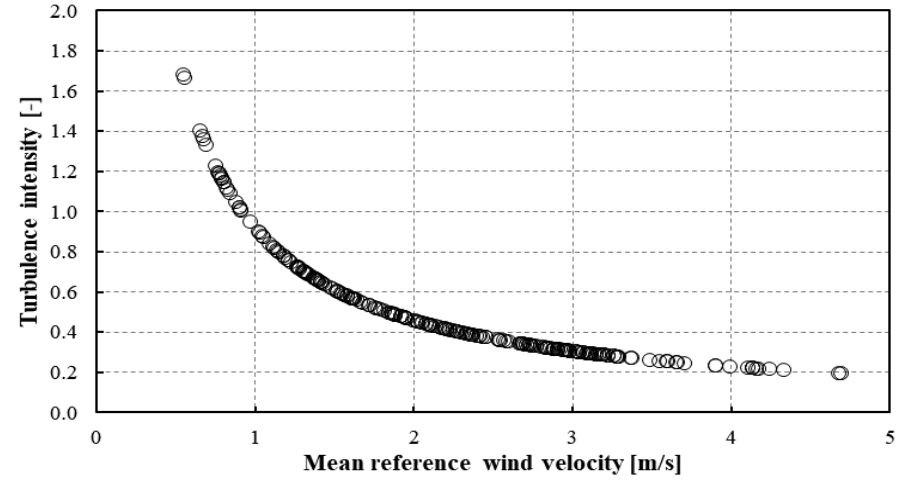

(c)

Figure 3.9. Turbulence intensity according to outdoor wind velocity; (a) case 1, (b) case 2, (c) case 3

3.2.2. Comparison of ventilation rate and velocity

Figures 3.10 demonstrate the ventilation rates quantified according to the outdoor wind velocity, inlet air velocity, and theoretical air velocity (V_{th}). The outdoor wind velocity and inlet air velocity were measured at the rooftop and center of the louvre openings, while the theoretical air velocity was calculated based on Eq (1.1) in chapter 1. The mean ventilation rate for all cases was 207.51 m^3/h, with maximum and minimum values of 701.85 m^3/h and 29.64 m^3/h, respectively. Despite the fluctuation of outdoor wind velocity among the cases tested, the results of this study show that the outdoor wind velocity was similar to the ventilation rate, inlet air velocity, and theoretical velocity. The study confirmed that the ventilation rate is affected by the velocities (outdoor wind velocity and inlet air velocity).

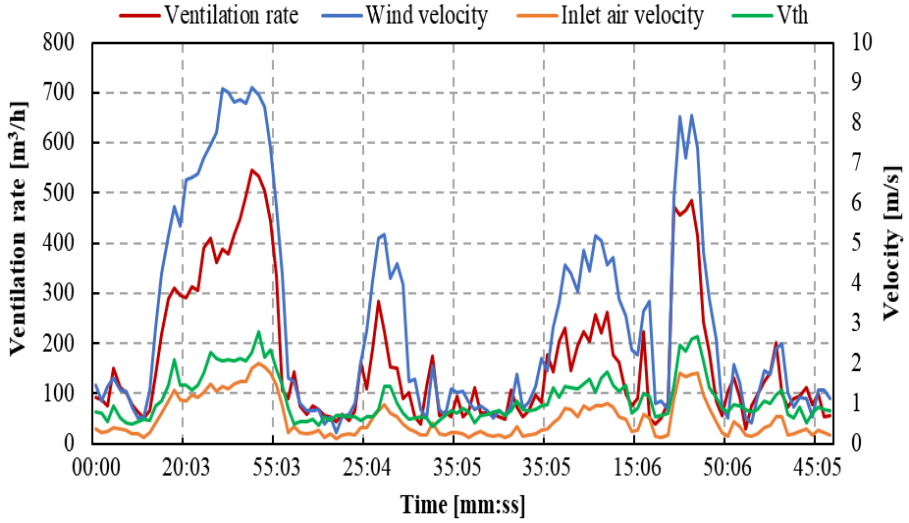

(a)

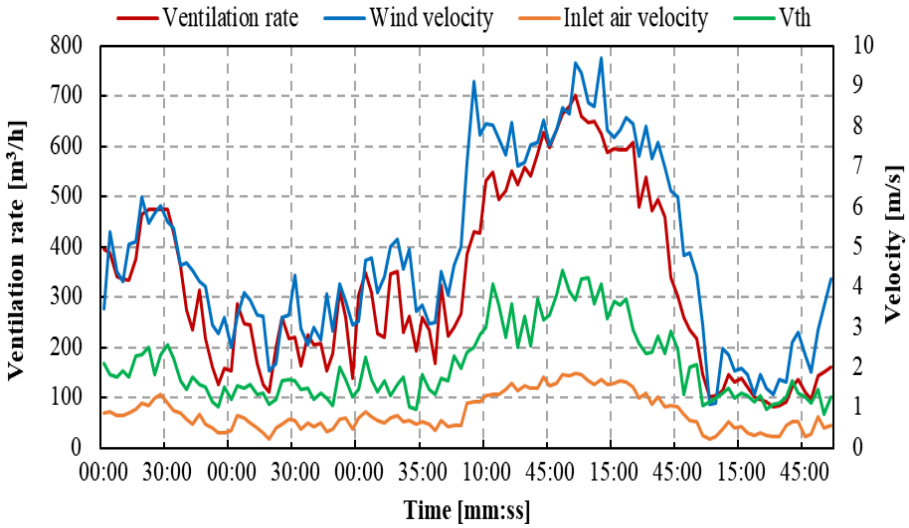

(b)

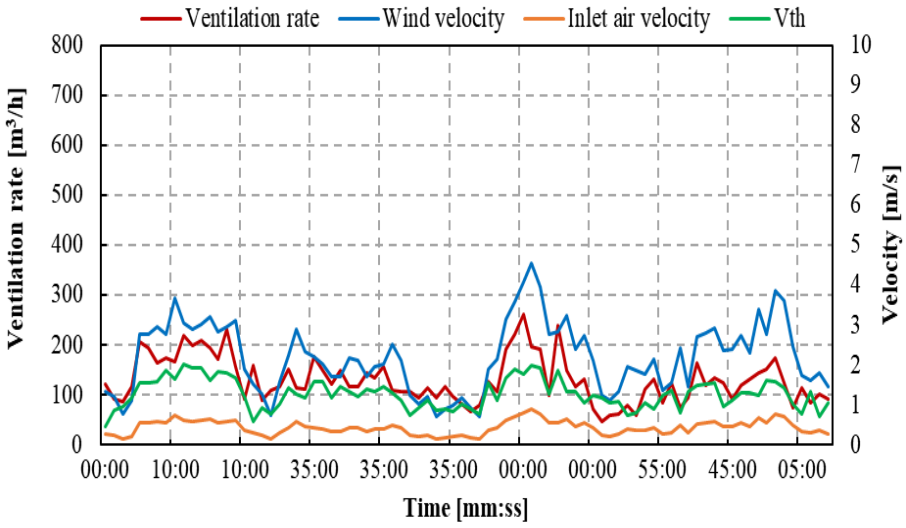

(c)

Figure 3.10. Comparison of velocity and ventilation rate: (a) case 1, (b) case 2, (c) case 3.

3.2.3. Relationship of ventilation rate, wind velocity, and pressure difference

Figures 3.11 - 3.13 present the relationship between ventilation rate, outdoor wind velocity, and pressure difference. According to outdoor wind velocity, the coefficient of determination (R^2) for all cases tested ranged from 0.35 to 0.84. Then, the correlation coefficient (R) was estimated to be between 0.59 and 0.92. This result means that the change in the outlet air velocity was significant concerning the change of ventilation rate in the louvre ventilation opening. A strong relationship between ventilation rate and outdoor wind velocity was observed.

Meanwhile, based on pressure difference, the coefficient of determination (R^2) and correlation coefficient (R) for all cases averaged to 0.50 and 0.70, respectively. This study reports that ventilation rate is mostly affected by outdoor wind velocity and pressure difference.

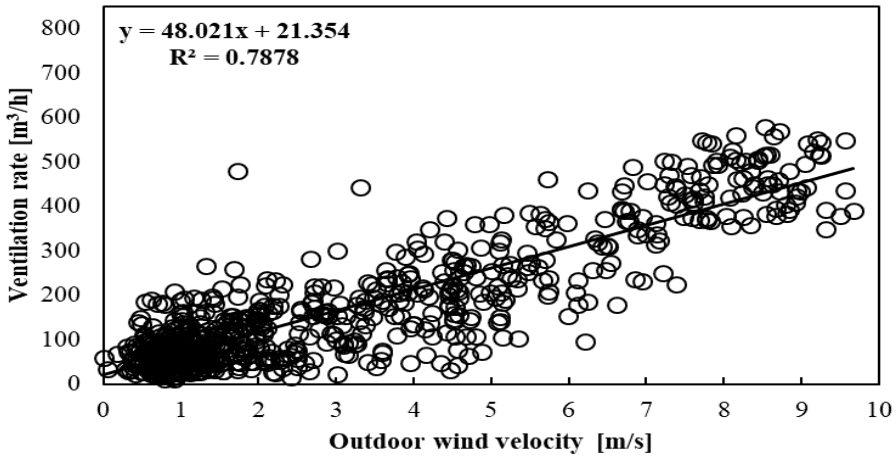

(a)

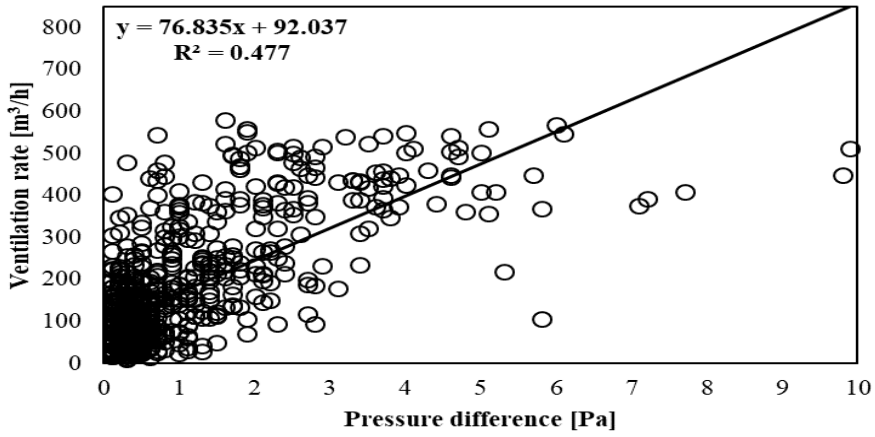

(b)

Figure 3.11. Relationship between ventilation rate and (a) outdoor wind velocity, (b) pressure difference for case 1

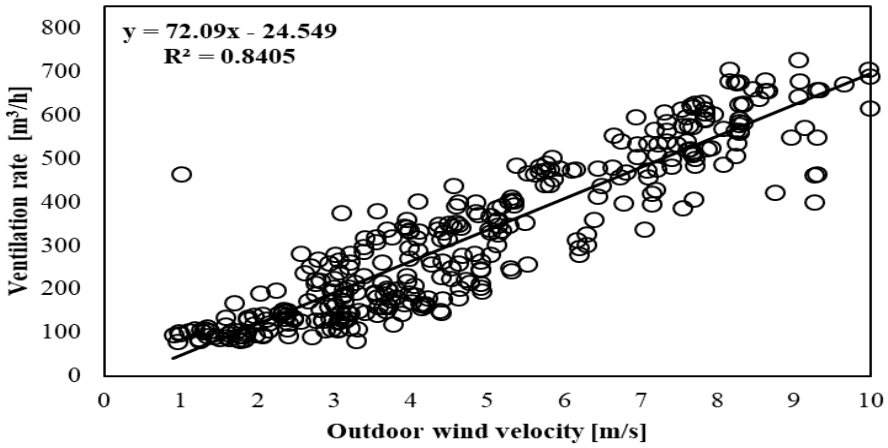

(a)

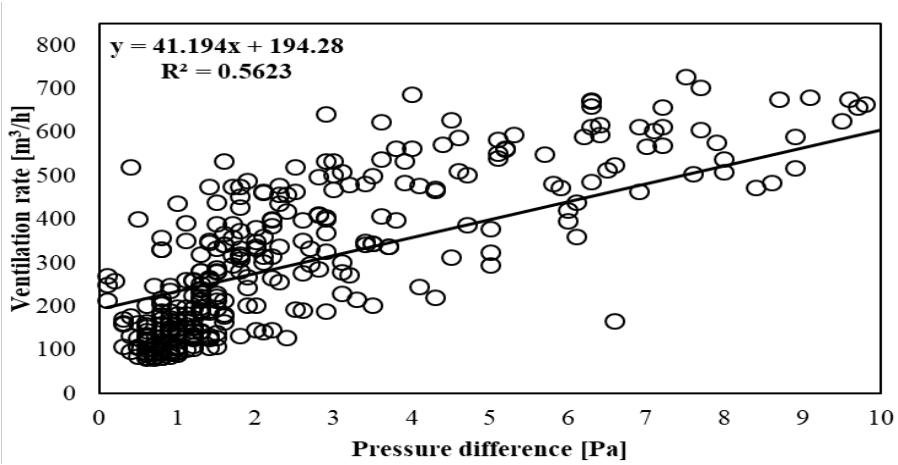

(b)

Figure 3.12. Relationship between ventilation rate and (a) outdoor wind velocity, (b) pressure difference for case 2

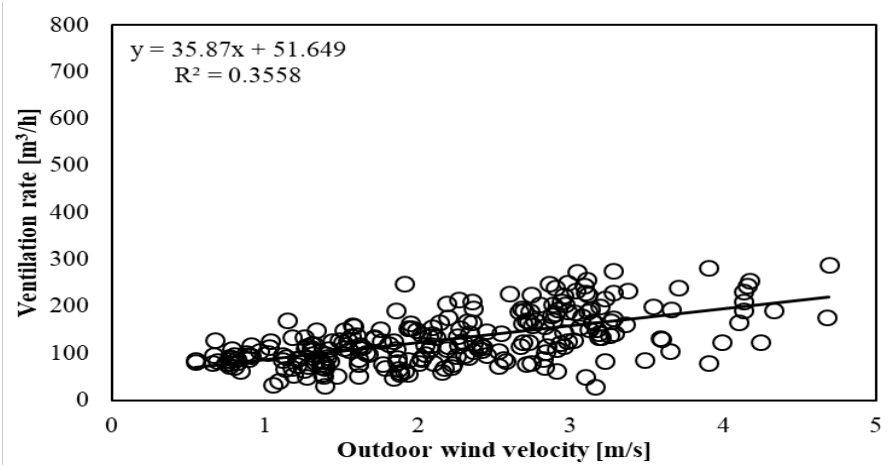

(a)

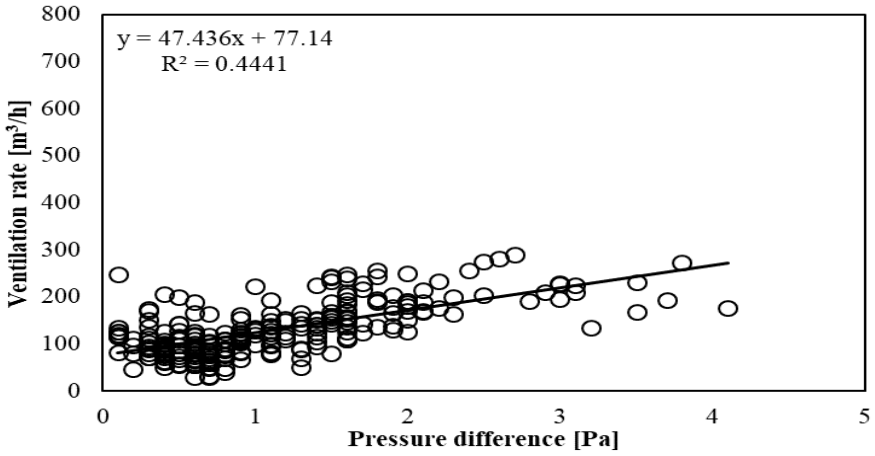

(b)

Figure 3.13. Relationship between ventilation rate and (a) outdoor wind velocity, (b) pressure difference for case 3.

3.2.4. Comparison of normalized ventilation rate against the outdoor wind velocity and pressure difference.

As discussed previously, the difference in the ventilation rate of the tested cases shows a significant concern owing to the unstable outdoor wind velocity. Therefore, a normalized ventilation rate (Q_N) was utilized to compare the ventilation rate for various external wind velocities and pressure differences among the examined case studies [8, 9]:

$$Q_N = \frac{Q}{A\,.\,Uref} \tag{3.2}$$

where Q_N is the normalized ventilation rate (−), Q is the ventilation rate (m^3/s), U_{ref} is the outdoor wind velocity (m/s), and A is the opening dimension of the louvre (m^2). The ventilation rate was transformed into Q (m^3/s) before normalization using Eq. (3.2).

Figure 3.14 shows a comparison of the normalized ventilation rate with outdoor wind velocity. The separation point of the normalized ventilation rate among the cases was clearly observed when the outdoor velocity was above 4 m/s. This means that a constant ventilation rate occurred at outdoor wind velocities above 2 m/s.

Even though the ventilation rate fluctuated when the outdoor wind velocity was low, the result mentions that Case 1 had the highest ventilation rate, followed by Cases 2 and 3. Interestingly, the results of this study confirmed that adding a sash with various angles to the louvre mainly affected the ventilation rate.

A comparison of the normalized ventilation rate with the pressure difference is shown in Figure 3.15. The normalized ventilation rate continued to change until the pressure difference was less than 1 Pa. Case 2 exhibited the highest ventilation rate at this stage. However, when the pressure difference was above 1 Pa, Case 1 was the highest, followed by Cases 2 and 3. This means that a stable value of the normalized ventilation rate occurred when the pressure difference was greater than 1 Pa. As a result, according to the pressure difference, installing a sash in the louvre opening also affected the normalized ventilation rate of the louvre openings.

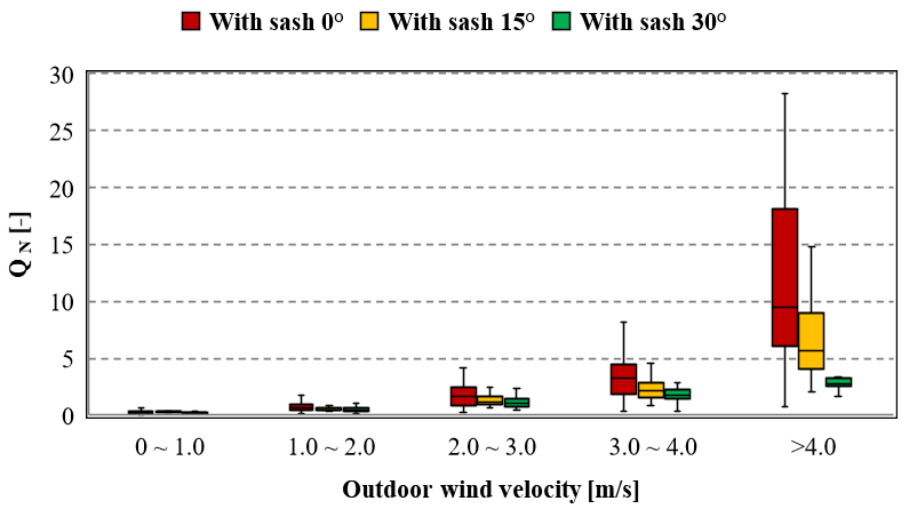

(a)

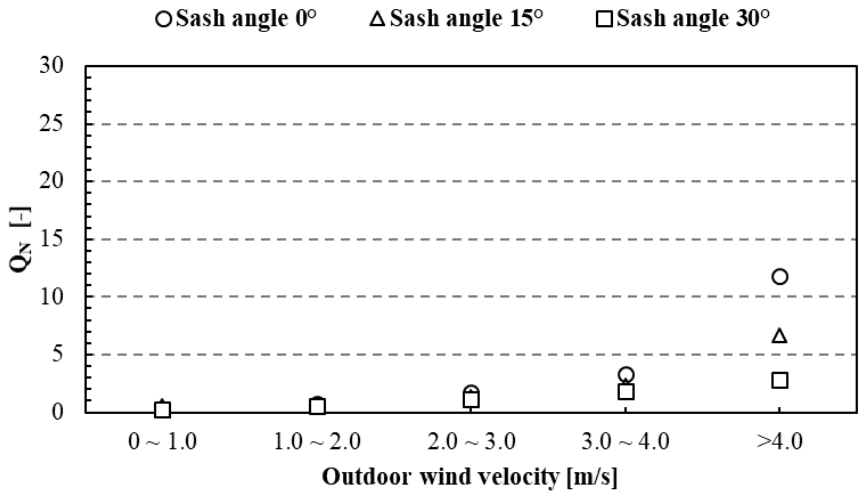

(b)

Figure 3.14. Comparison of normalized ventilation rates against outdoor wind velocity (a) box plot, (b) averaging value.

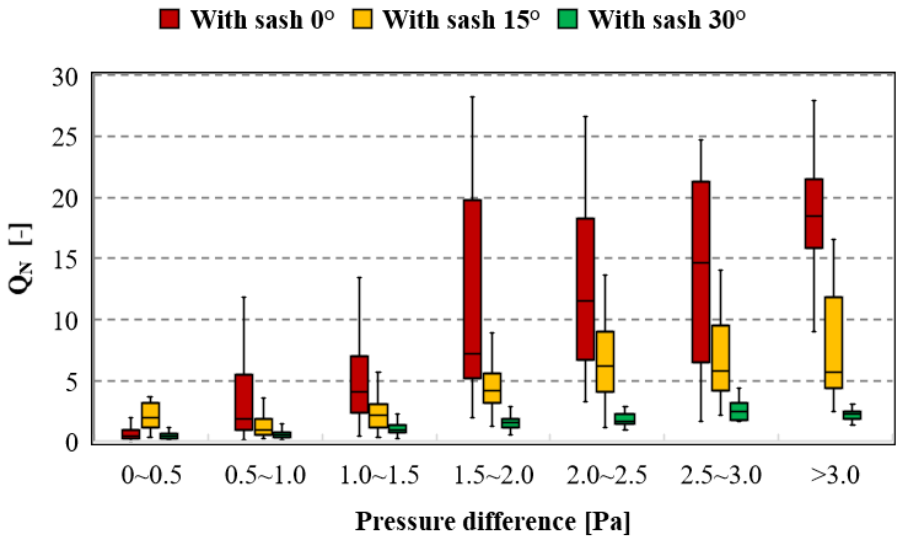

(a)

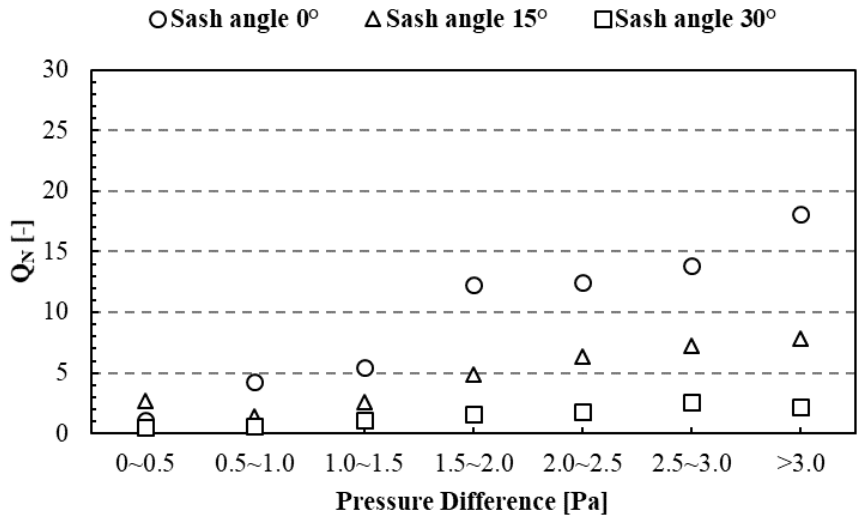

(b)

Figure 3.15. Comparison of normalized ventilation rates against pressure difference, (a) box plot, (b) averaging value.

3.2.5. The discharge coefficient

Figures 3.16 present the unsteady behavior of the discharge coefficient for the three cases and correspond to the inlet air velocity. The behavior of the discharge coefficient was calculated using Equation (1.3) as mention in chapter 1. Wind turbulence caused the unsteady behavior in the inlet air velocity and pressure difference.

Nevertheless, it has been proven that the turbulence patterns for the inlet air velocity and pressure difference are not identical because of the influence of wind on these quantities. Consequently, the calculated discharge coefficient also exhibited unsteady behavior instead of a constant one. The maximum and minimum values of discharge coefficients for case 1 were reported at 0.51 and 1.14, respectively. Interestingly, the discharge coefficient value tends to decrease with the addition of the sash angle of the louvre openings.

As a result, case 2, installed with a sash angle of 15° in the louvre, showed less discharge coefficient value than that of Case 1, with minimum and maximum at 0.27 and 1.23, respectively. In addition, the maximum and minimum discharge coefficient values for Case 3 with a sash angle of 30° were 0.26 and 0.57, respectively. Moreover, this result is similar to that of a previous study by Iqbal et al. [10] in which the discharge coefficient decreased with increasing sash opening angle in a fully formed turbulent flow of the central pivot roof window. Therefore, the standard discharge coefficient value for the louvre opening in this study was averaged to overcome the result.

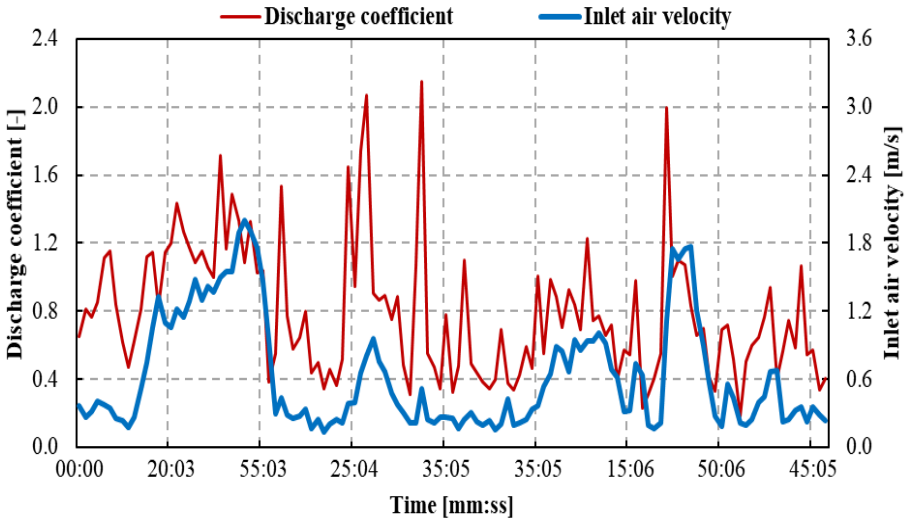
Discharge coefficient
Inlet air velocity
Discharge coefficient [-]
Inlet air velocity [m/s]
2.4
2.0
1.6
1.2
0.8
0.4
0.0
3.6
3.0
2.4
1.8
1.2
0.6
0.0
00:00
20:03
55:03
25:04
35:05
35:05
15:06
50:06
45:05
Time [mm:ss]

(a)

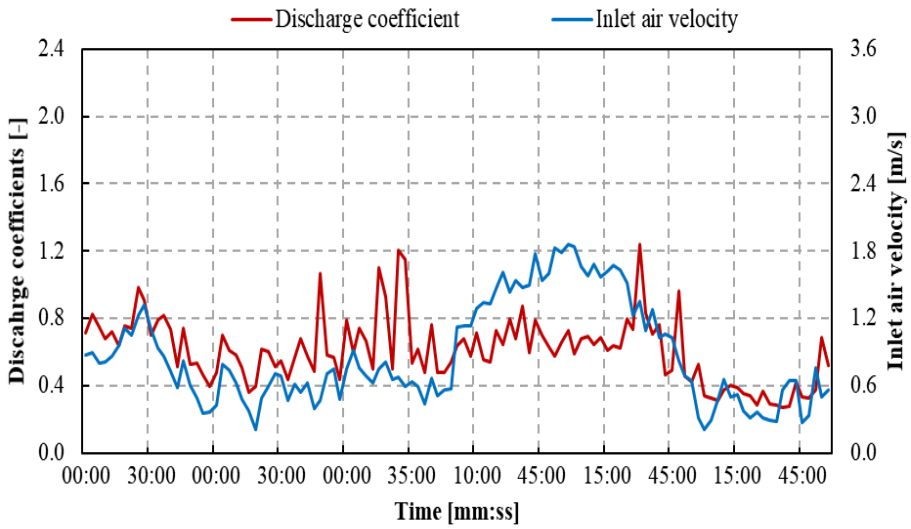
Discharge coefficient
Inlet air velocity
Discahrge coefficients [-]
Inlet air velocity [m/s]
2.4
2.0
1.6
1.2
0.8
0.4
0.0
3.6
3.0
2.4
1.8
1.2
0.6
0.0
00:00
30:00
00:00
30:00
00:00
35:00
10:00
45:00
15:00
45:00
15:00
45:00
Time [mm:ss]

(b)

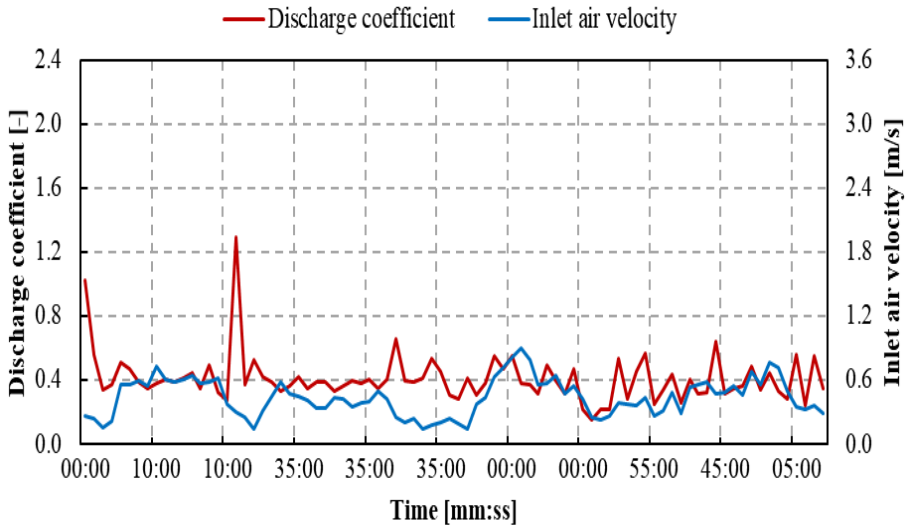

(c)

Figure 3.16. Discharge coefficients (a) case 1, (b) case 2, (c) case 3.

Furthermore, the discharge coefficient was evaluated based on outdoor wind velocity and pressure difference. Figure 3.17 and 3.18 present the ratio of the discharge coefficient among the cases tested based on the outdoor wind velocity and pressure difference. The discharge coefficient value continued to change according to the outdoor wind velocity, as shown in Figure 3.17. However, this study reveals that the discharge coefficient value is constant when the outdoor velocity reaches a stable and fixed position of the flow separation points at 2.5 m/s.

As a result, case 1 had the highest Cd value, followed by Cases 2 and 3. Meanwhile, according to the pressure difference, as shown in Figure 3.18, the discharge coefficient still fluctuated while the pressure difference value was below 1 Pa, where case 2 had the highest discharge coefficient, followed by cases 1 and 3. However, the discharge coefficient value is stable when the pressure difference is almost 1 Pa, with case 1 having the highest value, followed by cases 2 and 3. This result maintained a constant discharge coefficient until the pressure difference exceeded 3 Pa. In addition, the discharge coefficient decreased when the pressure difference was high. These findings are typical for natural ventilation measurements, owing to ordinary natural ventilation conditions.

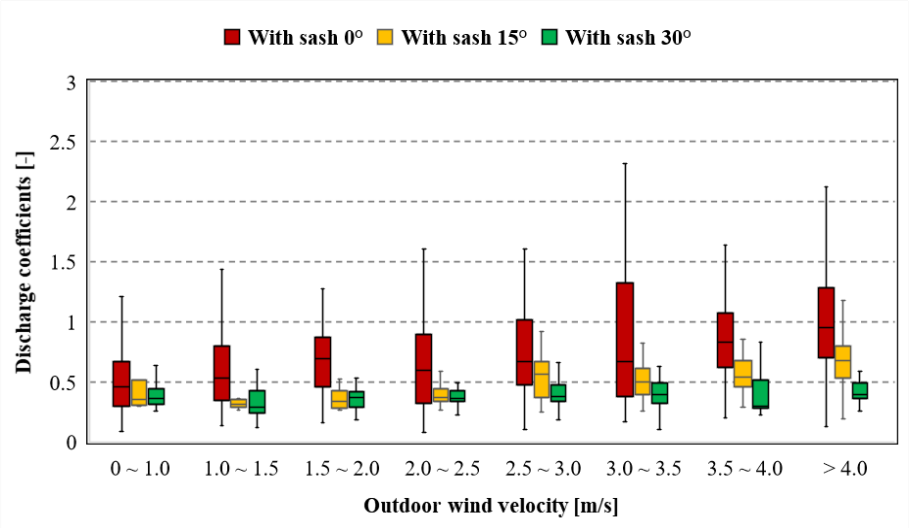

(a)

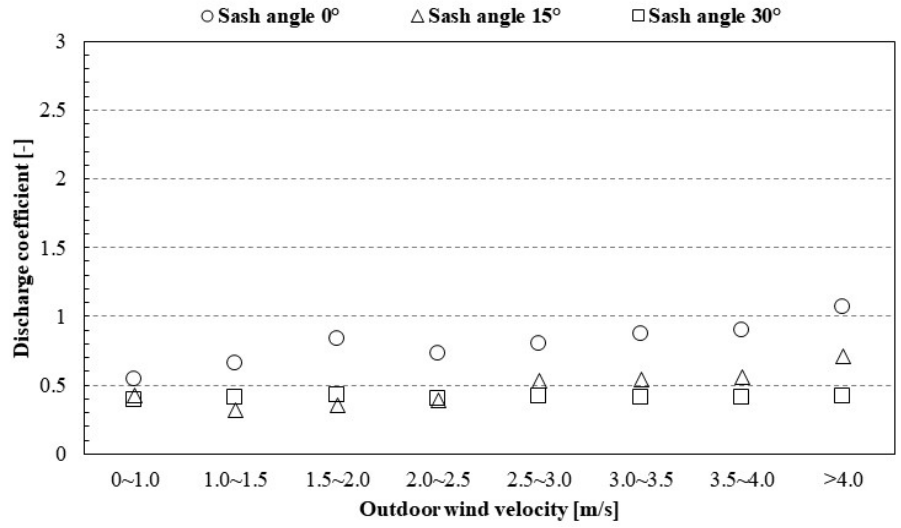

(b)

Figure 3.17. Ratio of discharge coefficient based on outdoor wind velocity, (a) box plot, (b) averaging value.

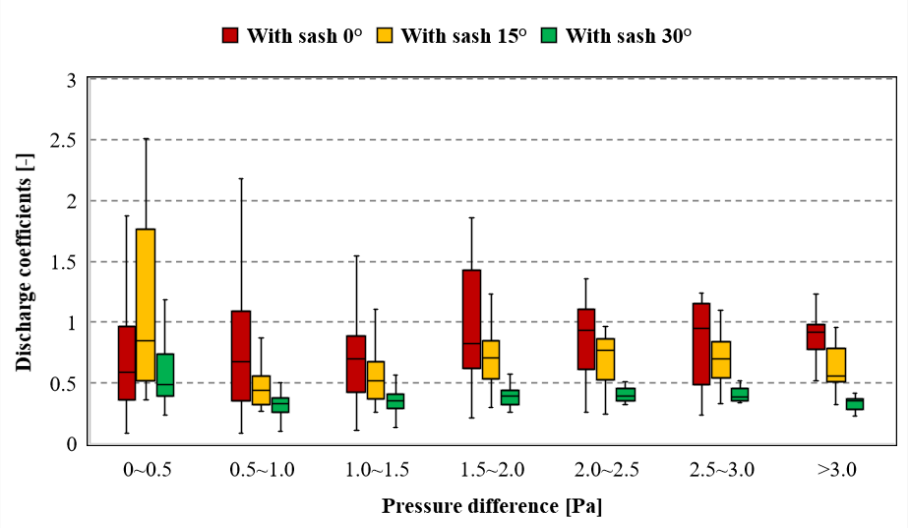

(a)

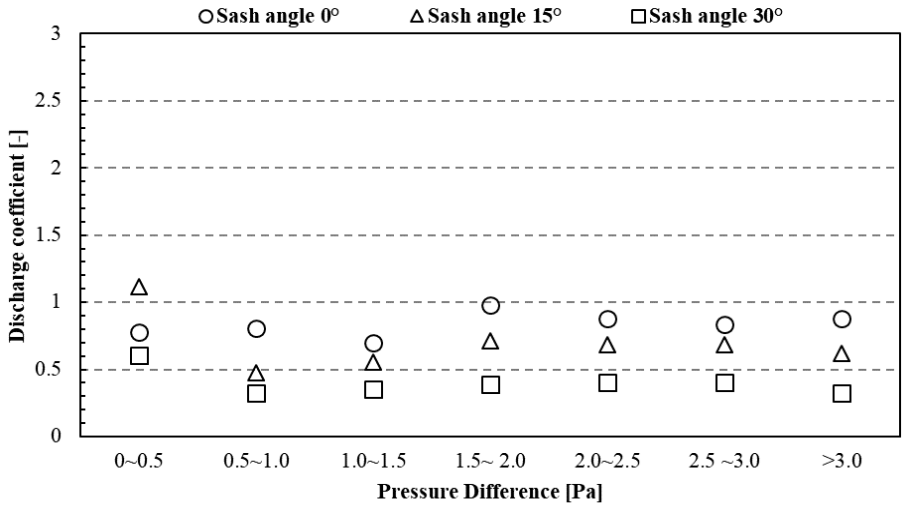

(b)

Figure 3.18. Ratio of discharge coefficient based on the pressure difference, (a) box plot, (b) averaging value.

By contrast, Heiselberg et al. [11] reported Cd reduction when the pressure difference increased, and an almost stable value was obtained when the pressure was above 10 Pa. It is evident that the pressure difference values were mainly below the threshold value of 10 Pa. The authors emphasize that pressure fluctuations of less than 10 Pa are common in the actual measurement of natural ventilation. Therefore, the discharge coefficient value observed in these experiments was considerable for naturally ventilated building settings. Furthermore, this study is significant for actual ventilation conditions, particularly louvre openings with a sash installed. As a result, we can conclude that the discharge coefficient value was average according to the outdoor wind velocity and the pressure

difference, where case 1 had the highest discharge coefficient value at 0.80, followed by Cases 2 and 3 at 0.62 and 0.41, respectively.

3.3. Wind Pressure Coefficients (Cp)

3.3.1. Calculation methods of wind pressure coefficients

The wind pressure coefficient, denoted as Cp, is a dimensionless parameter that represents the difference between the static pressure of the wind and the reference static pressure at a particular point on a structure or surface due to the action of wind. The wind pressure coefficient is commonly used in wind engineering to calculate wind loads on buildings, structures, or other surfaces. In addition, wind pressure coefficient describes the pressure distribution on the building surfaces. It is defined by the equation as shown below:

$$Cp = \frac{Px - Po}{Pd} \; ; \; \frac{\rho . Uref^2}{2} \tag{3.3}$$

where Px is the static pressure at a given point on the building facade (Pa), Po is the static reference pressure (Pa), Pd is the dynamic pressure (Pa), ρ is the air density (kg/m^3) and U_{ref} is the wind speed, which is often taken at building height h in the upstream undisturbed flow (m/s).

The value of the wind pressure coefficient depends on a wide range of parameters including building shape, envelope detailing, position on the façade, wind speed, wind direction, and turbulence intensity. Cóstola et al. [12] identify two main sources of Cp data. Primary sources including full-scale measurements, wind-tunnel measurements and Computational Fluid Dynamics (CFD) simulations, and secondary sources including databases and analytical models. In this chapter, the commercial code of CFD STAR-CCM+ is utilized to calculate wind pressure coefficients of the target building by including the surrounding environment condition, and target building (without surrounding environment) for comparison.

3.3.2. Overview of CFD

Computational Fluid Dynamics (CFD) is a numerical simulation technique used to study fluid flow and heat transfer. It involves solving a set of mathematical equations that describe the behavior of fluids, including the continuity equation, the equation of motion (e.g., Navier-Stokes equations), and the law of conservation of energy (e.g., energy equation or heat transfer equations).

The numerical analysis of CFD is roughly divided into finite difference method, finite element method, spectral method, and finite volume methods. Regarding to finite difference method, the governing equations are discretized using finite differences, which involve approximating the derivatives of the variables with respect to the spatial coordinates using difference quotients. Finite

difference methods are typically used on structured grids, where the computational domain is divided into a regular grid of points, and the equations are solved iteratively at these discrete grid points. Then, in the finite element method involves discretizing the governing equations using finite element basis functions, which are typically used to approximate the unknown variables within the computational domain. Finite element methods are well-suited for problems with irregular geometries and can handle complex boundary conditions. They are widely used in structural mechanics and solid-fluid interactions in CFD simulations.

Moreover, spectral methods involve approximating the unknown variables using a set of basis functions that are defined in the spectral domain, such as Fourier or Chebyshev basis functions. Spectral methods are known for their high accuracy and fast convergence rates, but they are typically used for problems with smooth solutions and regular geometries.

The finite volume method is a conservative approach where the governing equations are discretized over control volumes, which are typically defined as cells in a computational grid. The method involves computing fluxes across the faces of the control volumes to approximate the transport of the variables across the grid. Finite volume methods are widely used in CFD simulations due to their ability to accurately capture shocks, discontinuities, and other complex flow features. In addition, the finite volume method subdivides the computational domain into a finite number of minute volume spaces and considers the balance of each physical quantity in each minute space. The balance of the physical quantity is discretized and expressed by integrating the fundamental equation in each control volume. An unknown quantity is defined at the center of each control volume, and based on that value, the inflow and outflow of physical quantities at the boundaries of each control volume are calculated, and a solution is obtained by calculation using a discretization formula. Therefore, this research utilize the finite volume methods to calculated wind pressure coefficients of target building.

3.3.3. Input conditions for inflow wind speed

In CFD simulation setting up, specifying the inflow conditions at the boundary is crucial for accurately capturing the behavior of fluid flow. The wind conditions in the target area play a significant role in determining the appropriate inflow condition.

3.3.3.1. Nature of the wind

The characteristics of wind near the Earth's surface are affected by objects on the ground. The average wind speed near the ground surface tends to decrease or increase as it ascends vertically. This change in wind speed is influenced by the characteristics of the ground surface. The following formula provides the average wind speed at a specific height, denoted as Uz:

$$U(z) = U_s(\frac{Z}{Z_s})^{\alpha} \tag{3.4}$$

where Uz represents the average wind speed at ground level Z [m/s], and Us, which represents the average wind speed at reference ground height Zs [m/s]. The power exponent α, included in the equation, is influenced by the roughness of the ground surface near the ground level and increases in value as the ground surface becomes rougher. According to the Building Load Guidelines of the Architectural Institute of Japan [13], this value indicates the relationship between the condition of the ground surface and the power index based on observations of natural wind and ground surface roughness, as listed in Table 3.3. The situation of the ground surface and windward area is shown in Table 3.4.

Table 3.3. Ground roughness classification

Ground surface roughness classification	I	II	III	IV	V
Zg (sky wind altitude)	250	350	450	550	650
A	0.1	0.15	0.2	0.27	0.35

Table 3.4. Ground surface and windward area

Ground surface roughness classification	Situation of the ground surface of the construction site and the windward area
I	Area with almost no obstacles
II	Areas with obstacles like crops, such as countryside and grasslands, area where trees and low-rise buildings are scattered
III	Areas with many trees and low-rise buildings, areas with scattered middle-rise buildings
IV	Area where medium-rise buildings are the main
V	Urban area where high-rise buildings are densely packed

Moreover, the turbulence energy, which is the turbulence intensity of the fluid flow, is expressed by the following equation (3.5) from the wind speed and turbulence intensity (3.6).

$$I(z) = 0.1(\frac{Z}{Z_g})^{(-\alpha-0.05)} \tag{3.5}$$

$$k(z) = (I(z)U(z))^2 \tag{3.6}$$

where Iz is the turbulence strength at ground level Z. The dissipation factor, which indicates the speed at which turbulence disappears, is expressed by the following equation:

$$\varepsilon(z) = C_{\mu}{}^{1/2} k(z) \frac{U_s}{Z_s} \alpha \left(\frac{Z}{Z_s}\right)^{(\alpha-1)} \quad (3.7)$$

where Cμ is an eddy viscosity (common value of 0.09).

3.3.3.2. Wind properties of target area

The author used data from the AMeDAS Maehara Meteorological Observatory, located in Maehara Nishi, Itoshima City, Fukuoka Prefecture, as the study area is situated in Nishi Ward, Fukuoka City, Fukuoka Prefecture. The wind properties of the target area, such as average, maximum wind speed and wind direction, were assessed and presented in Table 3.5. The average wind speed over a 20-year period (2000-2020) was determined to be 2 m/s for all seasons, and this value was used as the input condition for Computational Fluid Dynamics (CFD) simulations.

Table 3.5. Monthly wind speed data for 20 years

Month	Average wind speed	Maximum wind speed	Wind direction
January	2.14	8.68	WNW
February	2.16	9.02	NE
March	2.3	9.87	NNW
April	2.22	9.64	NNW
May	2	8.55	NNW
June	1.93	8.58	NNW
July	2.01	8.85	SW
August	1.88	9.47	NNW
September	1.89	9.85	NNW
October	1.9	9.68	NNW
November	1.75	8.11	NW
December	2.05	8.8	WNW

Therefore, the inflow boundary condition for numerical simulation of wind pressure coefficients, including inflow wind speed, turbulence energy dissipation rate, and turbulence energy were calculated according to equation 3.5 – 3.7. Figure 3.19 present the input condition including inflow wind speed, turbulenece energy dissipation rate, and turbulence energy.

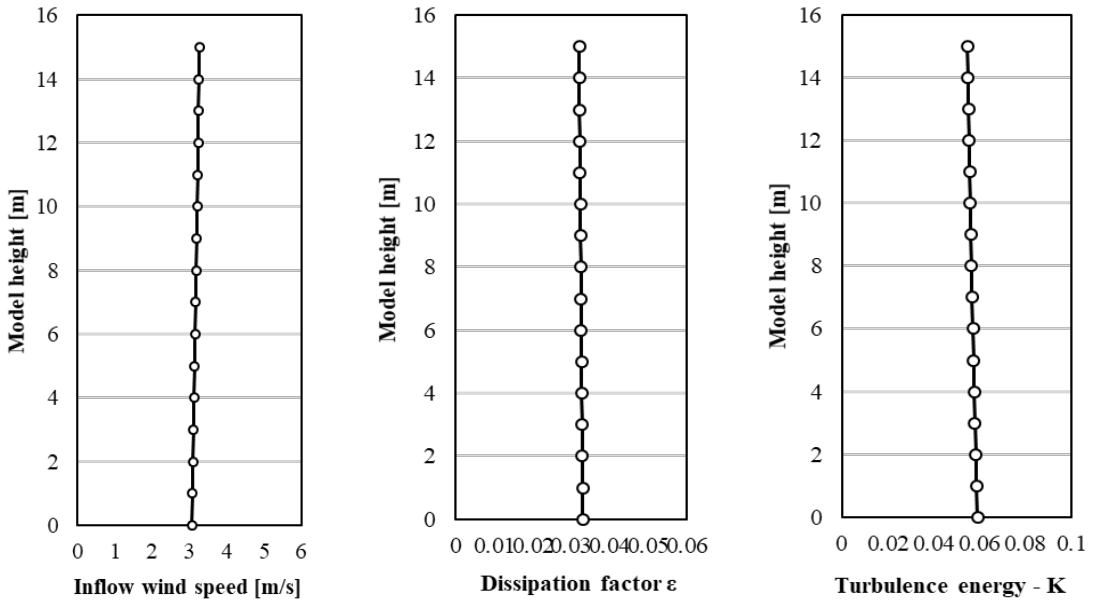

Figure 3.19. Input condition (a) inflow wind speed, (b) turbulence energy dissipation rate, (c) turbulence energy.

3.3.4. Analysis conditions

3.3.4.1. Analysis wind pressure coefficients including surrounding environment

The analysis condition of calculated wind pressure coefficients for louver openings with including surrounding environment is shown in Table 3.6, and the analysis domain is illustrated in Figure 3.20. The simulation utilize simplified model (512m × 512m × 170m) within the number of meshes of 6.220.164, and turbulence model is realizable k-ε model. In addition, the surrounding environment of target building is also included in this simulation.

Moreover, the wind pressure coefficient was calculated by considering wind inflow from 16 directions with reference to the north. The reference wind speed was assumed to be infinite, unaffected by the presence of the building, and measured at the same height as the meteorological station installed on the roof of the building of interest.

Table 3.6. Analysis conditions including surrounding environement

Content	Detail
Analysis software	STAR-CCM+
Analysis domain	512m(x)×512m(y)×170m(z)
Number of meshes	6,220,164.00
Inflow boundary condition	1/5 power law
Outflow boundary condition	Gradient 0 at outflow boundary
Speed reference point	Maebaru Meteorological Observatory
	Air/Side Boundary Conditions: Slip
Wall conditions	Floor surface: wall boundary condition based on wall function
	Target building: wall boundary condition based on wall function
Calculation algorithm	SIMPLE method
Turbulence model	Realizable k-ε model

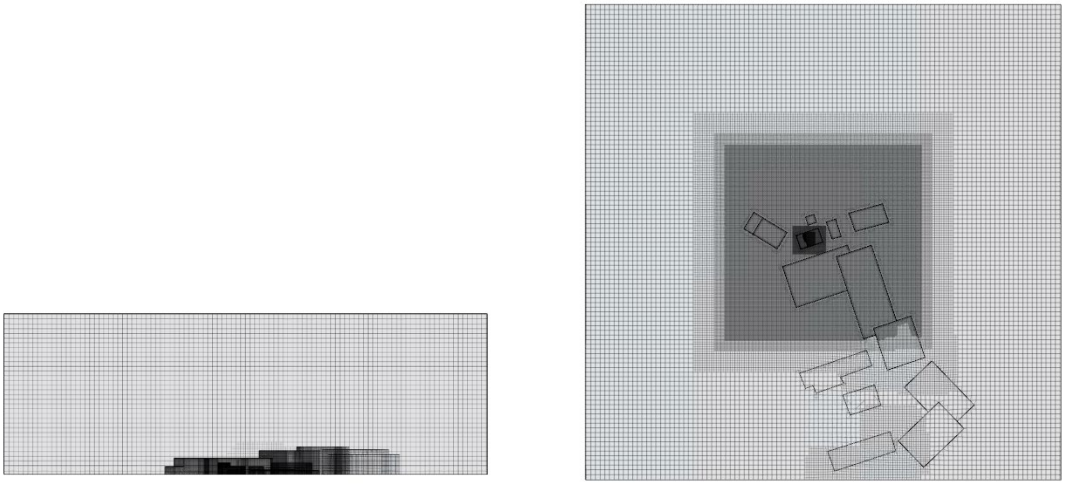

Figure 3.20. Analysis domain.

3.3.4.2. Analysis wind pressure coefficients of building without surrounding environement

This research also examined the case where the surrounding environment was excluded. Table 3.7 shows CFD calculation conditions and Figure 3.21 present the analysis domain for calculated wind pressure coefficients of target building. Based on the height of the building, the side boundary and the sky boundary were 5 times the standard, and the outflow boundary was 10 times the standard. In order to obtain the wind pressure coefficient in 16 directions, the analysis area was not changed, and the analysis was performed by changing the building angle. The reference wind speed was set at infinity,

where the building does not affect it, and at the same height as the meteorological station installed on the roof of the target building.

Table 3.7. Analysis conditions for target building only

Content	Detail
Analysis software	STAR-CCM+
Analysis domain	512m(x)×512m(y)×170m(z)
Number of meshes	6,220,164.00
Inflow boundary condition	1/5 power law
Outflow boundary condition	Gradient 0 at outflow boundary
Speed reference point	Maebaru Meteorological Observatory
	Air/Side Boundary Conditions: Slip
Wall conditions	Floor surface: wall boundary condition based on wall function
	Target building: wall boundary condition based on wall function
Calculation algorithm	SIMPLE method
Turbulence model	Realizable k-ε model

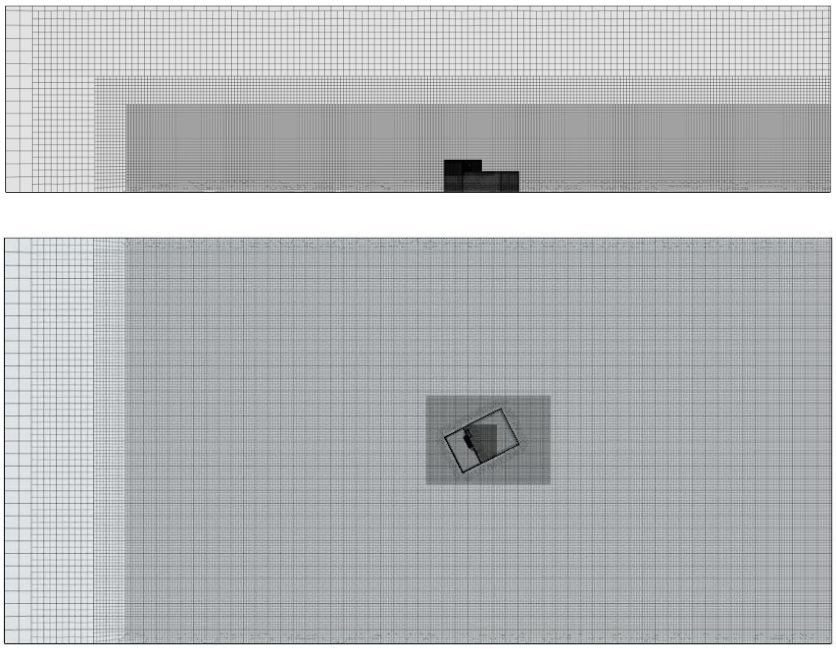

Figure 3.21. Analysis domain.

3.3.5. Result and discussion

The wind pressure coefficients of the target building, taking into account the surrounding environment, were computed and evaluated as depicted in Figure 3.22. The findings indicate that the wind pressure coefficient varies depending on the wind direction and is influenced by the nearby buildings and the shape of the surroundings around the opening. The simulation's accuracy is generally considered acceptable, although there is a possibility that the distance between the building and the boundary is not adequately considered near the inflow/outflow boundary in the calculation area. As a result, the wind pressure coefficients calculated by CFD are used as input data in the numerical simulation software THERB for HAM with NAF, which handles room data.

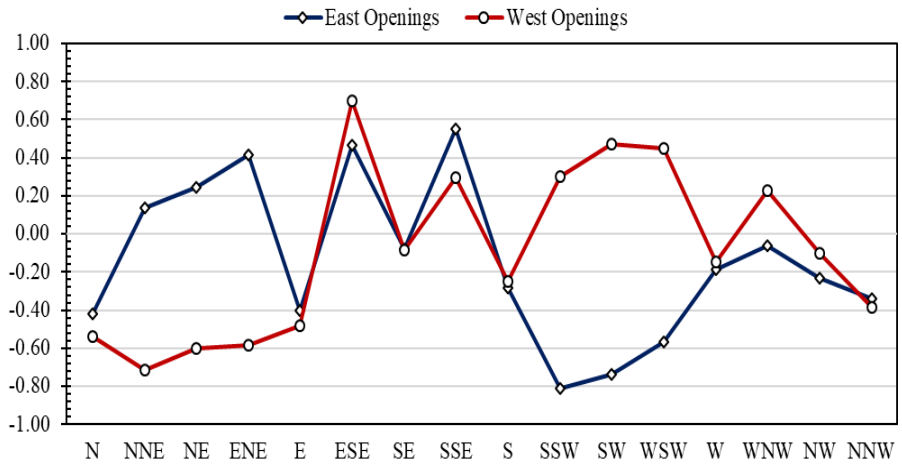

Figure 3.22. Wind pressure coefficients with including surrounding environment.

Furthermore, the wind pressure coefficients for the target building (isolated from the surrounding environment) exhibit variations. Figure 3.23 illustrates the wind pressure coefficient solely for the target building. Since it is not influenced by nearby buildings, it is possible to discern the relationship between the wind direction and high or weak wind pressure coefficients more clearly.

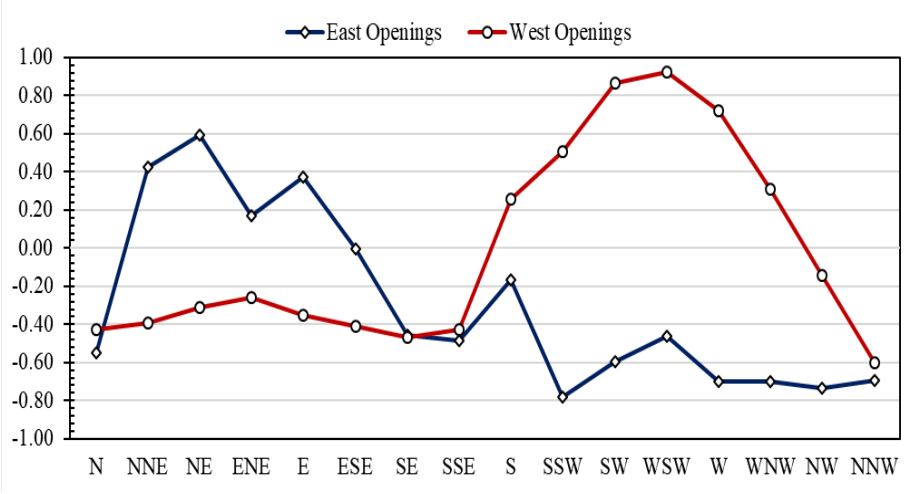

Figure 3.23. Wind pressure coefficients of target building.

3.4. Simulation accuracy verification

3.4.1. Overview of numerical simulation THERB for HAM

In many cases, simulation software designed to predict temperature, humidity, and heating/cooling loads of building spaces typically overlooks the moisture transfer that occurs in wall assemblies. The humidity calculation in most software tends to be influenced only by ventilation and primarily focuses on building spaces. However, THERB was specifically developed to provide detailed simulation of humidity conditions not only in building spaces but also in wall assemblies. It considers the moisture transfer that occurs within walls, offering a more comprehensive and accurate representation of the hygrothermal environment within buildings.

In addition, THERB incorporates detailed thermal theories related to conduction, convection, radiation, and ventilation, considering the complex phenomena associated with heat and moisture transfer. One progressive feature of THERB is the P-model, which utilizes the concept of water potential as a measure of thermodynamic energy. This model allows for the prediction of moisture transfer, including moisture sorption and desorption, within walls. As a result, THERB is capable of predicting the hygrothermal environment of entire buildings, considering the intricate relationship between heat and moisture transfer, as well as airflow. The detailed calculation method will be described later in the Appendix of this dissertation.

Therefore, this research calculates the indoor environmental condition using a dynamic simulation program called THERB [14]. This program is one of the official software approved by the Japanese government and is applied nationwide in Japan. It can calculate the time series of indoor temperatures, humidity, and heating/cooling loads for the whole building, considering the complete heat, air, and moisture (HAM) features with the network airflow model (NAF). The network airflow model is based on the equations of continuity, aperture, and crevice flow equations as follows:

$$\sum_{i=1}^{I} Q_i = 0 \tag{3.8}$$

$$Q_i = Cd_i A_i \sqrt{\frac{2g}{\gamma}|\Delta p_i|} \equiv 4Cd_i A_i \sqrt{|\Delta p_i|} \tag{3.9}$$

$$Q_i = a_i l_i \Delta p_i^{1/n} \tag{3.10}$$

where Q represents of air flow rate [m^3], A is an opening area [m^2], α: gap characteristic value [-], g: gravitational acceleration [=9.8m/s^2], l: gap length [m], ΔP: pressure difference [Pa], Cd: Discharge coefficient [-], γ: specific weight of air [kg/m^3], n = 1.5 (constant between 1 and 2). In addition, for an independent ventilation layer, the dimensionless flow rate is derived as a function of the dimensionless length of the ventilation layer. The modified Rayleigh number from the dimensionless energy equation, the equation of motion, continuity, and the actual ventilation rate, is also predicted.

A calculation model that finds the air volume by capturing the complex flow of ventilation air as a ventilation network, similar to an electric circuit as shown in Figure 3.24. The current, voltage, and resistance of the electric circuit correspond to the air volume, pressure difference, and flow resistance of the ventilation network.

The network airflow model, as explained, combines a thermal model and a plant model to calculate natural and forced ventilation quantities for individual zones in a building as shown in Figure 3.25. It takes into consideration factors such as air leakage, infiltration, and mechanical ventilation. The model also incorporates hydrodynamic analysis to estimate airflow in independent ventilated cavities within walls. Furthermore, the model permits the setting of constant ventilation quantities for all zones on an hourly basis. Overall, this comprehensive approach to estimating ventilation quantities in buildings is noteworthy, but it is crucial to validate its accuracy through real-world measurements and testing.

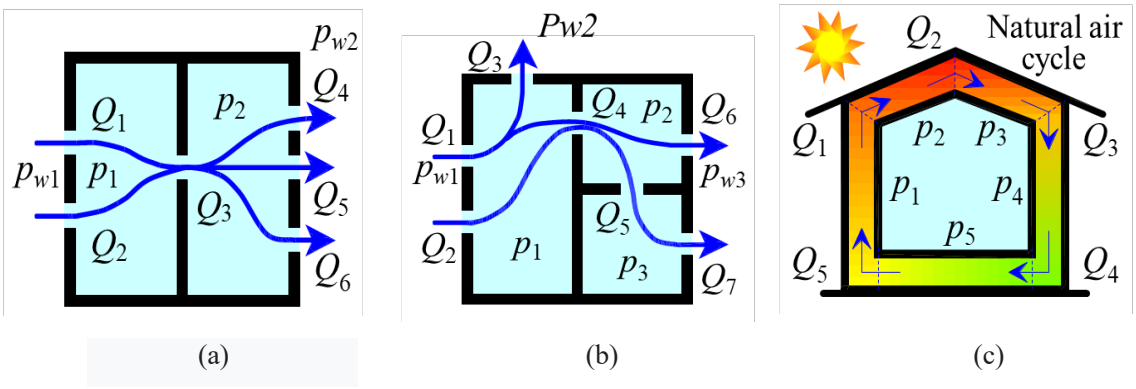

Figure 3.24. Circuit model, (a) calculated by combining resistance, (b) calculated by repeat calculation, and (c) natural air cycle

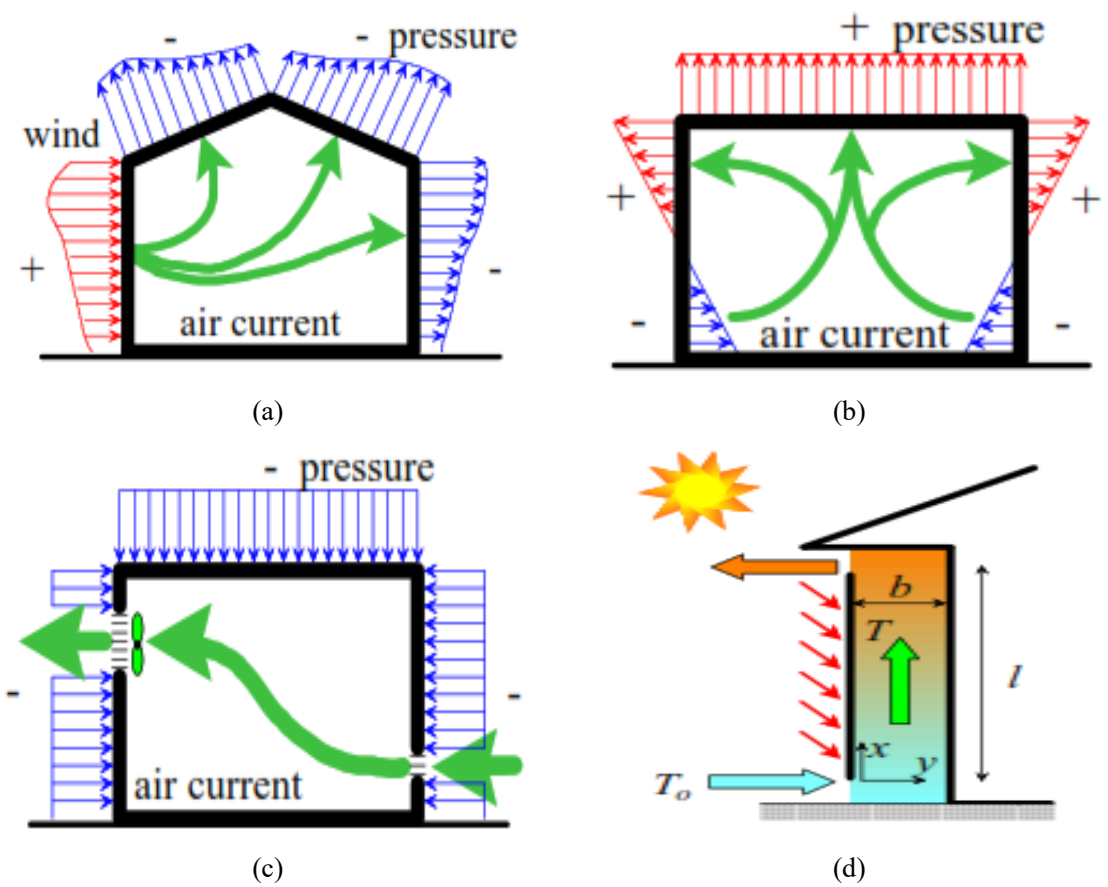

Figure 3.25. Mechanical or natural ventilation, (a) wind force ventilation, (b) buoyant ventilation, (c) mechanical ventilation, (d) cavity ventilation

3.4.2. Calculation conditions

The target building was the third floor of the environmental building of Kyushu University as mentioned previously. The calculation condition is demonstrated in Table 3.8. The calculation periods are referring to measurement periods during the summer. By considering the heat accumulation due to reinforced concrete of target building, the preliminary calculation was performed for more than 5 days with the time interval of 60 seconds. The weather data measured by AMeDAS meteorological station were used for temperature, relative humidity and solar radiation. In addition, the wind direction and wind velocity were employed the measured data at roof top of experimental building. This simulation requires the value of discharge coefficients and wind pressure coefficients for ventilation circuit network calculation. Therefore, the value of discharge coefficients and wind pressure coefficients are derived from experimental data analysis and CFD simulation result as previously mention.

Moreover, the wall configuration of target building is including outer wall, inner wall, floor/ceiling, roof glass, and ceiling as shown in Table 3.9. The summary of wind pressure coefficients for two openings on the target building with include environment and without environment are illustrated in Table 3.10 and Table 3.11. In addition, the summary of wind pressure coefficients from references is listed in Table 3.12. Based on the result of previous chapter, the discharge coefficients value for the cases tested is listed in Table 3.13.

Table 3.8. calculation conditions

Item	Parameters	Conditions
Basic conditions	Calculation periods	Refers to measured time
	Preliminary calculation	More than 5 days
	Calculation time interval	60 seconds
Target building	Location	Kyushu University (Ito Campus), Fukuoka City, Japan
	Type of construction	Reinforced concrete building
	Target room	Third floor
Input conditions	Temperature	AMeDAS Weather Data (Fukuoka)
	Relative humidity	AMeDAS Weather Data (Fukuoka)
	Solar radiation	AMeDAS Weather Data (Fukuoka)
	Wind direction	Measured on roof top of target building
	Wind velocity	Measured on roof top of target building
	Discharge coefficients	Experiment data
	Wind pressure coefficients	CFD

Table 3.9. Wall configurations

Element	Specifications	Thickness (mm)
Outer wall	Tile	20
	Air layer	120
	Polyurethane foam	30
	Concrete	150
	Sprayed tile (sand limestone)	2
Inner wall	Sprayed tile (sand limestone)	2
	Concrete	120
	Sprayed tile (sand limestone)	2
Floor/Ceiling	Extruded polystyrene foam insulation	30
	Concrete	180
Roof	Protective concrete	80
	Insulation sheet (vinyl cloth)	
	Extruded polystyrene foam insulation	30
	Concrete	130
	Air layer	50
Glass	Low-e glass	20
Ceiling pit	Extruded polystyrene foam insulation	25
	Gypsum board	10

Table 3.10. Wind pressure coefficients with surrounding environment

(a) East openings

NNE	**NE**	**ENE**	**E**	**ESE**	**SE**	**SSE**	**S**
0.14	0.24	0.42	-0.40	0.47	-0.08	0.55	-0.28
SSW	**SW**	**WSW**	**W**	**WNW**	**NW**	**NNW**	**N**
-0.81	-0.74	-0.57	-0.19	-0.06	-0.23	-0.34	-0.42

(b) West openings

NNE	**NE**	**ENE**	**E**	**ESE**	**SE**	**SSE**	**S**
-0.71	-0.60	-0.58	-0.48	0.70	-0.08	0.30	-0.25
SSW	**SW**	**WSW**	**W**	**WNW**	**NW**	**NNW**	**N**
0.30	0.47	0.45	-0.15	0.23	-0.10	-0.39	-0.54

Table 3.11. Wind pressure coefficients of target building only

(a) East openings

NNE	NE	ENE	E	ESE	SE	SSE	S
0.43	0.59	0.17	0.38	0.00	-0.46	-0.48	-0.17
SSW	**SW**	**WSW**	**W**	**WNW**	**NW**	**NNW**	**N**
-0.78	-0.60	-0.46	-0.70	-0.70	-0.73	-0.69	-0.55

(b) West openings

NNE	NE	ENE	E	ESE	SE	SSE	S
-0.39	-0.31	-0.26	-0.35	-0.41	-0.47	-0.42	0.26
SSW	**SW**	**WSW**	**W**	**WNW**	**NW**	**NNW**	**N**
0.51	0.87	0.93	0.72	0.31	-0.14	-0.60	-0.43

Table 3.12. Wind pressure coefficients obtained from references

(a) East openings

NNE	NE	ENE	E	ESE	SE	SSE	S
0.37	0.76	0.88	0.79	0.39	-0.24	-0.64	-0.48
SSW	**SW**	**WSW**	**W**	**WNW**	**NW**	**NNW**	**N**
-0.43	-0.30	-0.17	-0.31	-0.41	-0.48	-0.64	-0.22

(b) West openings

NNE	NE	ENE	E	ESE	SE	SSE	S
-0.40	-0.30	-0.17	-0.31	-0.41	-0.48	-0.65	-0.22
SSW	**SW**	**WSW**	**W**	**WNW**	**NW**	**NNW**	**N**
0.37	0.77	0.88	0.78	0.39	-0.23	-0.66	-0.48

Table 3.13. Discharge coefficient input value

Cases	East Openings	West Openings
Case 1	0.80	0.22
Case 2	0.62	0.22
Case 3	0.41	0.22

3.4.3. Accuracy verification

The accuracy verification was conducted by comparing the measured and simulated values of temperature, relative humidity, and ventilation volume. Measurements were taken at the center of the target building using CO_2 concentration methods for ventilation rate measurement, as mentioned earlier. The temperature, relative humidity, and ventilation volume were generally reproduced when the appropriate discharge coefficients and wind pressure coefficients were input. The study found that the simulation results were not significantly affected by differences in the calculation method of the wind pressure coefficient, indicating that using values from literature/references or CFD simulations yielded similar results.

To evaluate the accuracy of the simulations, two error indicators, namely the mean bias error (MBE) and the coefficient of variation of the root mean square error (CV(RMSE)), were calculated according to recognized standards and guidelines, such as ASHRAE [15], measurement and verification of federal energy projects [16], and the international performance measurement and verification protocol [17]. The MBE and CV(RMSE) [18, 19] were calculated using equations (3.11) and (3.12),

$$\mathrm{MBE} = \frac{\sum_{i=1}^{N}(M_i - S_i)}{N} \tag{3.11}$$

$$\mathrm{CV(RMSE)} = \frac{\sqrt{\sum_{i=1}^{N}((M_i \cdot S_i)^2 / N)}}{\frac{\sum_{i=1}^{N} M_i}{N}} \tag{3.12}$$

where Mi and Si are the measured and simulated data at the instant i, respectively. N is the number count of the calibration values.

Figure 3.26 - 3.34 present the simulation accuracy verification for three cases tested according to three types wind pressure coefficients source. The calibration criteria of the reasonable standards and guidelines, and the two calculated error indicators for the base case calibration are shown in Table 3.10. The measured values were expressed at 5 minutes interval of measurement using dotted line. The results show that the prediction mean bias errors (MBEs) and cross-validation root mean square

errors (CV(RMSE)s) were within the acceptable range, as defined by the validation criteria set by ASHRAE guidelines and IPMVP.

As a result, the calculated temperature and relative humidity present the result accurately compared to measured value of below 10 %. However, there were some errors in temperature and relative humidity depending on the time period. Two potential reasons for this discrepancy were identified. Firstly, errors in ventilation measurement (constant concentration method of CO_2), which could be up to 100 m^3/h, might impact the indoor environment. Secondly, the influence of neighbouring rooms, such as corridors and rooms with occupants, could affect the indoor environment due to factors such as air conditioner operation and blinds opening/closing.

Therefore, these findings suggest that THERB for HAM with NAF has the ability to accurately predict indoor air temperatures in naturally ventilated building.

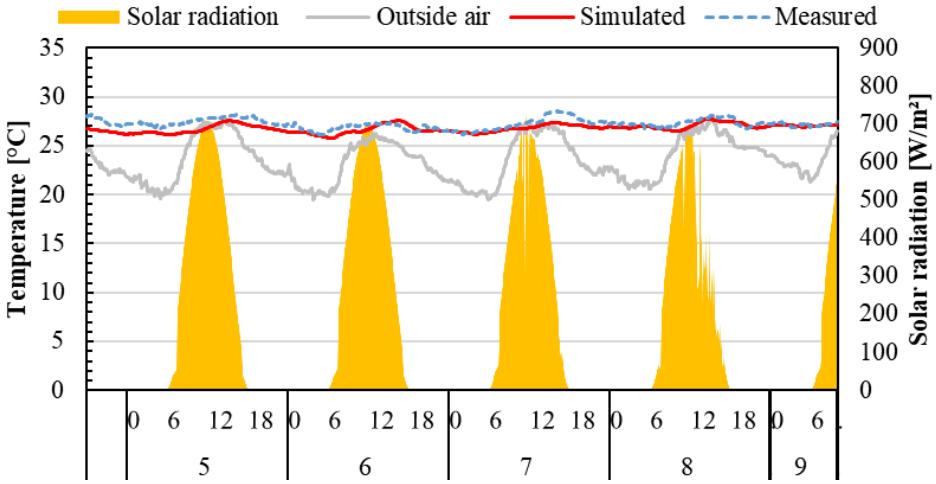

(a)

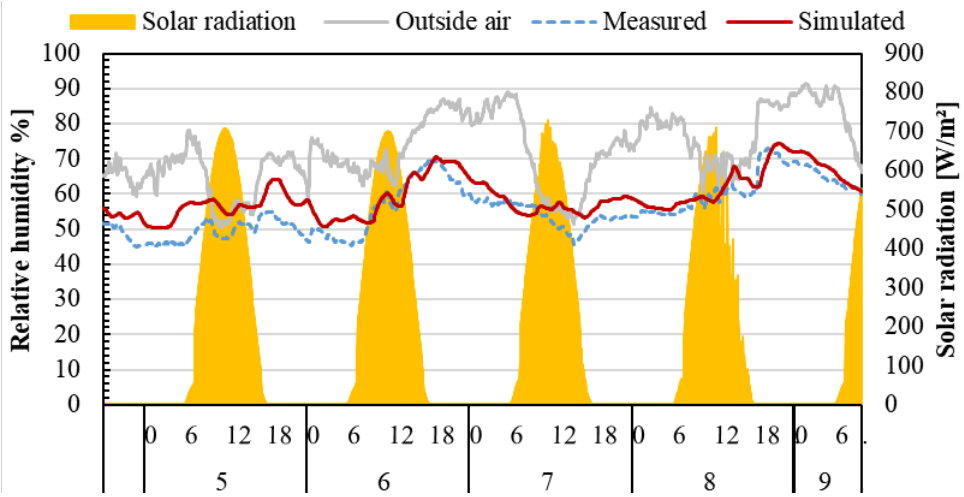

(b)

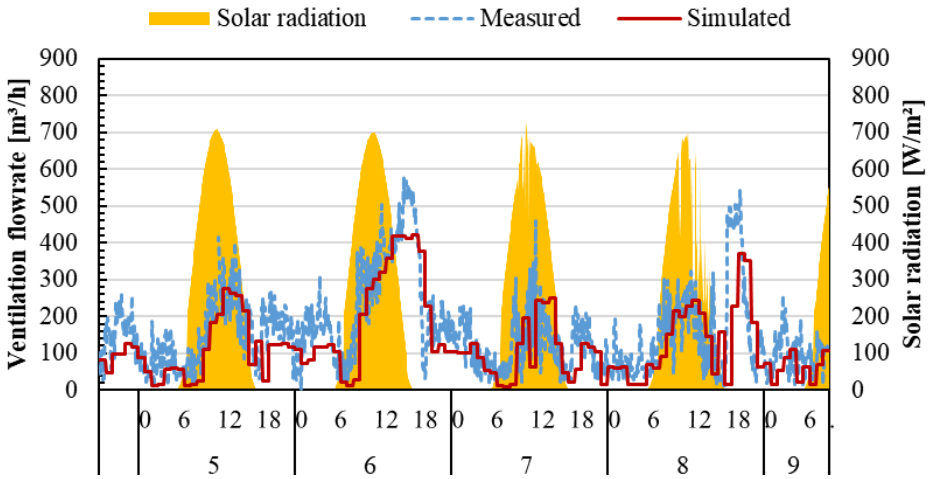

(c)

Figure 3.26. Comparison measured and simulated (Cp from CFD with include surrounding environment) for case 1, (a) temperature, (b) relative humidity, (c) ventilation rate

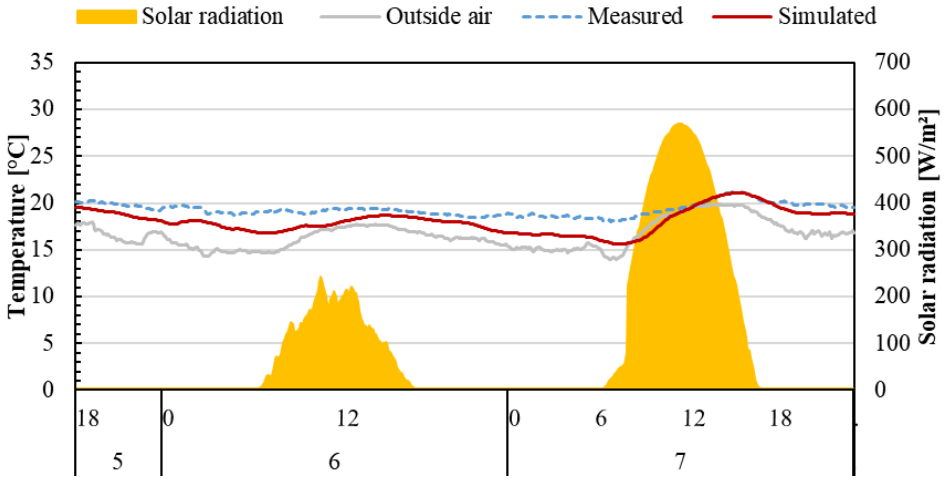

(a)

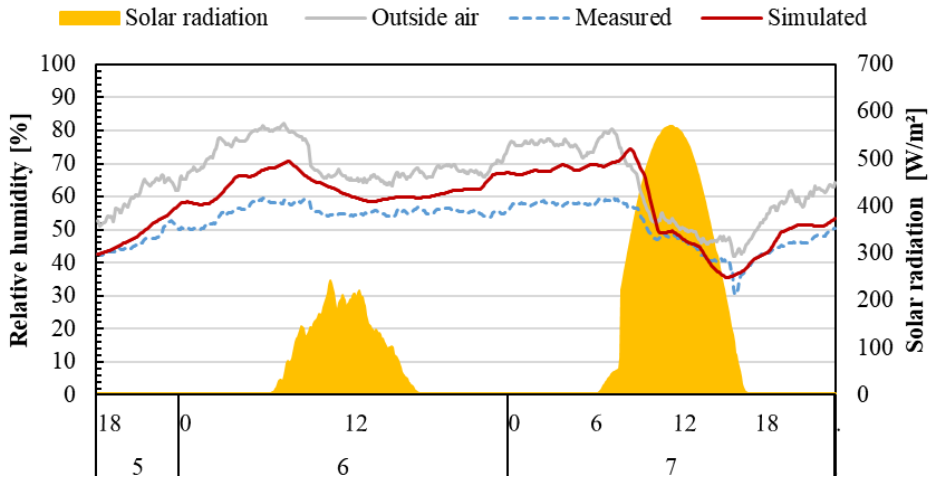

(b)

Figure 3.27. Comparison measured and simulated (Cp from CFD with include surrounding environment) for case 2, (a) temperature, (b) relative humidity.

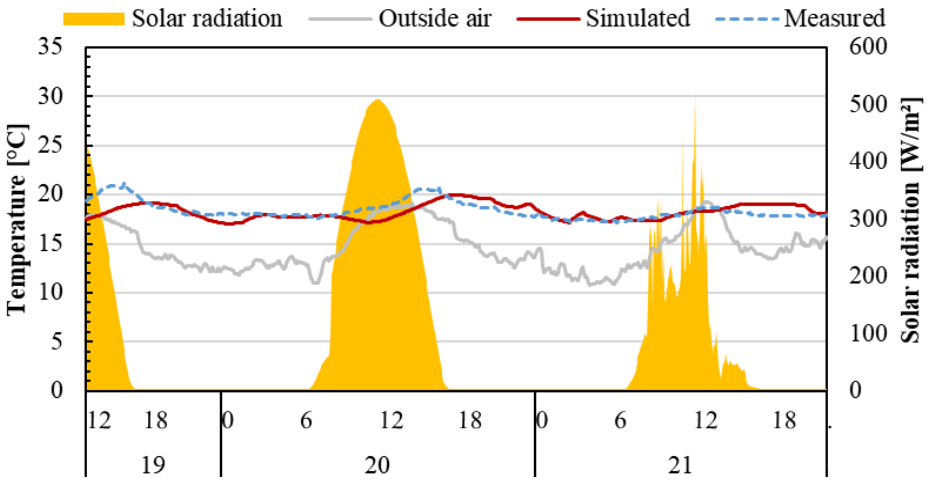

(a)

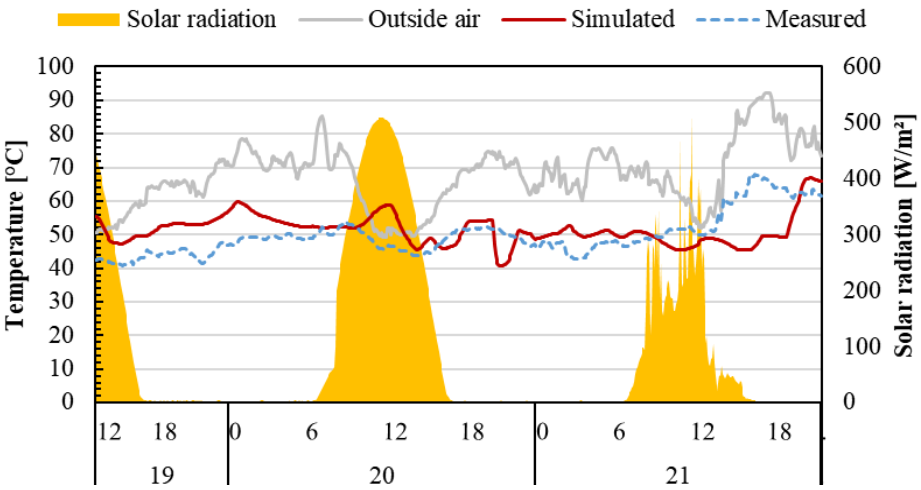

(b)

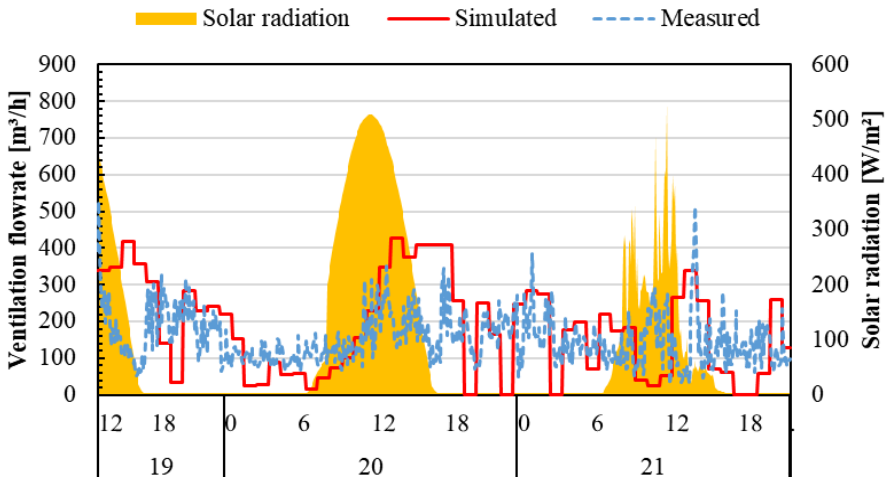

(c)

Figure 3.28. Comparison measured and simulated (Cp from CFD with include surrounding environment) for case 3, (a) temperature, (b) relative humidity, (c) ventilation rate

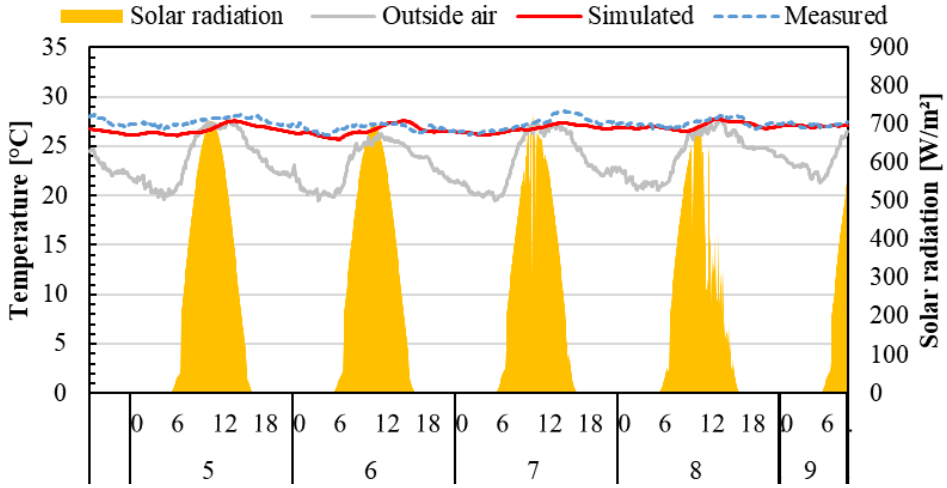

(a)

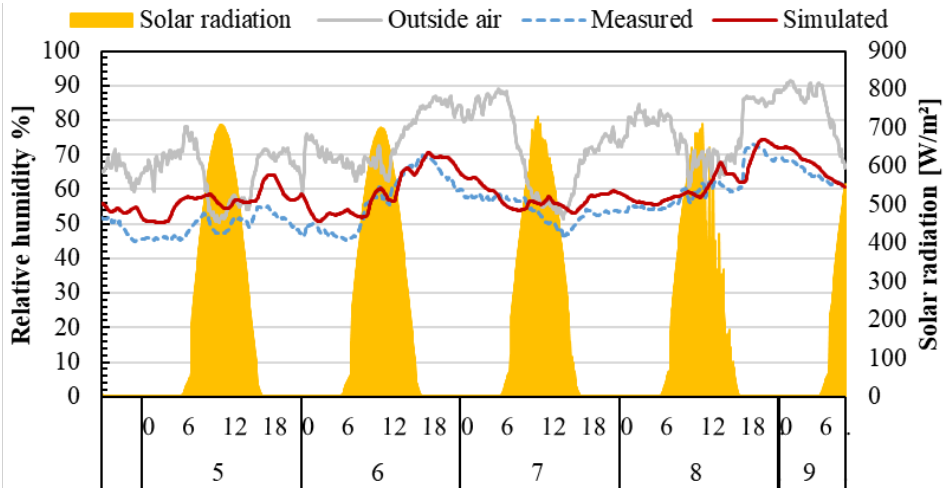

(b)

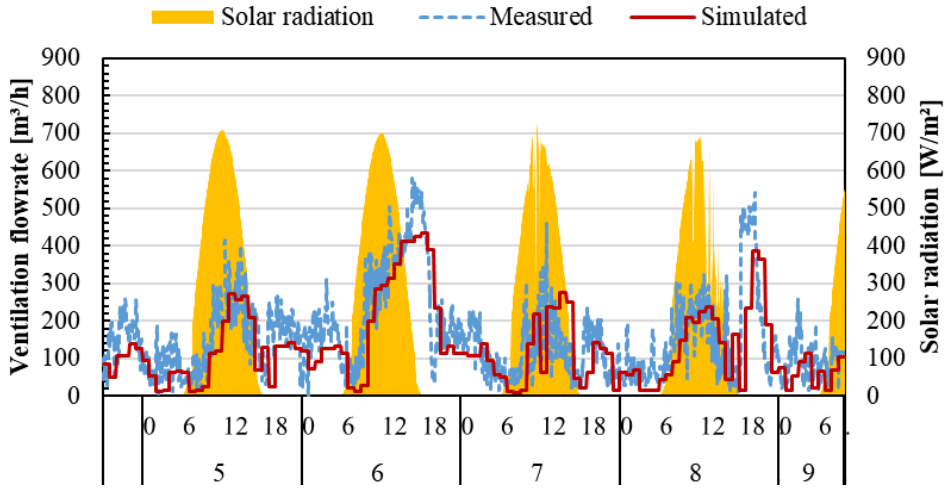

(c)

Figure 3.29. Comparison measured and simulated (Cp from CFD with target building only) for case 1, (a) temperature, (b) relative humidity, (c) ventilation rate

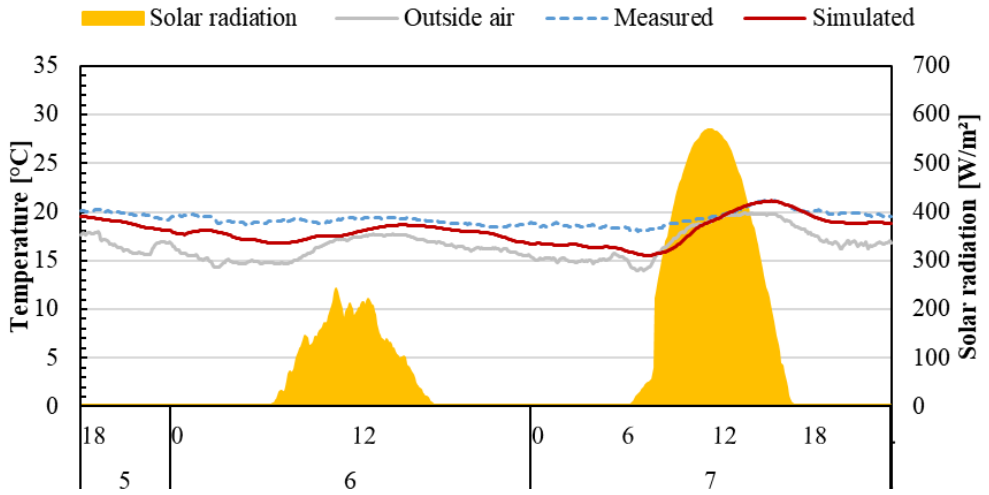

(a)

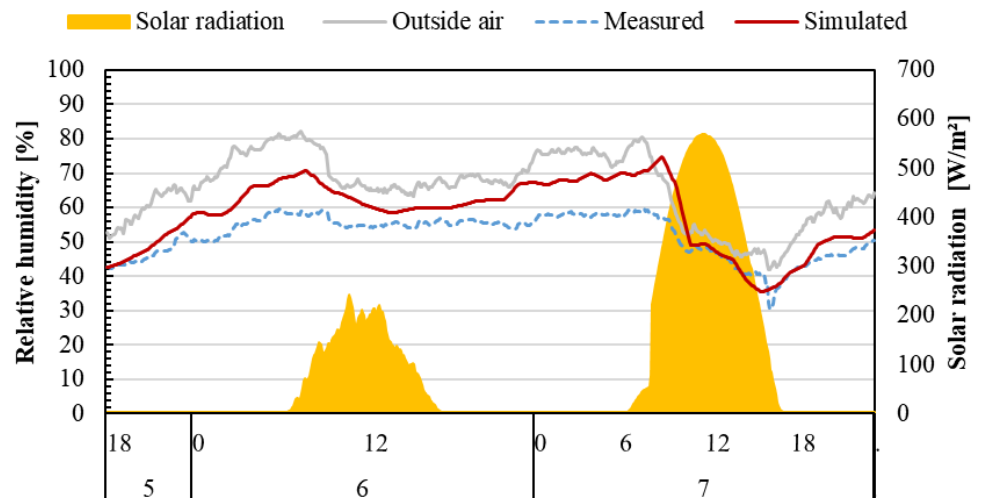

(b)

Figure 3.30. Comparison measured and simulated (Cp from CFD with target building only) for case 2, (a) temperature, (b) relative humidity

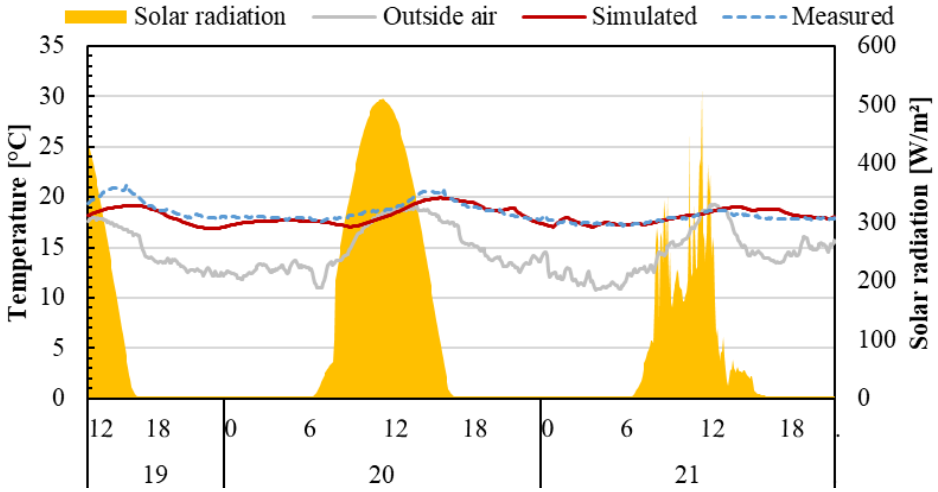

(a)

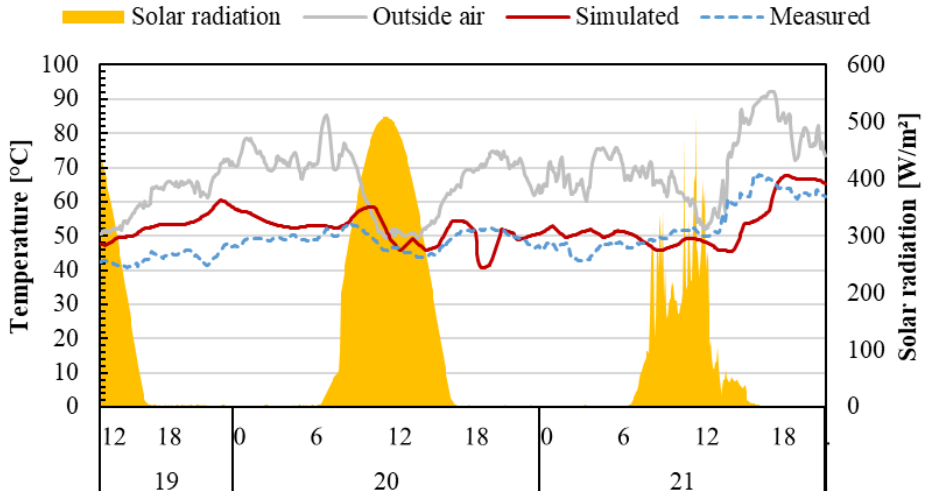

(b)

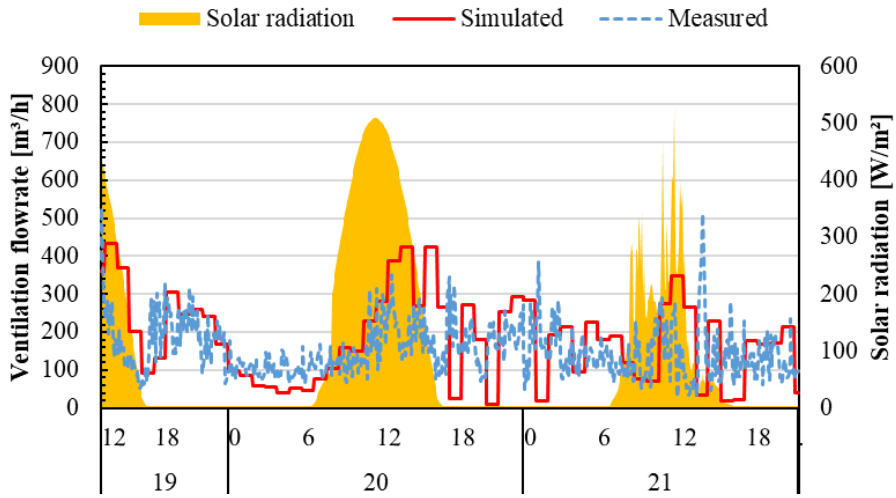

(c)

Figure 3.31. Comparison measured and simulated (Cp from CFD with target building only) for case 3, (a) temperature, (b) relative humidity, (c) ventilation rate

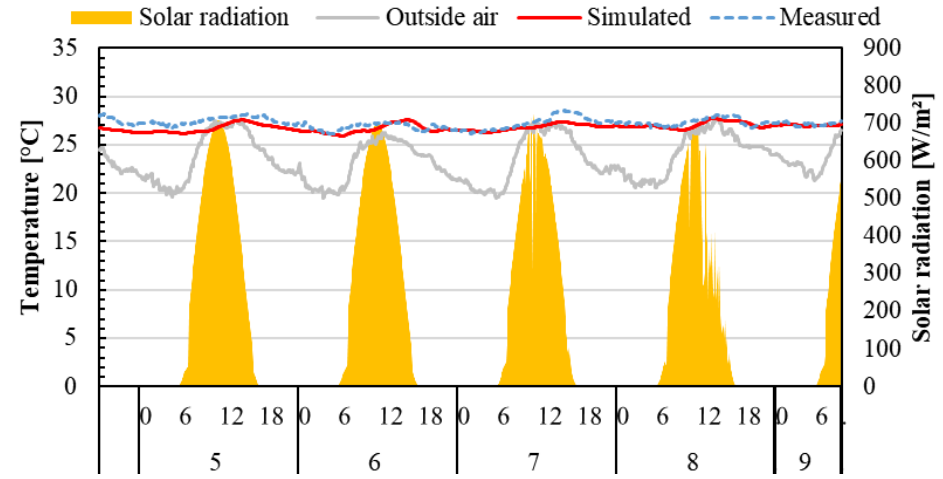

(a)

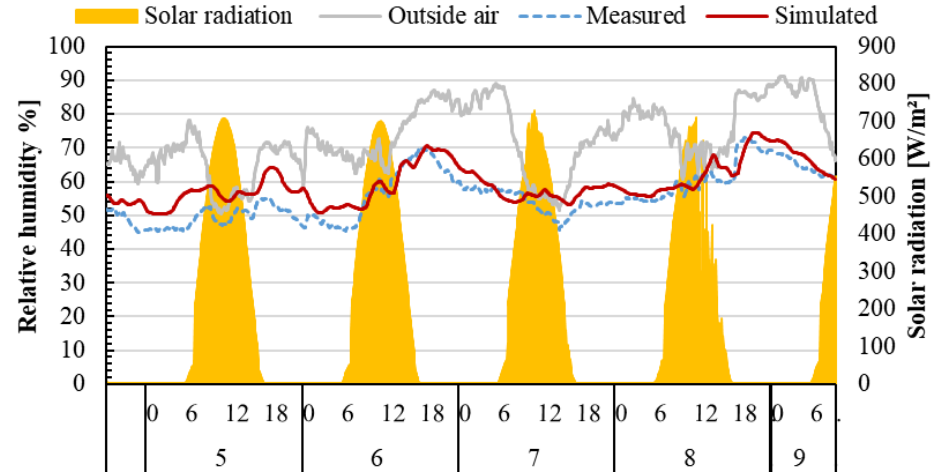

(b)

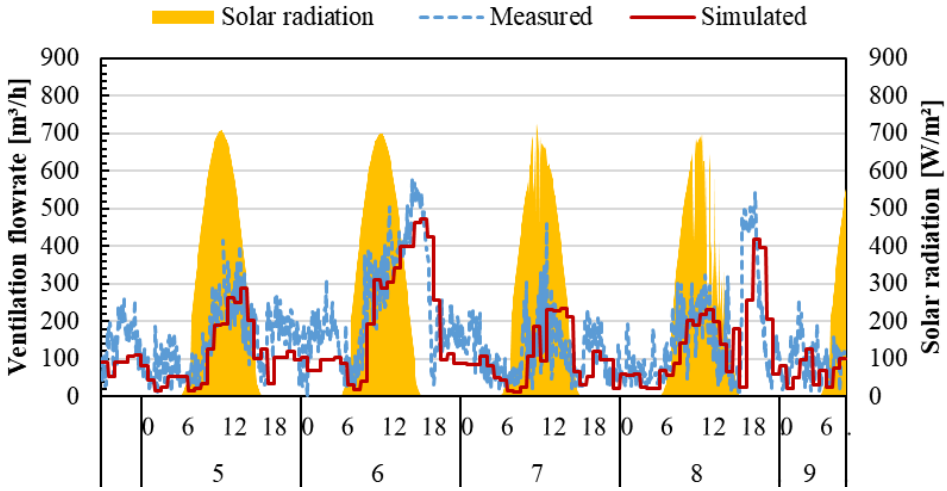

(c)

Figure 3.32. Comparison measured and simulated (Cp from references value) for case 1, (a) temperature, (b) Relative humidity, (c) Ventilation rate

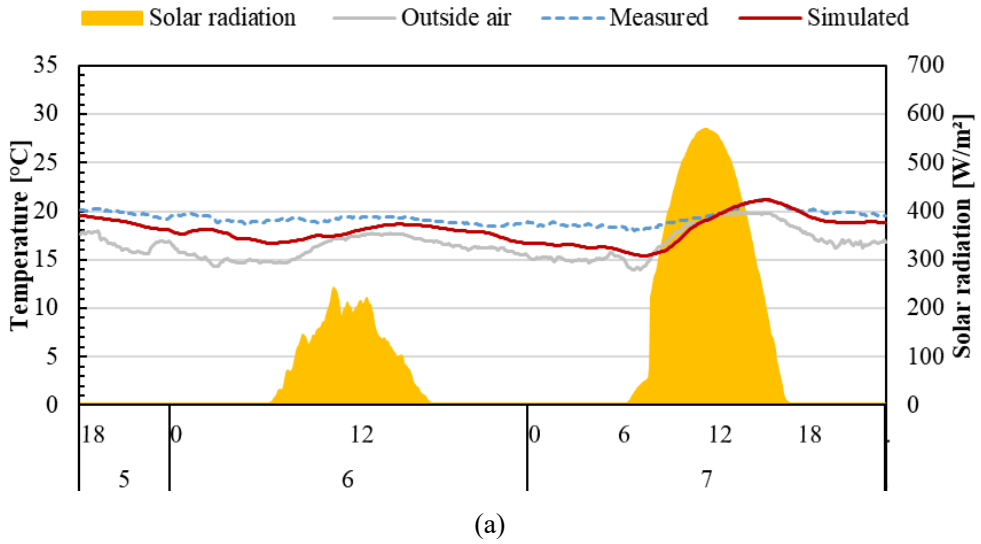

(a)

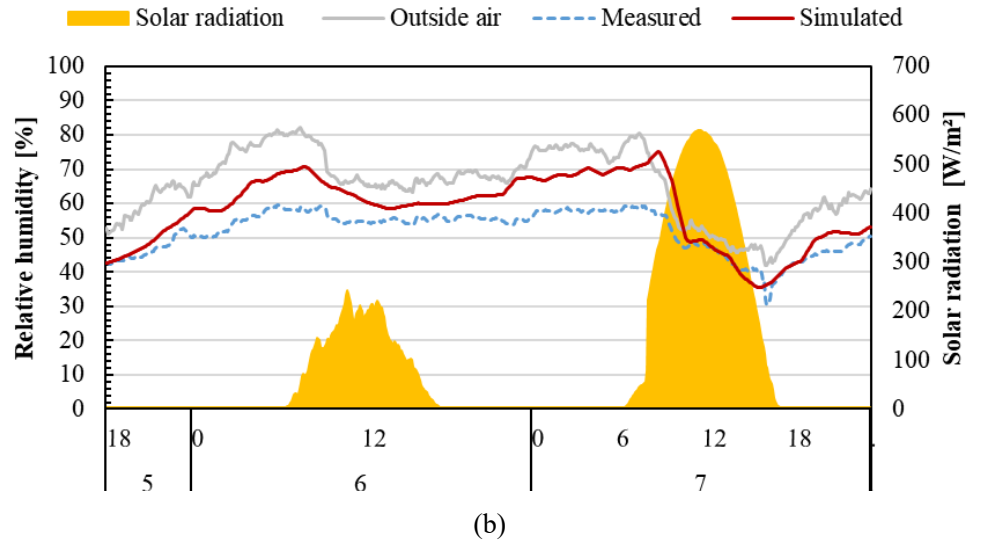

(b)

Figure 3.33. Comparison measured and simulated (Cp from references value) for case 2,

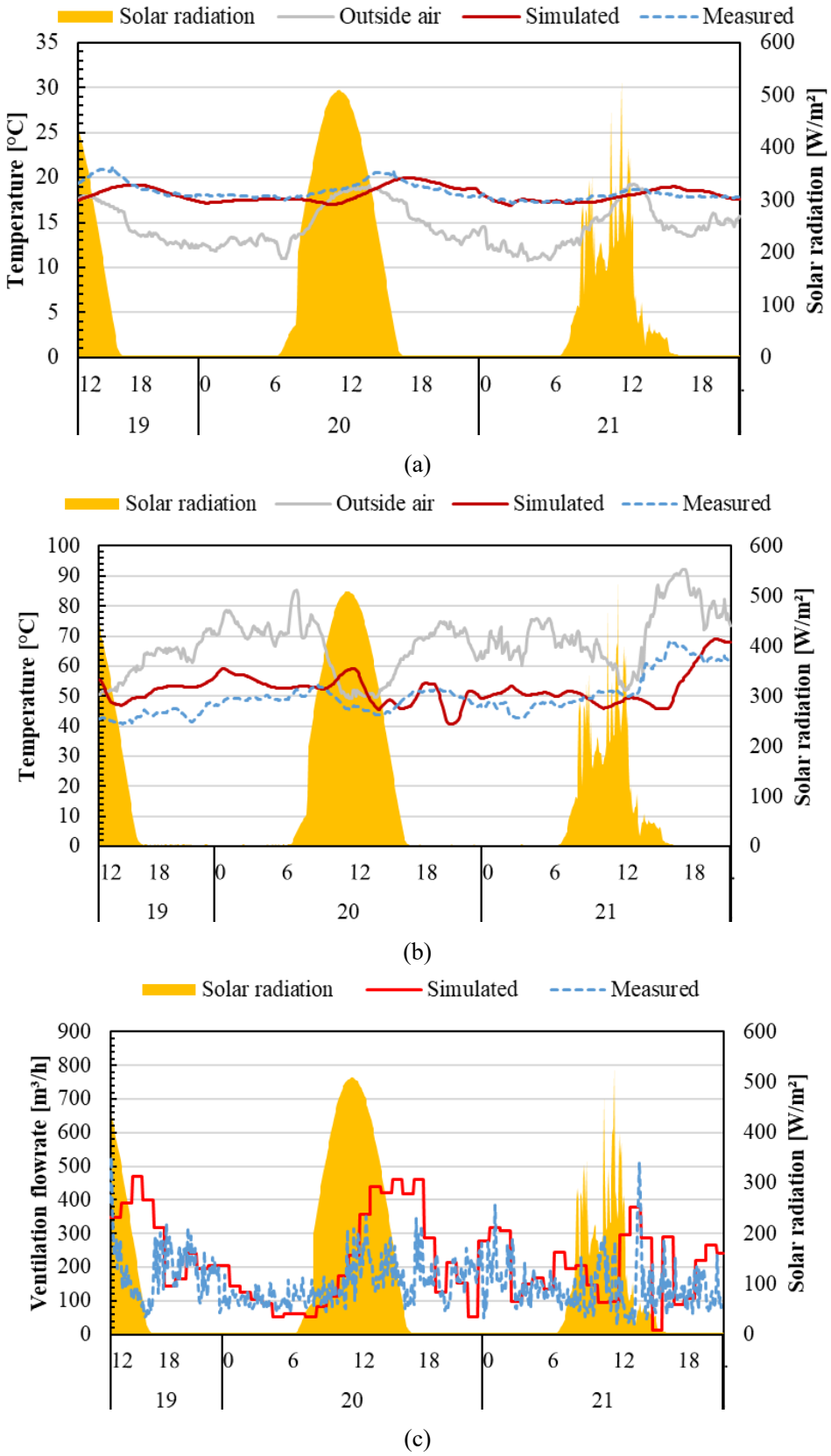

Figure 3.34. Comparison measured and simulated (Cp from references value) for case 3, (a) temperature, (b) Relative humidity, (c) Ventilation rate

Table 3.10. Calibration criteria and prediction error

(a) Cp value from CFD with include environment condition

Cases	Indicator	Prediction error			Standard		
		Temperature	RH	Ventilation rate	ASHRAE	IPMVP	FEMP
Case 1	MBE	1.69%	6.43%	19.96%	± 10%	± 10%	± 5%
	CV (RMSE)	2.49%	3.40%	3.53%	< 30%	< 30%	< 20%
Case 2	MBE	4.43%	11.78%	-	± 10%	± 10%	± 5%
	CV (RMSE)	4.75%	4.76%	-	< 30%	< 30%	< 20%
Case 3	MBE	1.09%	1.02%	19.07%	± 10%	± 10%	± 5%
	CV (RMSE)	2.43%	1.42%	3.53%	< 30%	< 30%	< 20%

(b) Cp value from CFD with target building only

Cases	Indicator	Prediction error			Standard		
		Temperature	RH	Ventilation rate	ASHRAE	IPMVP	FEMP
Case 1	MBE	1.78%	6.54%	17.58%	± 10%	± 10%	± 5%
	CV (RMSE)	2.55%	3.43%	3.31%	< 30%	< 30%	< 20%
Case 2	MBE	4.52%	11.91%	-	± 10%	± 10%	± 5%
	CV (RMSE)	4.80%	4.79%	-	< 30%	< 30%	< 20%
Case 3	MBE	1.76%	3.26%	20.00%	± 10%	± 10%	± 5%
	CV (RMSE)	3.09%	2.53%	3.61%	< 30%	< 30%	< 20%

(c) Cp value from references

Cases	Indicator	Prediction error			Standard		
		Temperature	RH	Ventilation rate	ASHRAE	IPMVP	FEMP
Case 1	MBE	1.65%	6.42%	19.04%	± 10%	± 10%	± 5%
	CV (RMSE)	2.46%	3.39%	3.45%	< 30%	< 30%	< 20%
Case 2	MBE	6.59%	12.15%	-	± 10%	± 10%	± 5%
	CV (RMSE)	5.84%	4.84%	-	< 30%	< 30%	< 20%
Case 3	MBE	1.91%	2.61%	41.86%	± 10%	± 10%	± 5%
	CV (RMSE)	3.21%	2.26%	5.23%	< 30%	< 30%	< 20%

3.5. Conclusions

The objective of this study is to evaluate the discharge coefficients for louvre openings with various sash angle installations according to the pressure difference and outdoor wind velocity in real-time measurements.

The constant concentration method for CO_2 quantifies the ventilation rate in an indoor environment. Three cases of louvre openings are presented: (1) louvre opening with a sash angle of 0°, (2) louvre opening with a sash angle of 15°, and (3) louvre opening with a sash angle of 30°. The conclusions of this study are as follows:

1. The ventilation rate has a tendency similar to that of the inlet air velocity, outdoor wind velocity, and theoretical velocity.
2. The normalized ventilation rate fluctuated according to the outdoor wind velocity and the pressure difference. A constant value for the airflow rate occurred when the outdoor velocity was above 2 m/s and the pressure difference was greater than 1 Pa.
3. The discharge coefficient of the louvre opening with the installation of the sash varied according to the angle. The value decreased with increasing sash angle, and the summary values of the discharge coefficient for louvres with sash angles of 0°, 15°, and 30° were 0.80, 0.62, and 0.41, respectively.
4. Wind pressure coefficients of the target building was simulated by CFD STAR CCM+ with include surrounding environment and target building only. In addition, wind pressure coefficients from literature review is also performed for comparison of accuracy verification of developed model. There are no significant different of simulation result due to different of wind pressure coefficients source.
5. The calculated temperature and relative humidity present the result accurately compared to measured value of below 10 %. Meanwhile, the deviation for ventilation rate is also within the acceptable range for some cases, with no more than 20 %.
6. These findings suggest that THERB for HAM with NAF has the ability to accurately predict indoor air temperatures in naturally ventilated building.

The findings presented in this study are aimed at understanding the geometrical patterns of louvre ventilation openings and their effects on the ventilation rate and discharge coefficient value according to outdoor wind velocity and pressure difference. These findings can be implemented for houses in tropical climates to increase the indoor thermal environment of naturally ventilated buildings, especially in Indonesia. In addition to improve of naturally ventilated house in Indonesia, THERB for HAM with NAF can be used for numerical simulation.

References

[1] S. Tong, J. Wen, N. H. Wong, and E. Tan, “Impact of façade design on indoor air temperatures and cooling loads in residential buildings in the tropical climate,” Energy Build, vol. 243, p. 110972, 2021.

[2] E. Prianto and P. Depecker, “Optimization of architectural design elements in tropical humid region with thermal comfort approach,” Energy Build, vol. 35, no. 3, pp. 273–280, 2003.

[3] A. M. Nugroho, “Tropical Nusantara’s Contemporary House for Liveable Environment,” MATEC Web of Conferences, vol. 280, p. 03021, 2019.

[4] M. H. Sherman, “Tracer-gas techniques for measuring ventilation in a single zone,” Build Environ, vol. 25, no. 4, pp. 365–374, Jan. 1990.

[5] P. Kapalo, S. Vilčeková, F. Domnita, C. Bacotiu, and O. Voznyak, “Determining the ventilation rate inside an apartment house on the basis of measured carbon dioxide concentrations - Case study,” 10th International Conference on Environmental Engineering, ICEE 2017, no. October, 2017.

[6] T. Yang, “CFD and Field Testing of a Naturally Ventilated Full-scale Building,” no. May, pp. 1–227, 2004.

[7] Y. Choi and D. Song, “How to quantify natural ventilation rate of single-sided ventilation with trickle ventilator?,” Build Environ, vol. 181, no. April, p. 107119, 2020.

[8] H. L. Gough et al., “Field measurement of natural ventilation rate in an idealised full-scale building located in a staggered urban array: Comparison between tracer gas and pressure-based methods,” Build Environ, vol. 137, no. January, pp. 246–256, 2018.

[9] J. S. Park, “Long-term field measurement on effects of wind speed and directional fluctuation on wind-driven cross ventilation in a mock-up building,” Build Environ, vol. 62, pp. 1–8, 2013.

[10] A. Iqbal, A. Afshari, H. Wigö, and P. Heiselberg, “Discharge coefficient of centre-pivot roof windows,” Build Environ, vol. 92, pp. 635–643, 2015.

[11] P. Heiselberg, K. Svidt, and P. V. Nielsen, “Characteristics of airflow from open windows,” Build Environ, vol. 36, no. 7, pp. 859–869, Aug. 2001.

[12] D. Cóstola, B. Blocken, and J. L. M. Hensen, “Overview of pressure coefficient data in building energy simulation and airflow network programs,” Build Environ, vol. 44, no. 10, pp. 2027–2036, 2009.

[13] AIJ, “AIJ Recommendations for Loads on Buildings (2015) Architectural Institute of Japan,” 2019, [Online]. Available: https://www.aij.or.jp/

[14] A. Ozaki and T. Tsujimaru, “Prediction of hygrothermal environment of buildings based upon combined simulation of heat and moisture transfer and airflow,” IBPSA 2005 - International Building Performance Simulation Association 2005, pp. 899–906, 2005.

[15] ASHRAE 14, “Measurement of Energy, Demand, and Water Savings,” ASHRAE Guideline 14-2014, vol. 4, pp. 1–150, 2014, [Online].
Available: www.ashrae.org%0Awww.ashrae.org/technology.

[16] U.S. Department of Energy–Federal Energy Management Program, “M&V guidelines: measurement and verification for performance-based contracts -Version 4.0,” U.S. Department of Energy, vol. 3, no. November, pp. 1–108, 2015.

[17] Efficiency Valuation Organization, “International Performance Measurement & Verification Protocol,” Handbook of Financing Energy Projects, vol. I, no. January, p. 122, 2016.

[18] G. Mustafaraj, D. Marini, A. Costa, and M. Keane, “Model calibration for building energy efficiency simulation,” Appl Energy, vol. 130, pp. 72–85, 2014.

[19]M. Royapoor and T. Roskilly, “Building model calibration using energy and environmental data,” Energy Build, vol. 94, pp. 109–120, 2015.

Chapter 4. Performance improvement plan of naturally ventilated house in tropical climate regions, Indonesia

4.1. Research methods

This study comprises four key steps, as depicted in Figure 4.1. The initial step involves conducting on-site measurements of temperature and humidity both indoors and outdoors. These measurements are then utilized to validate the accuracy of a base simulation model. Additionally, the housing configuration details are determined for the numerical simulation. Moving on to the second step, a base simulation model of the test house is developed. This model serves as a foundation for further analysis and improvements. The third step focuses on devising an energy-saving improvement plan specifically tailored to Indonesian housing. The primary areas of improvement include the louver opening area and insulation level. Finally, in the fourth step, the validated model is employed to simulate the annual cooling loads in various regions of Indonesia. This step aims to identify the appropriate improvement plan suited for each region.

4.1.1. Overview of the test house

The configuration of the test house for the numerical analysis is based on an existing house where people are living, as shown in Figure 4.2. The house is a housing prototype, built in large numbers after the tsunami attack in 2004 in Indonesia. By 2008, approximately 104,200 permanent residences had been built based on this floor plan by various sponsors, including the Indonesian government and local and international non-governmental organizations [1]. The experimental houses are low-cost, with a building envelope comprising a combination of concrete and brickwork, and feature a zinc roof material, as shown in Table 4.1. The configuration of this house is typical in Indonesian households and was classified as a detached modern house [2] with a total floor area of 54 m^2 and averaging four-person occupancy. The material employed exhibited high thermal conductivity, which affected the process of rapid heat transfer from outdoors to indoors.

Most low-income occupants primarily rely on window and door openings to avoid excessive indoor temperature during the daytime at peak heat conditions, rather than operating the air conditioner for cooling. In tropical buildings, window openings can be effective to reduce heat buildup, which in turn can lower indoor air temperatures and nighttime cooling loads [3]. For free cooling, the opening ratio design significantly affects the ventilation rate. Louver-attached windows, which can partly improve the comfort level by increasing air velocity, are among the traditional design factors of Indonesian housing [4]. Louvers are typically arranged in a pattern, either horizontally or vertically, and are usually made from wood, although modern homes may also use metal or plastic materials.

Notably, the building material functions as a barrier between the outside temperature, from sources such as solar radiation, and inside temperature. Therefore, factors such as material properties, thickness, air cavity, and outer surface configurations should be considered. Because most occupants spend sufficient time in the living room during daily activities, this study set the living room as a target of simulation. In addition, the temperature and relative humidity were measured inside the living room

and outside using a USB Temperature and Humidity Data Logger DS 102. The specifications of the measurement devices are listed in Table 4.2.

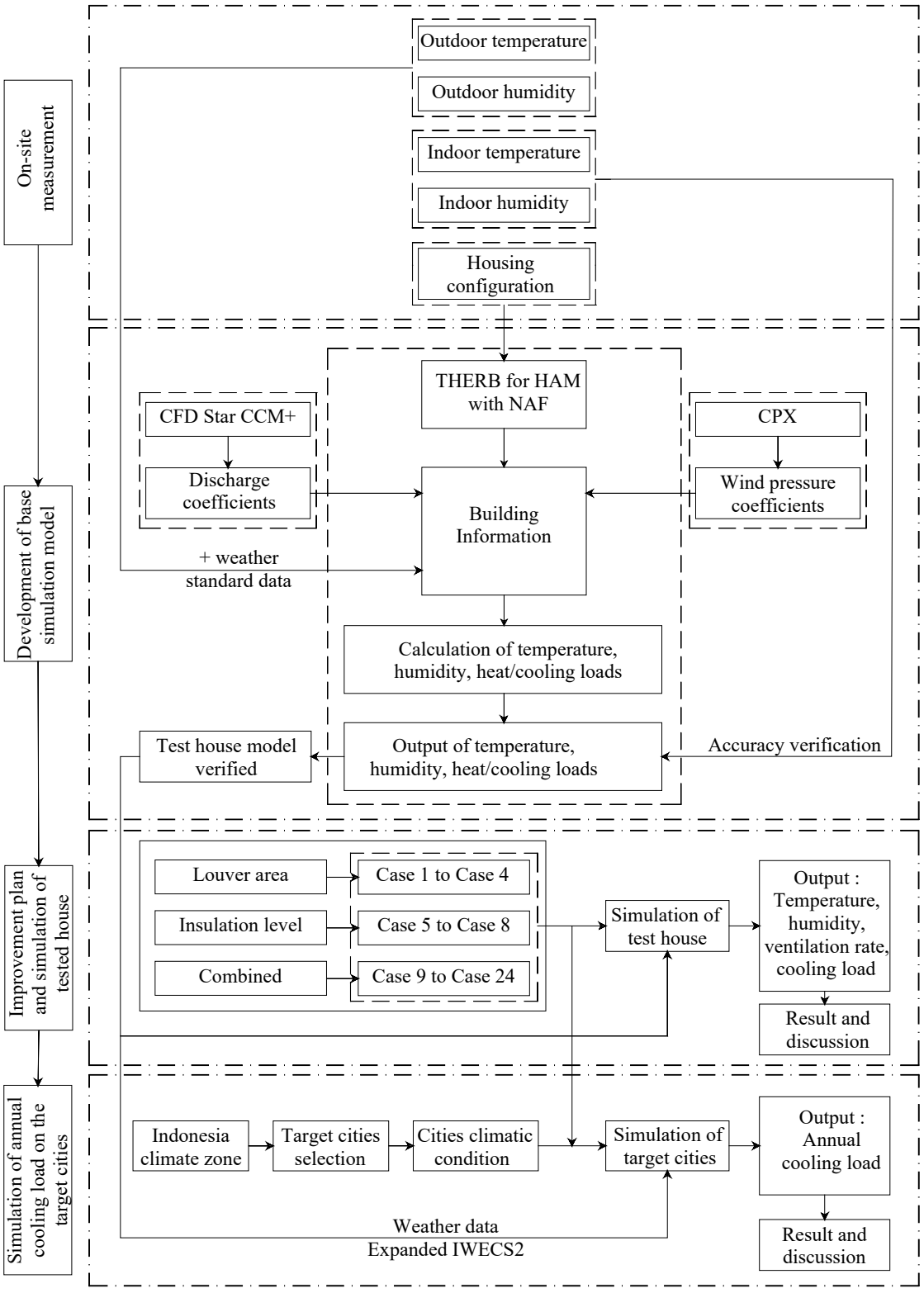

Figure 4.1. Research process

Table 4.1. Building envelope information of the test house

Category	Layer	Thickness [m]	Thermal conductivity [W/(m·K)]	Specific heat [J/(kg·K)]	Specific gravity [kg/m3]	Moisture conductivity [kg/(m·s·Pa)]	Moisture capacity [kg/(m3(kJ/kg)]
Roof (U-Value = 8.13 W/(m².K))	Zinc plate	0.00025	110	896	2800	-	-
Ceiling (U-Value = 5.48 W/(m².K))	Plywood	0.004	0.120	1880.0	556.0	5.670E-13	2.200E-01
Exterior wall (U-Value = 2.90 W/(m².K))	Cement mortar	0.03	1.910	917.0	2009.0	4.570E-12	1.830E-01
	Brickwork	0.1	0.807	880.0	1792.0	2.600E-11	1.072E-02
Floor (U-Value = 4.50 W/(m².K))	Sand	0.1	1.910	840.0	1764.0	0.000E+00	0.000E+00
	Concrete	0.05	1.619	890.0	2206.0	1.020E-12	1.881E+00
	Cement mortar	0.02	1.910	917.0	2009.0	4.570E-12	1.830E-01
	Concrete tile	0.009	1.1	837	2100	-	-

Table 4.2. Measurement devices

Description	Specification
Measures temperature range	-40 °C to + 60 °C
Measures humidity range	1%RH – 99%RH
Temperature accuracy	+/-1°C under 0-50 °C
Humidity accuracy	+/-4% under 20%-80%
Logging interval	8 seconds to 4 hours

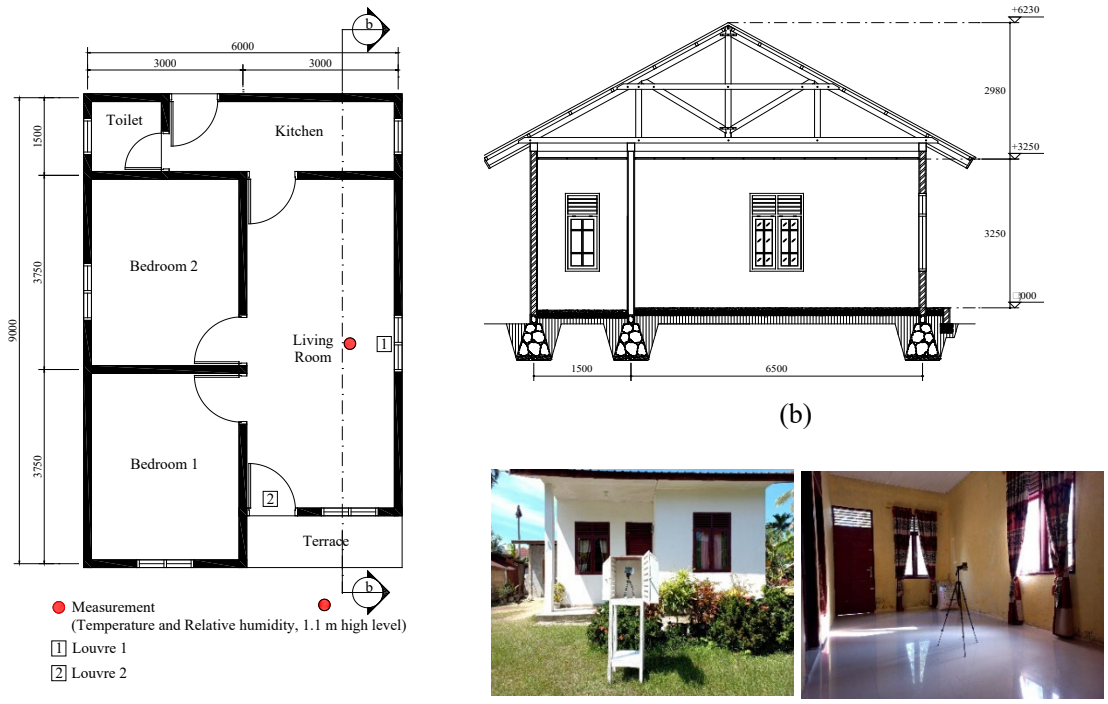

Figure 4.2. Plan and section of test house (unit: mm): (a) floor plan, (b) cross-section, and (c) measurement photograph

4.1.2. Climate zone and time zone of Indonesia

Indonesia is a nation consisting of multiple islands situated near the equator, showcasing diverse landscapes and various land utilization practices. The unique climate characteristics in different regions of Indonesia have been shaped by a multitude of intricate global, regional, and local climatic phenomena. These phenomena encompass a wide range of atmospheric processes, including surface and upper air circulations, as well as interactions between the atmosphere and the surrounding ocean. Based on koppen's climate classification [5], Indonesia climate is divided into three zone, namely: equatorial climate (Af), monsoon climate (Am), and tropical savanna climate (Aw), as shown in Figure 4.3. However, according to the integrated climate zone as shown in Figure 4.4, the climatic zones in Indonesia are determined by the temperature range and wind speed. This zonation is more detailed and optimal than koppen's climate classification, which divides Indonesia into eight climate zones: equatorial, sub-equatorial, high land tropical, extremely high land tropical, monsoonal, sub-monsoonal, savanna, and sub-savanna zones [6].

Moreover, Indonesia, with its vast territory across the archipelago, spans multiple time zones. Figure 4.5 presents the time zones in Indonesia, which are divided into three categories [7]. The primary time zone in Indonesia is Western Indonesia Time (WIB), which is UTC+7. This time zone includes cities such as Sumatra (consisting of Aceh, Bengkulu, Jambi, Lampung, North Sumatra, Riau,

South Sumatra, and West Sumatra), Riau Islands, Bangka Belitung Islands, Java (consisting of Banten, Jakarta, West Java, Central Java, the Special Region of Yogyakarta, and East Java), West Kalimantan, and Central Kalimantan. Additionally, there are two other time zones in Indonesia. Central Indonesia Time (WITA) is observed in regions such as South Kalimantan, East Kalimantan, North Kalimantan, Nusantara, Sulawesi (consisting of North Sulawesi, Gorontalo, Central Sulawesi, West Sulawesi, South Sulawesi, and Southeast Sulawesi), Bali, West Nusa Tenggara, and East Nusa Tenggara, and is UTC+8. Eastern Indonesia Time (WIT) is followed in areas including Maluku, North Maluku, Central Papua, Highland Papua, South Papua, Southwest Papua, West Papua, and Papua, and is UTC+9.

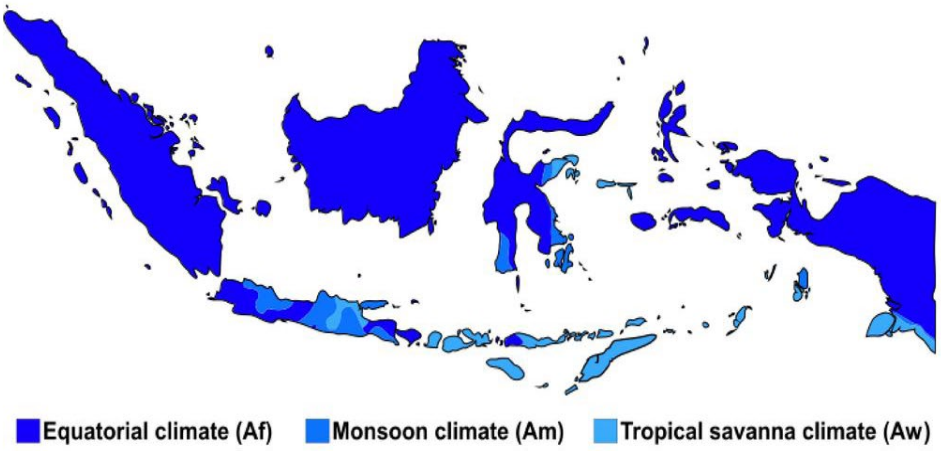

Figure 4.3. Koppens climate classsification of Indonesia

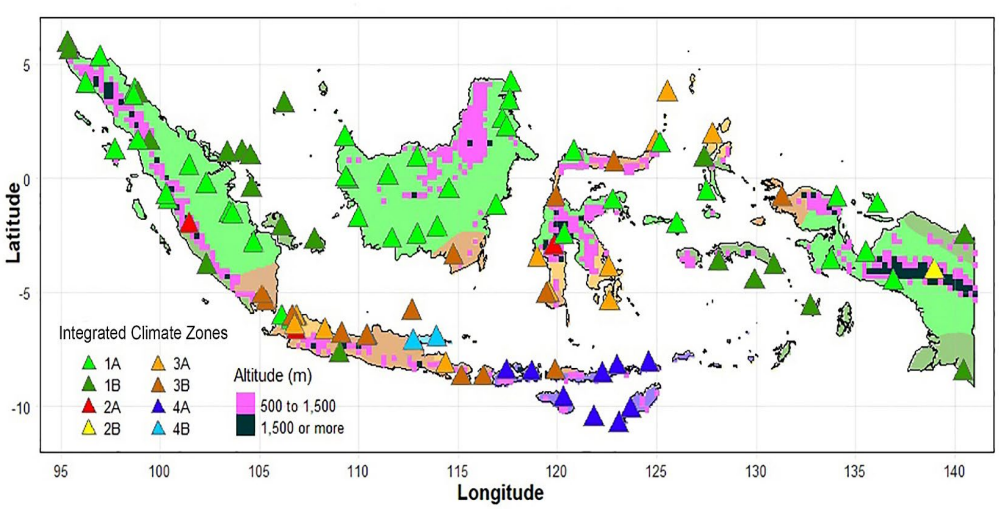

Figure 4.4. Integrated Indonesia climate zone

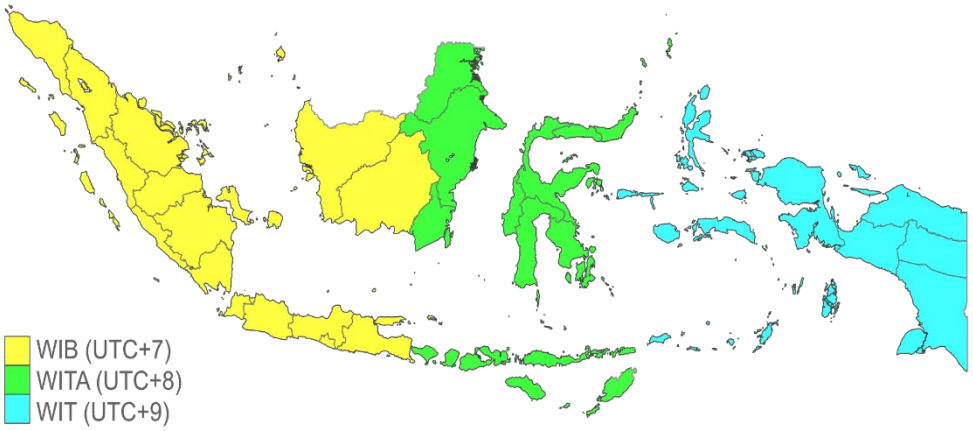

Figure 4.5. Indonesia time zone

4.1.3. Target cities and calculation condition

This study proposes a passive design based on an optimal combination of passive design measures, which is determined through thermal load simulation. The classification of these zones significantly depends on the criteria of thermal climatic zones and local climatic conditions. Therefore, this study selects 13 cities that are uniformly distributed across the thermal climatic regions, require cooling loads to maintain indoor temperatures, and have weather data available for simulation. The selected cities include two in the equatorial, two in the sub-equatorial, one in the highland, two in the monsoonal, two in the sub-monsoonal, two in the savanna, and two in the sub-savanna zones.

Furthermore, to investigate the hourly performance of the target room in the test house, the simulation was conducted for two weeks in the dry season (July) with an interval of 60 seconds, and the data were averaged hourly. The selection time of the simulation was predicted as the peak of hot and humid conditions in Indonesia. Meanwhile, to calculate the daily cooling load, the simulation periods were one year (January 1 to December 31), and the data were divided by 365. In addition, to simulate the selected cities, the weather data were expanded from IWEC2 recommended by ASHRAE for building simulation. The simulation conditions for the annual cooling loads of the target cities are listed in Table 4.3. Figure 4.6 illustrates the locations of the cities on the Indonesia map, and Table 4.4 presents their climatic conditions.

Figure 4.6. Various target cities on the Indonesia map

Table 4.3. Simulation condition for annual cooling loads

	Condition
Calculation period	January 1 to December 31
Calculation interval	Temperature and RH : 60 seconds
	Ventilation rate : 60 minutes
Calculation target	Living room
Indoor set-point of temperature and RH	Temperature : 24 °C
	RH : 60%
Space conditioning time	6-9, 12-13, 17-22 (Living schedule of a family)
CD Value	CFD (Star CCM+)
CP Value	CPX2
Weather data	Expanded IWEC2 Weather Data

Table 4.4. Climate condition of target cities

City	Temperature [°C]			Relative humidity [%]			Wind velocity [m/s]			Solar radiation [w/m²]		
	Min	Max	Average	Min	Max	Average	Min	Max	Average	Min	Max	Average
Lhokseumawe	18.60	37.90	26.98	44	100	81.58	0	30.80	1.68	0	1134	111.01
Banda Aceh	19.10	36.90	26.94	34	100	80.07	0	25.70	1.74	0	1149	162.29
Kerinci	9.50	30.70	22.70	32	100	82.62	0	27.80	1.50	0	925	147.15
Cilacap	2.50	55.60	26.36	18	100	82.65	0	48.30	2.03	0	1250	111.58
Sumbawa Besar	18.30	38.80	26.86	24	100	78.21	0	15.40	1.62	0	874	136.34
Waingapu	12.10	39.00	26.84	24	100	76.95	0	12.90	2.13	0	922	150.67
Surabaya	19.00	37.70	27.93	16	100	75.10	0	20.60	2.70	0	889	187.55
Balikpapan	22.00	37.00	27.49	50	100	85.36	0	30.80	2.19	0	887	178.51
Maluku Utara	21.00	34.40	26.78	41	100	86.01	0	11.30	1.17	0	868	135.64
Semarang	14.30	37.40	28.16	22	100	74.26	0	29.90	2.77	0	940	202.51
Gorontalo	20.70	34.60	27.16	41	100	82.33	0	27.80	1.49	0	917	218.44
Bima	18.20	36.30	27.51	25	100	78.49	0	25.70	2.20	0	943	271.95
Madura	21.20	34.10	27.76	47	100	81.10	0	39.10	3.86	0	955	205.40

4.1.4. Improvement plan

Several studies have explored optimizing passive design techniques, such as the insulation level of building envelopes, window-to-wall ratio (opening ratio), overhang depth, air leakage, and energy performance of glazing, for residential buildings [3, 8, 9, 10, 11]. Passive design is significantly influenced by climate conditions and is an effective means of reducing energy consumption in residential buildings. The external wall insulation level is the most significant parameter in terms of its impact on the annual thermal load, contributing to approximately 70% of the total impact [8].

In tropical climates, the opening ratio of windows in residential buildings has a significant impact on the indoor environment and energy consumption. When the window-to-wall ratio is reduced from 1 to 0.4, the largest reductions in indoor air temperature are observed [3]. Additionally, window openings are effective in reducing nighttime cooling loads because they promote heat dissipation during the daytime [3]. Therefore, the opening ratio and insulation level of the building envelope are effective to maintain indoor environment conditions and control the annual cost of cooling loads in tropical regions. Consequently, the performance of the improvement plan in this study was dependent on various opening ratios (louver) and insulation levels.

Because the louver shape of the test house is commonly used in low-cost houses in Indonesia, this study examines the impact of the louver by enlarging and reducing the area and comparing it to existing conditions. The insulation consisted of four integrated levels: external wall, roof, and ceiling insulations. A study has reported that the material composition of the building envelope significantly reduces annual cooling loads and indoor environmental conditions. Ashouri et al. investigated two insulation materials, rockwool and glasswool. They reported that the optimal thicknesses resulted in annual cost savings of 1.6028 \$/m^2 for glasswool and 0.7658 \$/m^2 for rockwool [12].

Therefore, this study employs two primary insulation materials (glasswool and rockwool), and another material, particle board or plywood, is used for comparison. For the roof part, the insulation of the proposed cases was strengthened by more than 100% compared with that of the existing case. In addition, external wall insulation is upgraded by adding glasswool, plywood, and particle boards, including air cavities. The U-value of the external wall is 0.51 W/(m^2.K), whereas that of the existing condition is 3.29 W/ (m^2.K). A significant improvement was also achieved on the ceiling by adding 100 mm of rockwool. The ceiling proposed in this study could reduce the U-value to 0.33 W/ (m^2.K) compared with the existing value of 5.48 W/ (m^2.K).

In addition, various combinations of louver opening ratios and insulation levels were combined to determine the best performance among the test cases. Case N represents the actual condition of the test house, and this study examines 24 cases of improved plans. Figure 4.7 demonstrates the insulation improvement plan, and Table 4.5 illustrates the configuration of the simulation cases.

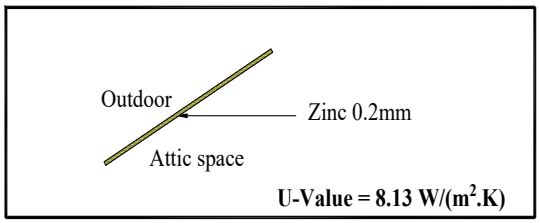

(a1) Roof existing (N, C5)

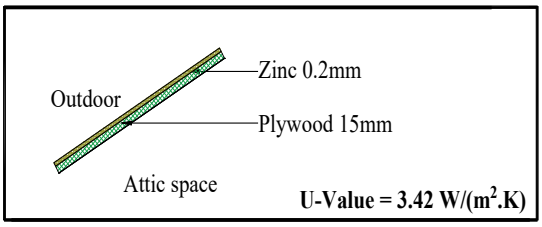

(a2) Roof insulation 1 (C6)

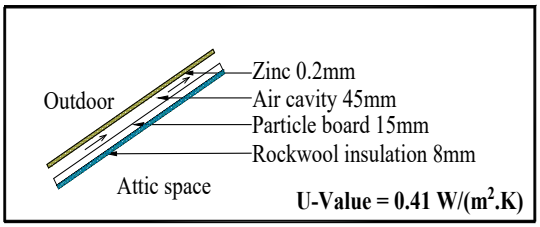

(a3) Roof insulation 2 (C7, C8)

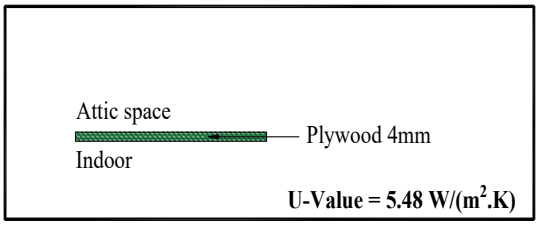

(b1) Ceiling existing (N, C5)

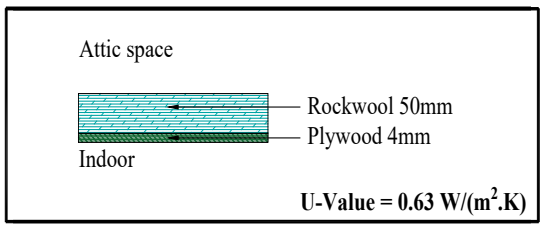

(b2) Ceiling insulation 1 (C6)

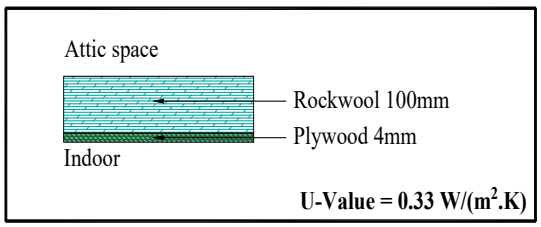

(b3) Ceiling insulation 2 (C7, C8)

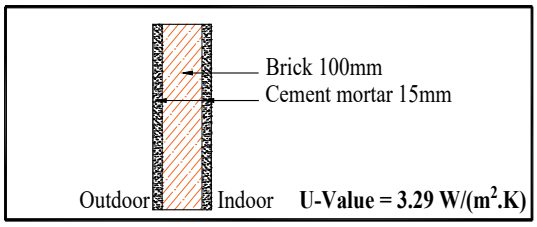

(c1) External wall existing (N)

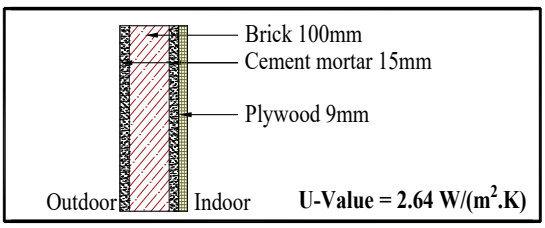

(c2) External wall insulation 1 (C5, C6, C7)

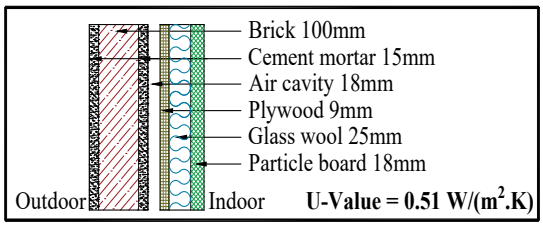

(c3) External wall insulation 2 (C8)

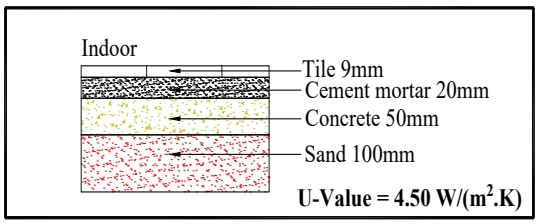

(d1) Floor existing (N, C1 – C24)

Figure 4.7. Insulation improvement plan.

Table 4.5 Simulated cases configuration

Cases	Louver area		Insulation level					Remarks
	Louver 1 [m²]	Louver 2 [m²]	No Insulation	Insulation 1	Insulation 2	Insulation 3	Insulation 4	
N	0.32	0.19	√					Existing the test house
Case 1	0.16	0.095	√					Reduce louver area (louver area existing x 0.5)
Case 2	0.08	0.048	√					Reduce louver area (louver area existing x 0.25)
Case 3	0.64	0.38	√					Enlarge louver area (louver area existing x 2)
Case 4	1.28	0.76	√					Enlarge louver area (louver area existing x 4)
Case 5	0.32	0.19		√				Insulation 1 (a1, b1, c2, d1)
Case 6	0.32	0.19			√			Insulation 2 (a2, b2, c2, d1)
Case 7	0.32	0.19				√		Insulation 3 (a3, b3, c2, d1)
Case 8	0.32	0.19					√	Insulation 4 (a3, b3, c3, d1)
Case 9	0.16	0.095		√				Combined 1 (case 1 and case 5)
Case 10	0.16	0.095			√			Combined 2 (case 1 and case 6)
Case 11	0.16	0.095				√		Combined 3 (case 1 and case 7)
Case 12	0.16	0.095					√	Combined 4 (case 1 and case 8)
Case 13	0.08	0.048		√				Combined 5 (case 2 and case 5)
Case 14	0.08	0.048			√			Combined 6 (case 2 and case 6)
Case 15	0.08	0.048				√		Combined 7 (case 2 + case 7)
Case 16	0.08	0.048					√	Combined 8 (case 2 + case 8)
Case 17	0.64	0.38		√				Combined 9 (case 3 + case 5)
Case 18	0.64	0.38			√			Combined 10 (case 3 + case 6)
Case 19	0.64	0.38				√		Combined 11 (case 3 + case 7)
Case 20	0.64	0.38					√	Combined 12 (case 3 + case 8)
Case 21	1.28	0.76		√				Combined 13 (case 4 + case 5)
Case 22	1.28	0.76			√			Combined 14 (case 4 + case 6)
Case 23	1.28	0.76				√		Combined 15 (case 4 + case 7)
Case 24	1.28	0.76					√	Combined 16 (case 4 + case 8)

4.2. Development-based simulation model and simulation validation

This study calculated the indoor environmental conditions using a dynamic simulation program termed THERB [13]. As previous mention in chapter 3, this program is an official software approved by the Japanese government with nationwide application. It can calculate the time series of indoor temperatures, humidity, and heating/cooling loads for the entire building, considering the complete heat, air, and moisture (HAM) features with the network airflow model (NAF).

4.2.1. Discharge coefficient

The discharge coefficient (Cd) takes into account the impact of flow contraction and frictional losses when fluid passes through an opening. Typically, a value of Cd = 0.6 is commonly used and can be determined mathematically for a sharp-edged orifice opening [14, 15]. Awbi et al. demonstrated that the value of the discharge coefficient varies depending on the characteristics of the opening's geometry and the pressure difference caused by external factors [16].

Since the louver openings in the test house possess a specific and unidentified geometry as mentioned in the references, this study employed computational fluid dynamics (CFD) to examine the discharge coefficients. The numerical analysis of Computational Fluid Dynamics (CFD) can be categorized into different approaches, including finite difference, finite element, spectrum, and finite volume methods. For this particular study, a finite volume method was utilized for the numerical analysis. This approach involves partitioning the computational domain into multiple small volumes referred to as control volumes. The primary objective of this method is to ensure the conservation of various physical quantities within these control volumes. To achieve this, the balance equation for each physical quantity is discretized and integrated within each control volume. The unknown value of the quantity is assigned at the center of each control volume, and based on this value, the inflow and outflow of physical quantities at the boundaries of each control volume are determined.

Additionally, a solution is obtained by applying a discretization formula. The characteristics of the wind in close proximity to the Earth's surface undergo variations due to the presence of objects on the ground. The average wind velocity near the ground surface diminishes or intensifies as it extends vertically upwards. This alteration in wind speed is influenced by the characteristics of the ground surface. The Building Load Guidelines established by the Architectural Institute of Japan [17] define this value as the correlation between the ground surface condition and the power index, based on observations of natural wind and the roughness of the ground surface.

Moreover, the inflow boundary condition for the numerical simulation of the flow coefficients, including the inflow wind speed, turbulence energy dissipation rate, and turbulence energy, is shown in Figure 4.8. The analysis conditions of the calculated discharge coefficients for louver openings are shown in Table 4.6.

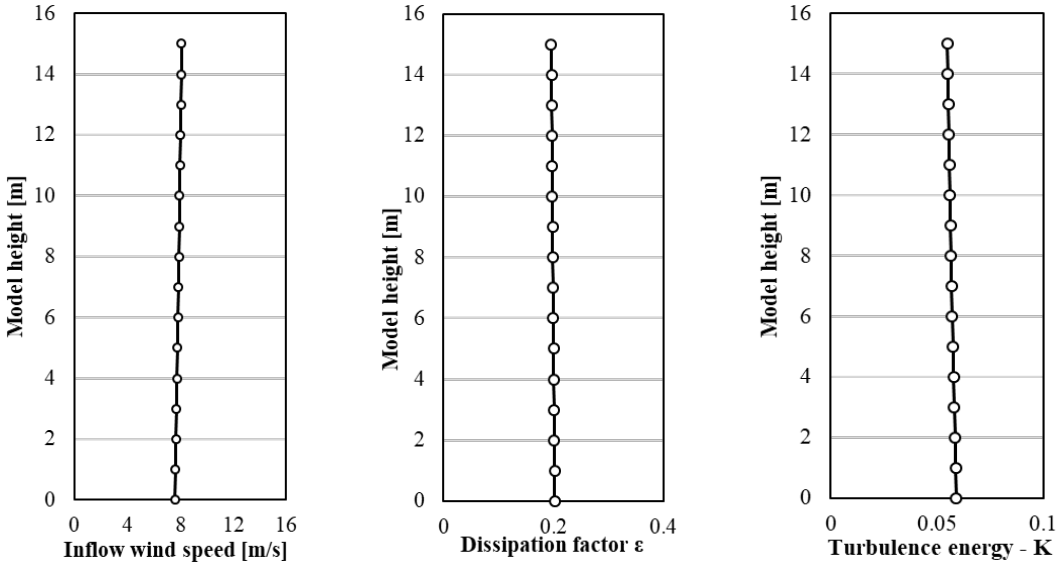

(a) (b) (c)

Figure 4.8. Inflow boundary condition (a) inflow wind speed, (b) turbulence energy dissipation rate, and (c) turbulence energy.

Table 4.6. Analysis conditions

Content	Detail
Analysis software	STAR-CCM+
Analysis domain	50m (x) x 90m (y) x 25m (z)
Number of meshes	3,300,000
Inflow boundary condition	1/5 power law
Outflow boundary condition	Gradient 0 at the outflow boundary
Air/Side Boundary Conditions	Slip
Wall conditions	Floor surface: wall boundary condition based on wall function
	Target building: wall boundary condition based on wall function
Calculation algorithm	SIMPLE method
Turbulence model	Realizable k-ε model

Therefore, the discharge coefficients are averaged to obtain the result: Louvers 1 and 2 are 0.57 and 0.68, respectively. In addition, the values of the discharge coefficients are used as input data, which are building data, in the numerical simulation software.

4.2.2. Wind pressure coefficient

The wind pressure coefficient (Cp) expresses the degree to which a building receives wind force and describes the pressure distribution on the building surfaces. The value of the wind pressure coefficient depends on a wide range of parameters, including building shape, envelope detailing, position on the façade, wind speed, wind direction, and turbulence intensity.

Cóstola et al. (2009) identified two main sources of Cp data. The primary sources include full-scale measurements, wind-tunnel measurements, and CFD simulations, and the secondary sources include databases and analytical models. In this study, the wind pressure coefficients utilize the database for natural ventilation design that is compiled into CP-X [19].

This database employs a wind tunnel experiment to determine the wind pressure coefficients, including those of detached houses that are similar to that of the test house. The standard values of the wind pressure coefficients of the test house according to reference is shown in Figure 4.9. They are used as the input values of the wind pressure coefficients in the room data of the numerical simulation.

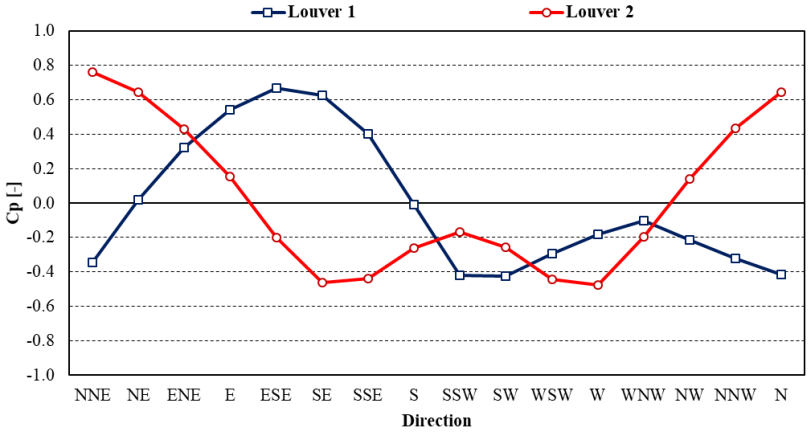

Figure 4.9. Wind pressure coefficients

4.3. Simulation accuracy verification

The temperature and relative humidity of the test houses located in Lhokseumawe, Indonesia, were measured during the peak of the dry season for 26 days, from June 20 to July 15, 2022. Outdoor measurement data and Indonesia meteorological standard data were used for the simulation. The accuracy of the simulation was verified by comparing the simulated and measured results. Figure 4.10 compares the simulated and measured results of the temperature and humidity of the living rooms. Two error indicators, mean bias error (MBE) and coefficient of variation of the root mean square error (CV(RMSE)), were calculated for the base case according to reasonable standards and guidelines, including ASHRAE [20], the measurement and verification of federal energy projects [21], and the international performance measurement and verification protocol [22].

The MBE and CV(RMSE) [23, 24] were calculated using Equations (4.1) and (4.2). The calibration criteria of the reasonable standards and guidelines and the two calculated error indicators for the base-case calibration are listed in Table 4.7. The measured values were expressed at 10-min intervals using dotted lines.

The results show that the predicted MBEs and cross-validation root mean square errors (CV(RMSE)s) were within the acceptable range, as defined by the validation criteria set by ASHRAE guidelines and IPMVP, with no more than 5% deviation, respectively. These findings suggest that THERB for HAM with NAF can accurately predict indoor air temperatures in naturally ventilated houses.

$$\mathrm{MBE} = \frac{\sum_{i=1}^{N}(M_i - S_i)}{N} \tag{4.1}$$

$$\mathrm{CV(RMSE)} = \frac{\sqrt{\sum_{i=1}^{N}((M_i \cdot S_i)^2/N)}}{\frac{\sum_{i=1}^{N} M_i}{N}}, \tag{4.2}$$

where Mi and Si are the measured and simulated data at an instant i, respectively, and N is the number of calibration values.

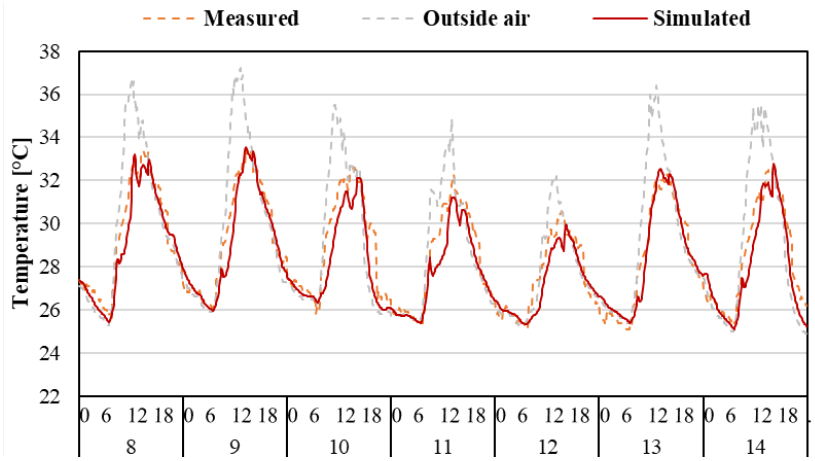

(a)

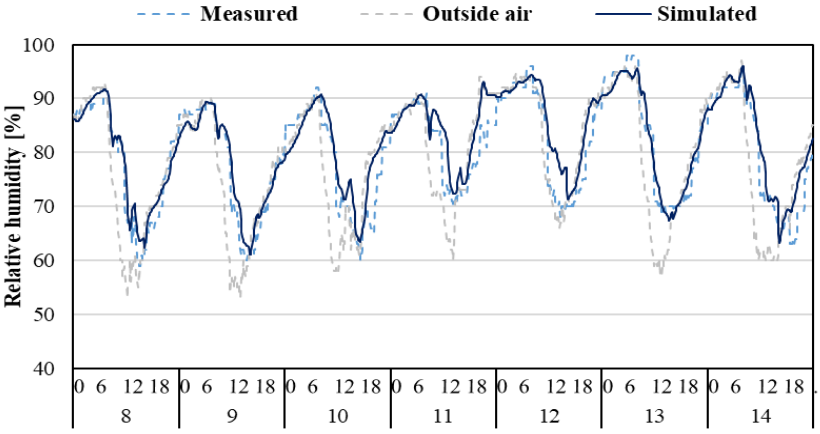

(b)

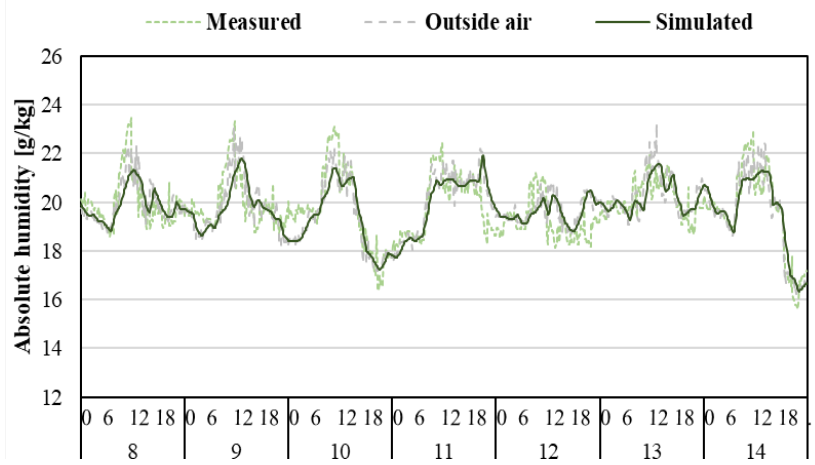

(c)

Figure 4.10. Comparison of the measured and simulated values: (a) temperature, (b) relative humidity, and (c) absolute humidity

Table 4.7. Calibration criteria and prediction error

Indicator	Prediction error			Standard		
	Temperature	RH	Abs. humidity	ASHRAE	IPMVP	FEMP
MBE	2.06%	3.05%	3.22%	± 10%	± 10%	± 5%
CV (RMSE)	2.69%	3.97%	4.01%	< 30%	< 30%	< 20%

4.4. Simulation result and discussion

4.4.1. Louver improvement

Various louver openings in the living room with an area ranging from 0.08 to 0.76 m^2 are evaluated, as shown in Figure 4.11. The tendency of hourly air temperature slightly decreased with large louver areas at night from 10:00 pm to 08:00 am, by approximately 0.3 °C. However, the situation was considerably reversed during the daytime, when the temperature increased by 1 °C for large louvers. Meanwhile, the hourly indoor relative humidity increased at night by approximately 86% at peak conditions and dropped significantly by 56% during the day for the largest louver. However, the situation reversed for the lowest louver area. In addition, the absolute humidity slightly fluctuated for all louvers tested, where the highest absolute humidity occurred at 10.00 pm by approximately 19.4 g/kg' and dropped significantly until 18 g/kg' during daytime.

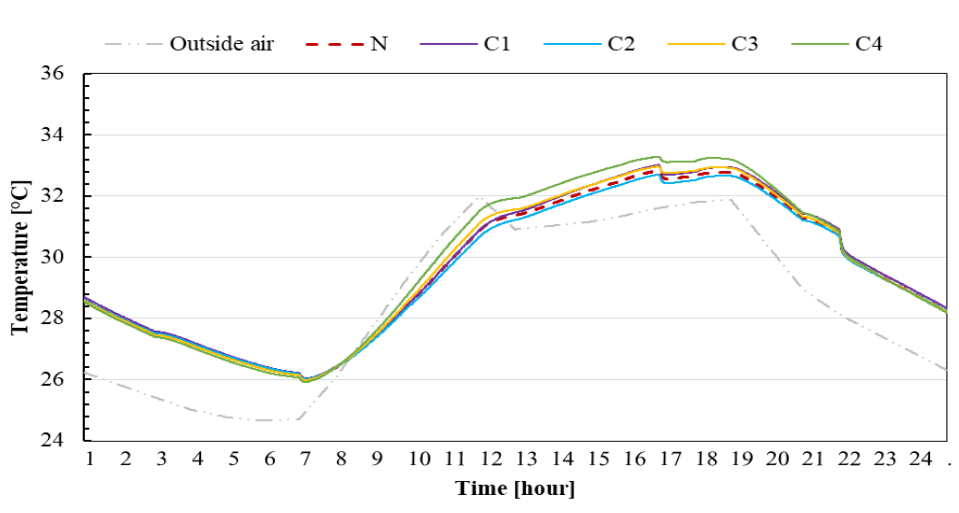

(a)

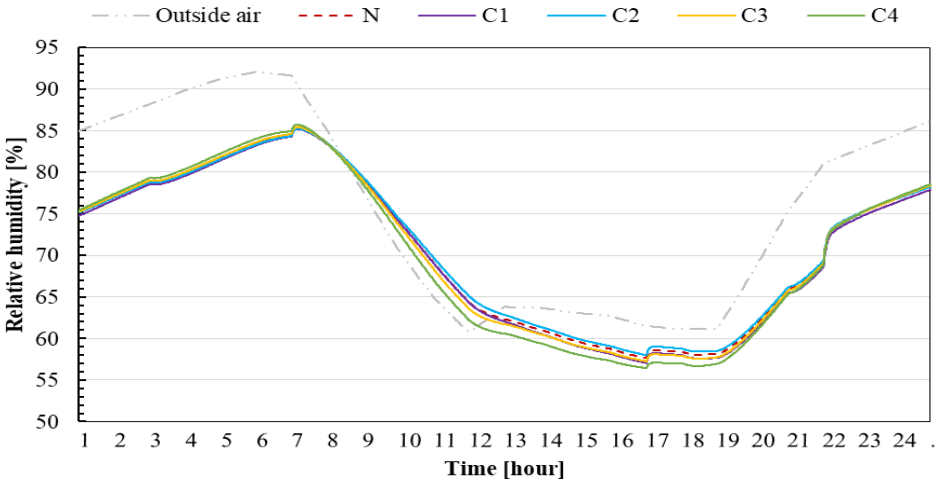

(b)

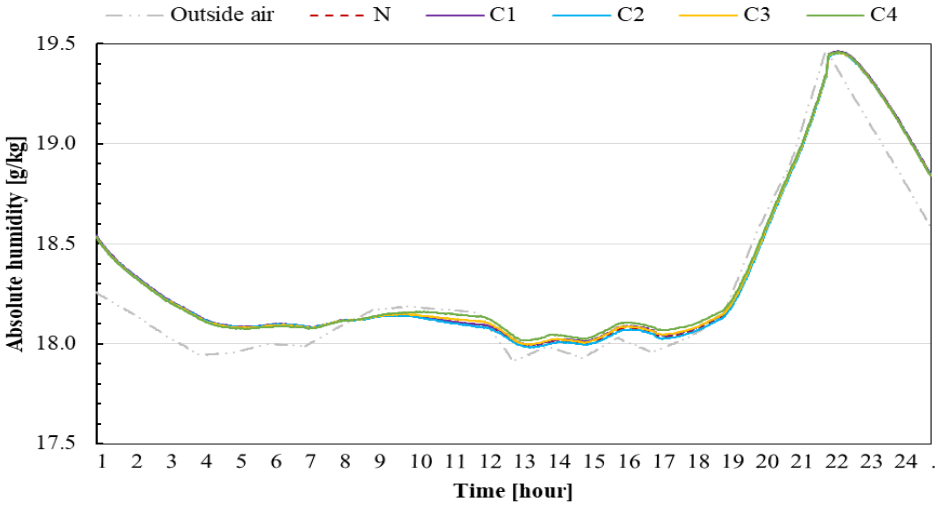

(c)

Figure 4.11. Comparison of living room conditions by louvers cases developed: (a) temperature, (b) relative humidity, and (c) absolute humidity

The daily cooling loads of the louver area cases are calculated, as shown in Figure 4.11. Unlike in the existing case, the lowest cooling load is classified in Case 2 with a value of 9.98 kWh (92.9%). However, when we enlarge the opening areas (C3 and C4), the daily cooling loads increase gradually until 14.25 kWh (132.7%).

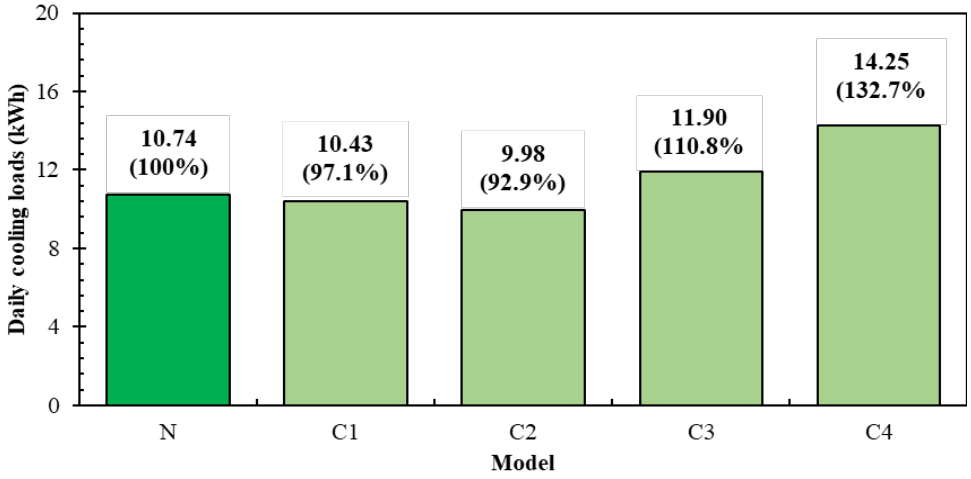

Figure 4.12. Daily cooling loads of louvers cases

4.4.2. Insulation improvement

The insulation improvement plan in this study is optional for maintaining indoor environment conditions. The impacts of insulation under external wall insulation, roof insulation, ceiling insulation, and their combinations were investigated. Figure 4.15 compares the hourly indoor temperature, relative humidity, and absolute humidity between the existing and developed cases. The hourly indoor temperature obtained by adding insulation level 1 reduces the temperature from 0.5 to 0.9 °C at night and during the day at peak conditions. However, combining the insulations of the external wall, roof, and ceiling (level 4) significantly reduces the indoor temperature from 1.0 to 2.1 °C compared with the existing case at peak conditions. However, relative humidity significantly decreased to 7% when the temperature increased at night and during the daytime. Moreover, the absolute humidity slightly fluctuated according to the cases developed, where the maximum value was introduced at night at 19.8 g/kg and dropped extremely until 17.8 g/kg during the day.

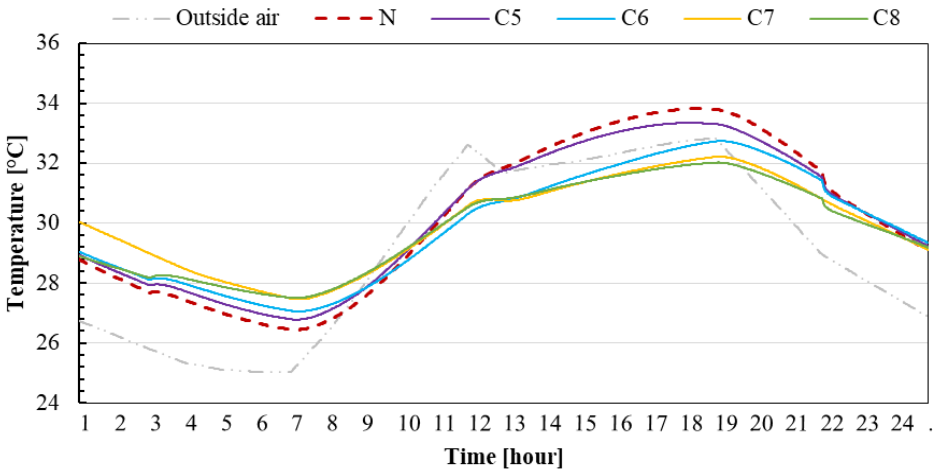

(a)

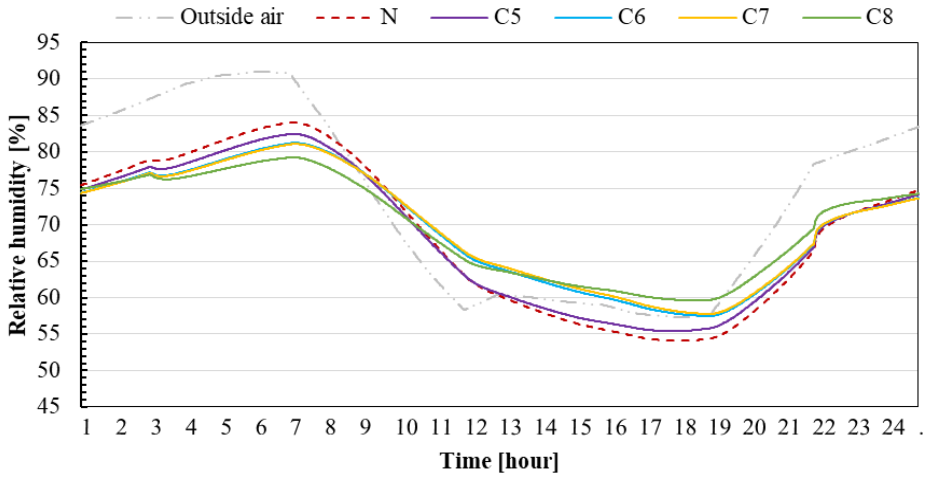

(b)

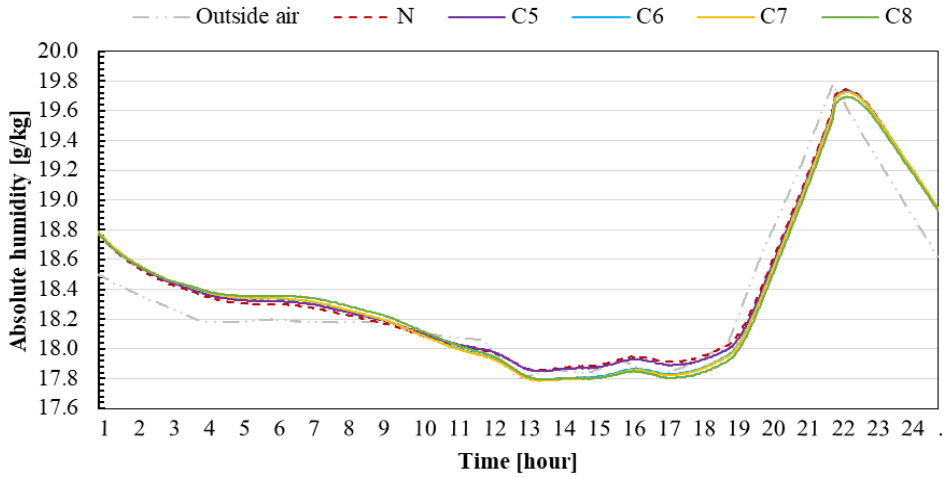

(c)

Figure 4.13. Comparison of living room conditions by insulation cases developed: (a) temperature, (b) relative humidity, and (c) absolute humidity

In addition, the daily cooling loads of the target room are gradually reduced by various additional insulation levels, as shown in Figure 4.18. The daily cooling loads are decreased on insulation level 4 (Case 8) by approximately 16.4% compared with that of the existing case.

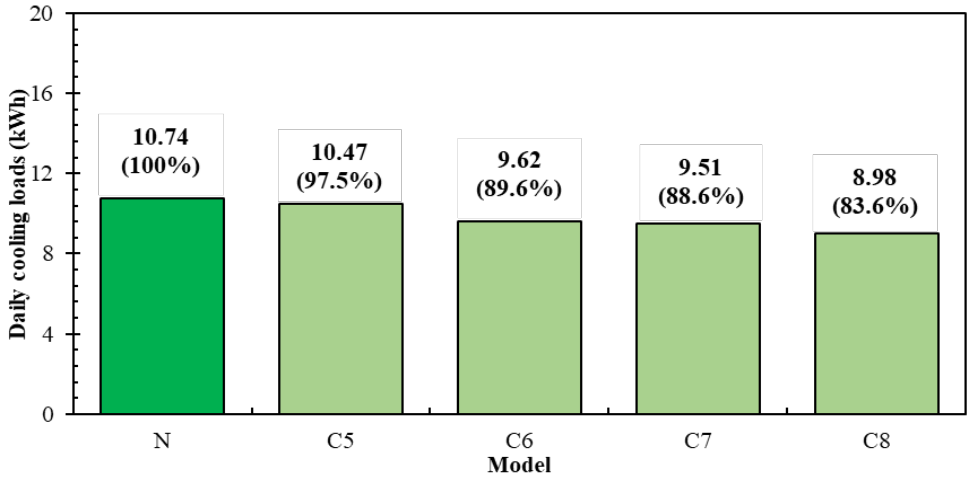

Figure 4.14. Daily cooling loads of insulation cases

4.4.3. Combined model

The combined model between the louver opening area and various levels of insulation was analyzed for 16 simulated cases. The impacts of various cases on the indoor environment are identified, as shown in Figure 4.19. The hourly indoor temperature is reduced from 1.6 to 2.2 °C compared with existing cases at peak daytime conditions. The relative humidity is decreased from 6% to 8% and stabilizes at 60% during the day and 78% at night. The absolute humidity presents a similar condition with the insulation cases developed, where a maximum of 19.7 g/kg' occurred at 10.00 pm and dropped extremely until 17.75 g/kg during the day.

Therefore, this study confirms that combining the louver opening area and insulation by reducing the louver area of the existing case and adding insulation of level 4 on an external wall, roof, and ceiling can effectively maintain indoor environment conditions compared with the existing case. In addition, the daily cooling loads of the target room for the combined cases show various results for the entire case, as illustrated in Table 4.8. The result shows that optimizing an improvement plan by combining the louver opening area (C2) and adding an insulation level 4 (C8) declines the daily cooling loads by 25.09% compared with the existing case.

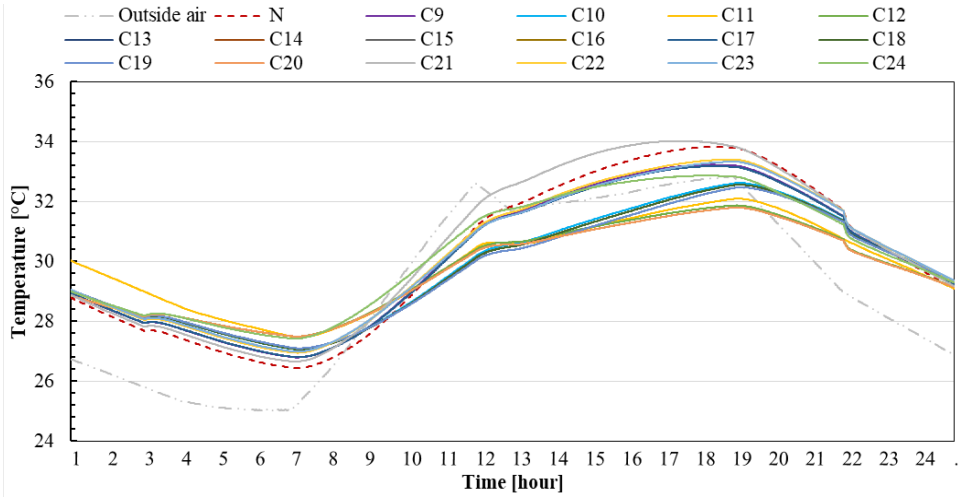

(a)

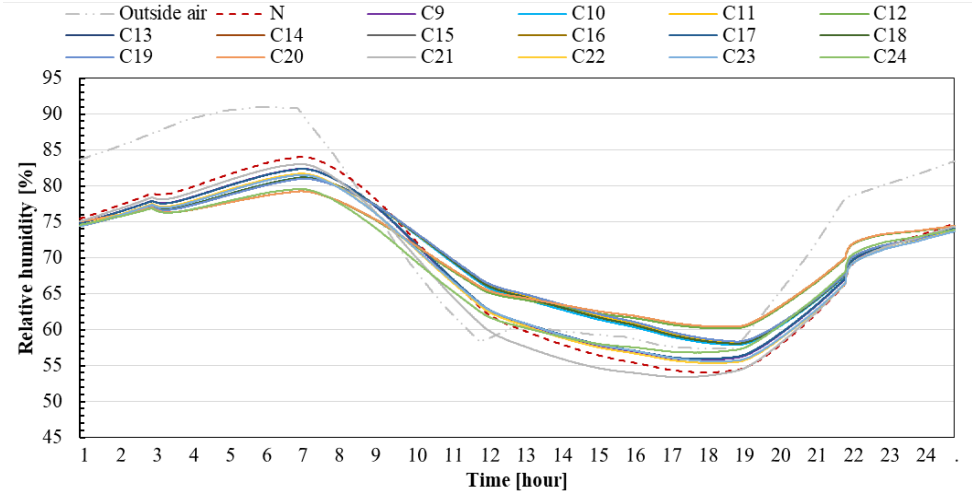

(b)

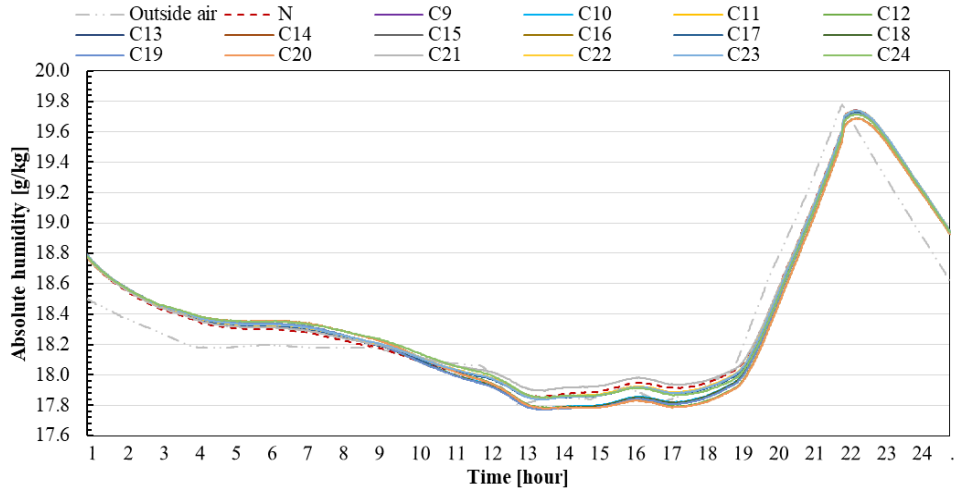

(c)

Figure 4.15. Comparison of living room conditions by combined cases developed: (a) temperature, (b) relative humidity, and (c) absolute humidity

Table 4.8. Daily cooling load of the developed cases in selected area

Cases	Parameters	Daily cooling loads	
		kWh	%
N	Existing Model	10.74	100.00
Case 1	Reduce louvre 1	10.43	97.18
Case 2	Reduce louvre 2	9.98	92.98
Case 3	Enlarge louvre 1	11.90	110.88
Case 4	Enlarge louvre 2	14.25	132.77
Case 5	Insulation 1	10.47	97.53
Case 6	Insulation 2	9.63	89.67
Case 7	Insulation 3	9.51	88.60
Case 8	Insulation 4	8.98	83.67
Case 9	Case 1 + Case 5	9.94	92.57
Case 10	Case 1 + Case 6	9.08	84.54
Case 11	Case 1 + Case 7	8.94	83.24
Case 12	Case 1 + Case 8	8.36	77.88
Case 13	Case 2 + Case 5	9.68	90.21
Case 14	Case 2 + Case 6	8.75	81.48
Case 15	Case 2 + Case 7	8.63	80.41
Case 16	Case 2 + Case 8	8.04	74.91
Case 17	Case 3 + Case 5	11.70	108.97
Case 18	Case 3 + Case 6	10.93	101.79
Case 19	Case 3 + Case 7	10.80	100.60
Case 20	Case 3 + Case 8	10.32	96.13
Case 21	Case 4 + Case 5	14.05	130.89
Case 22	Case 4 + Case 6	13.35	124.39
Case 23	Case 4 + Case 7	13.27	123.64
Case 24	Case 4 + Case 8	12.88	120.01

Figure 4.16 – 4.18 show the cumulative graphs of the temperature and the temperature distribution of the tested room from July 1 to 15 based on louver improvement, insulation improvement and combined. The cumulative graph indicates the ratio of data when the temperature value is higher than temperature corresponding to x-axis among the data within the period. For the louver improvement as shown in Figure 4.16(a) and 4.16(b), the distribution graph reveals that the distributions of temperature in case 2 is lower than other cases tested. In particular, the distribution occupies the highest ratio at 29-31 °C. In cumulative graph, the cumulative rate of more than 50% of the living room temperature indicates about 29 °C in case 2 while other cases is about 30 °C - 31 °C. Based on insulation improvement as shown in Figure 4.17(a) and 4.17(b), the distribution graph indicates that the distribution of inside temperature in case 8 is the lowest among of cases tested, followed by case 7, case 6, case 5, and case N. In addition, according to combination cases between louver openings and insulation improvement (Figure 4.18(a) and 4.18(b)), the distribution of inside temperature in case 16 and 20 is the lower than all of the cases tested. This result indicates that optimizing insulation and adequate openings area is significance against indoor temperature for naturally ventilated house.

Figures 4.19 to 4.21 display the distribution of relative humidity in an indoor living room, as well as the cumulative graph of relative humidity from July 1 to 15. The distribution graph reveals that in case 2, the relative humidity is higher compared to the other cases. The louver improvement results in case 2 having the highest distribution ratio of 70%, followed by case 1, case N, case 3, and case 4. The cumulative graph shows that the relative humidity exceeds 50% for approximately 70% to 75% of the time, as depicted in Figure 4.19(a) and 4.19(b). Furthermore, Figure 4.20(a) and Figure 4.20(b) illustrate the impact of insulation improvement, with case 8 exhibiting the highest relative humidity, followed by case 7, case 6, case 5, and case N. Additionally, the combination of insulation and louver ratio improvements is demonstrated in Figure 4.21(a) and 4.21(b), where case 16 and case 20 show a higher relative humidity distribution compared to the other cases. Consequently, the level of insulation and the ratio of louver openings significantly influence the distribution and cumulative relative humidity, and the combined improvement of insulation and louver ratio contributes to better indoor temperature and relative humidity.

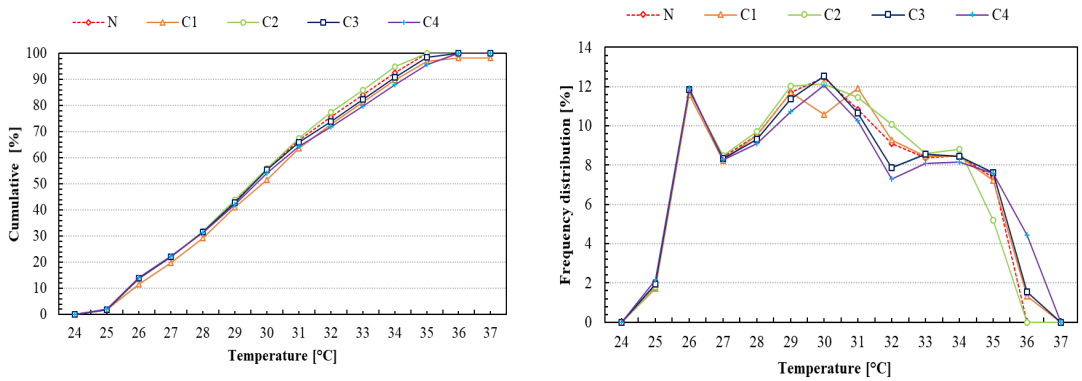

(a) (b)

Figure 4.16 Temperature of living room in July according to louver improvement: (a) cumulative rate (b) frequency distribution

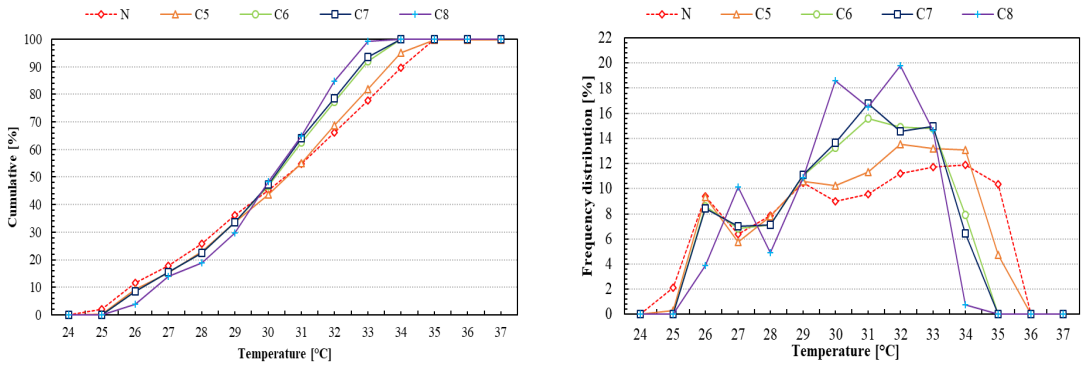

(a) (b)

Figure 4.17. Temperature of living room in July according to insulation improvement: (a) cumulative rate (b) frequency distribution

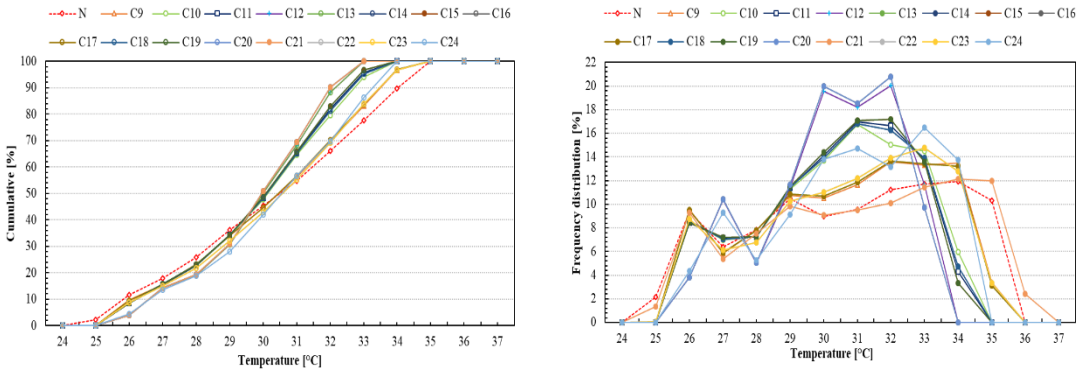

(a) (b)

Figure 4.18. Temperature of living room in July according to combined improvement: (a) cumulative rate (b) frequency distribution

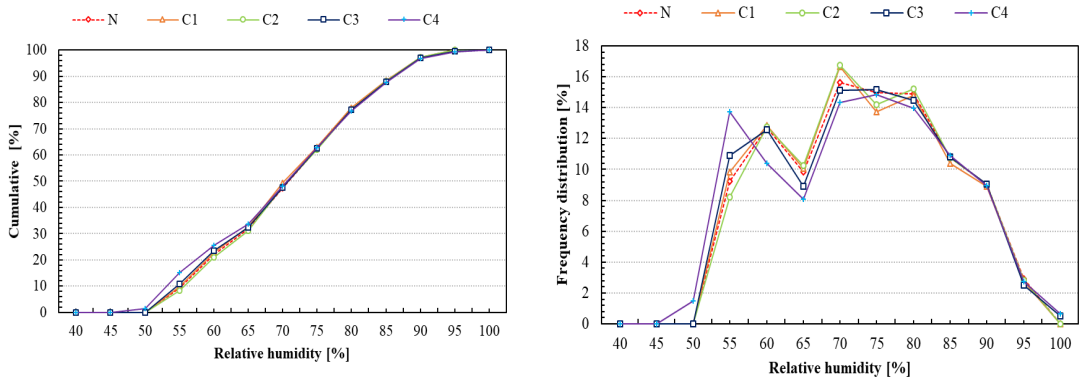

(a) (b)

Figure 4.19 Relative humidity of living room in July according to louver improvement: (a) cumulative rate (b) frequency distribution

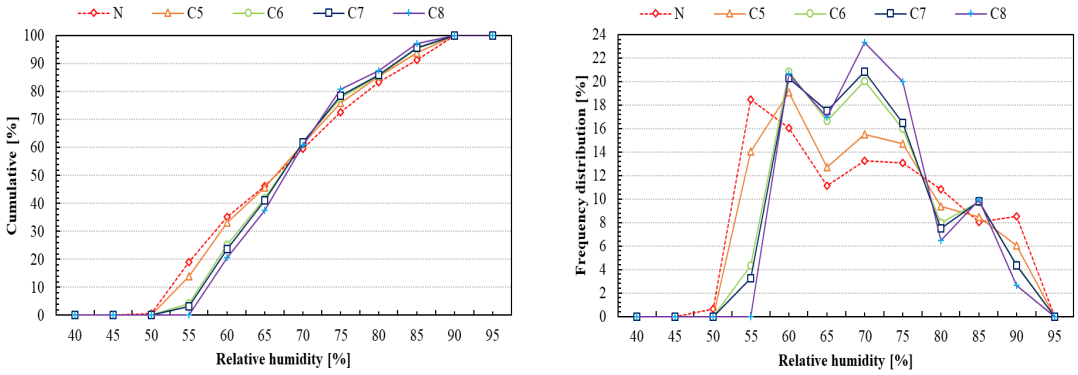

(a) (b)

Figure 4.20 Relative humidity of living room in July according to insulation improvement: (a) cumulative rate (b) frequency distribution

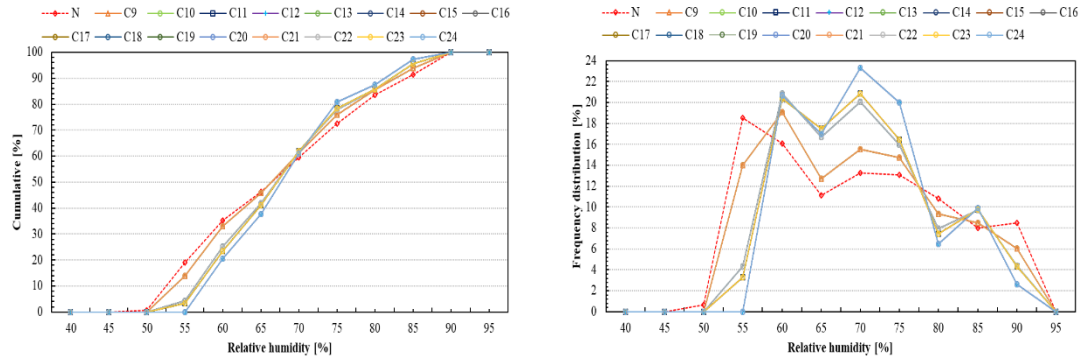

(a) (b)

Figure 4.21. Relative humidity of living room in July according to combined improvement: (a) cumulative rate (b) frequency distribution

4.4.4. Ventilation rate

The impact of ventilation rate on indoor temperature in a naturally ventilated house is an important consideration. Increasing the ventilation rate can effectively eliminate surplus heat from the indoor environment. In addition, adequate ventilation enables the exchange of indoor and outdoor air, facilitating the dissipation of heat and enhancing air circulation. As a result, this study includes the calculation of the ventilation rate for the existing louver opening ratio (referred to as type N) to assess its impact on the indoor temperature.

Figure 4.22 shows the tendency of ventilation rate and inside/outside temperature. Figure 4.23-4.24 present temperature difference and the relationship of the ventilation rate against inside temperature. During the daytime (08:00 am – 02:00 pm), the ventilation rate starts to increase gradually, and the inside air temperature is lower than the outside air temperature. However, as the ventilation rate decreases gradually (at 02:00 pm), the inside temperature becomes higher than the outside temperature. This is followed by a decrease in the ventilation rate. Therefore, this study reveals that the inside temperature is mostly affected by the ventilation rate. Specifically, a higher openings ratio leads to a higher ventilation rate and a lower inside temperature during the daytime. Moreover, the relationship between inside temperature against ventilation rate is significant in terms of the change of ventilation rate of louvre openings, which the coefficient determination (R^2) is 0.7987.

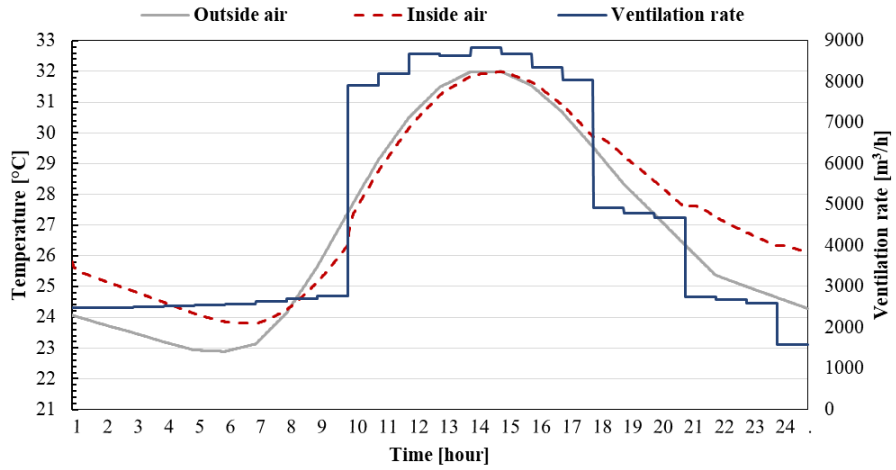

Figure 4.22. Temperature of living room in July according to cases developed

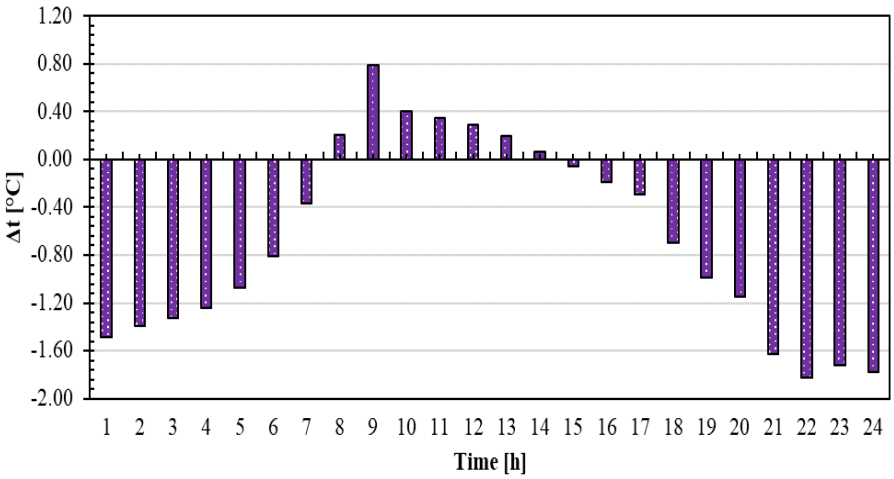

Figure 4.23. Temperature difference

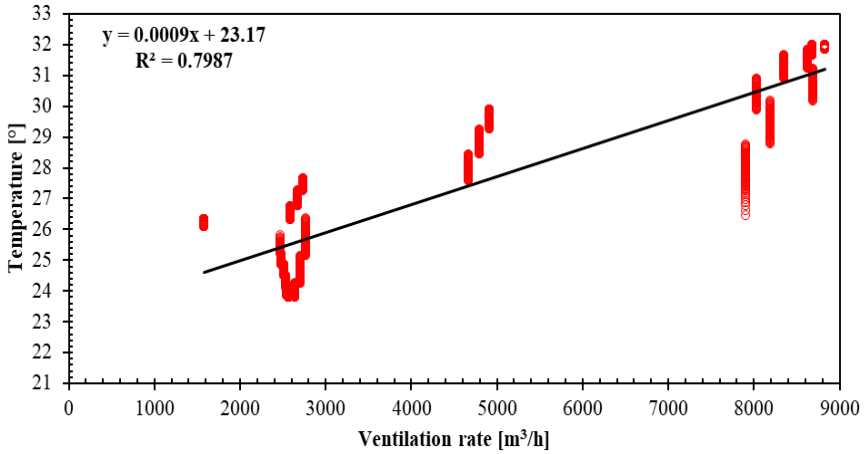

Figure 4.24. Relationship inside temperature against ventilation rate

4.4.5. Annual cooling loads on the target cities

The annual cooling loads for the existing and improved cases of the 13 cities are analyzed, as illustrated in Table 4.9. Notably, a large amount of data is described in a part, and those corresponding to the optimal level of case examination are highlighted. This study reports that the maximum annual cooling loads for existing cases are classified in Semarang at approximately 24.93 GJ/year, followed by Surabaya at 22.93 GJ/year and Bima at 22.58 GJ/year. The other cities are evaluated as averaging 15.54 GJ/year, with a minimum occurring at Kerinci.

By modifying the louver opening area, the annual cooling loads decreased approximately by14.26% in Bima, followed by Madura at 13.66%, Kerinci at 12.90%, Semarang at 10.69 %, and Gorontalo at 9.96 %. The average decrease in annual cooling loads for all cities simulated is 1.47 GJ/year (9.48 %) compared with the existing case.

Meanwhile, adding the insulation level into the test house to control annual cooling loads is better than modifying louver openings, approximately 1.80 GJ/year (12%) for the entire cities. The annual cooling loads of Kerinci is decreased by 31.03%, followed by Gorontalo at 16.84%, Banda Aceh at 16.80%, and Lhokseumawe at 16.33% compared to each existing case.

Moreover, combination case 16 (C16) shows the best optimization of energy consumption reduction for all simulated cases. The maximum annual cooling loads is decreases by approximately 6.55 GJ/year (29%) in Bima, followed by Madura 5.39 GJ/year (23.93%), Semarang at 5.08 GJ/year (20.37%), and Gorontalo at 4.19 GJ/year (27.97%) compared with existing cases. Notably, the estimation of total annual cooling by applying the optimizing cases of this study was 155.30 GJ/year, and it could save the annual cooling load by 46.63 GJ/year (23.09%) for the entire simulated cities compared with the existing case.

Table 4.9. Annual cooling load of the developed cases for 13 target cities

Cases	Para-meters	Annual Thermal load per unit of living room (63.37 m³) for each city ((GJ/year) and (%))												
		Lhokseumawe	Banda Aceh	Kerinci	Cilacap	Sumbawa Besar	Waingapu	Surabaya	Balikpapan	Maluku Utara	Semarang	Gorontalo	Bima	Madura
N	Existing Model	14.11	12.69	1.64	11.45	15.35	6.28	22.93	18.04	14.52	24.93	14.97	22.58	22.50
		(100%)	(100%)	(100%)	(100%)	(100%)	(100%)	(100%)	(100%)	(100%)	(100%)	(100%)	(100%)	(100%)
Case 1	Reduce louvre 1	13.71	12.42	1.60	11.05	14.48	6.15	22.08	17.71	14.06	23.45	14.26	20.50	20.38
		(97%)	(98%)	(97%)	(97%)	(94%)	(98%)	(96%)	(98%)	(97%)	(94%)	(95%)	(91%)	(91%)
Case 2	Reduce louvre 2	13.12	11.83	1.43	10.54	13.66	5.83	21.24	17.14	13.54	22.27	13.48	19.36	19.43
		(93%)	(93%)	(87%)	(92%)	(89%)	(93%)	(93%)	(95%)	(93%)	(89%)	(90%)	(86%)	(86%)
Case 3	Enlarge louvre 1	15.64	13.94	1.98	13.19	17.73	7.07	25.67	19.49	16.10	29.43	17.28	26.33	26.78
		(111%)	(110%)	(120%)	(115%)	(115%)	(113%)	(112%)	(108%)	(111%)	(118%)	(115%)	(117%)	(119%)
Case 4	Enlarge louvre 2	18.73	16.63	2.58	16.28	22.35	8.61	30.99	22.60	19.40	37.12	21.40	32.96	33.36
		(133%)	(131%)	(157%)	(142%)	(146%)	(137%)	(135%)	(125%)	(134%)	(149%)	(143%)	(146%)	(148%)
Case 5	Insulation 1	13.76	12.31	1.51	11.26	15.07	6.17	22.51	17.73	14.20	24.67	14.58	22.08	22.28
		(98%)	(97%)	(92%)	(98%)	(98%)	(98%)	(98%)	(98%)	(98%)	(99%)	(97%)	(98%)	(99%)
Case 6	Insulation 2	12.65	11.37	1.32	10.38	14.12	5.70	21.48	16.91	13.50	23.60	13.32	20.55	21.16
		(90%)	(90%)	(81%)	(91%)	(92%)	(91%)	(94%)	(94%)	(93%)	(95%)	(89%)	(91%)	(94%)
Case 7	Insulation 3	12.50	11.24	1.22	10.32	14.01	5.66	21.26	16.65	13.44	23.42	13.08	20.38	21.00
		(89%)	(89%)	(74%)	(90%)	(91%)	(90%)	(93%)	(92%)	(93%)	(94%)	(87%)	(90%)	(93%)
Case 8	Insulation 4	11.80	10.56	1.13	9.82	13.44	5.38	20.60	16.02	12.92	22.76	12.45	19.54	20.38
		(84%)	(83%)	(69%)	(86%)	(88%)	(86%)	(90%)	(89%)	(89%)	(91%)	(83%)	(87%)	(91%)
Case 9	C1+C5	13.06	11.75	1.35	10.62	13.91	5.87	21.42	17.12	13.51	22.88	13.58	19.68	20.00
		(93%)	(93%)	(82%)	(93%)	(91%)	(93%)	(93%)	(95%)	(93%)	(92%)	(91%)	(87%)	(89%)
Case 10	C1+C6	11.93	10.70	1.18	9.93	12.94	5.37	20.23	16.18	12.78	21.74	12.41	18.05	18.80
		(85%)	(84%)	(72%)	(87%)	(84%)	(86%)	(88%)	(90%)	(88%)	(87%)	(83%)	(80%)	(84%)
Case 11	C1+C7	11.74	10.59	1.13	9.63	12.81	5.33	20.10	15.91	12.72	21.55	12.03	17.86	18.65
		(83%)	(83%)	(69%)	(84%)	(83%)	(85%)	(88%)	(88%)	(88%)	(86%)	(80%)	(79%)	(83%)
Case 12	C1+C8	10.99	9.87	0.96	9.12	12.20	5.02	19.39	15.26	12.17	20.84	11.33	16.98	17.98
		(78%)	(78%)	(58%)	(80%)	(79%)	(80%)	(85%)	(85%)	(84%)	(84%)	(76%)	(75%)	(80%)
Case 13	C2+C5	12.73	11.50	1.33	10.29	13.32	5.70	20.90	16.77	13.23	21.98	13.08	18.90	19.22
		(90%)	(91%)	(81%)	(90%)	(87%)	(91%)	(91%)	(93%)	(91%)	(88%)	(87%)	(84%)	(85%)
Case 14	C2+C6	11.49	10.44	1.12	9.45	12.31	5.22	19.71	15.77	12.70	20.79	11.72	17.24	18.01
		(81%)	(82%)	(68%)	(82%)	(80%)	(83%)	(86%)	(87%)	(87%)	(83%)	(78%)	(76%)	(80%)
Case 15	C2+C7	11.34	10.27	1.04	9.26	12.21	5.17	19.52	15.54	12.37	20.60	11.50	16.96	17.82
		(80%)	(81%)	(63%)	(81%)	(80%)	(82%)	(85%)	(86%)	(85%)	(83%)	(77%)	(75%)	(79%)

Case 16	C2+C8	10.57	9.53	0.92	8.69	11.57	4.85	18.79	14.87	11.81	19.85	10.78	16.03	17.12
		(75%)	(75%)	(56%)	(76%)	(75%)	(77%)	(82%)	(82%)	(81%)	(80%)	(72%)	(71%)	(76%)
Case 17	C3+C5	15.37	13.60	1.87	13.00	17.51	6.94	25.38	19.21	15.82	29.15	17.19	25.85	26.51
		(109%)	(107%)	(114%)	(113%)	(114%)	(111%)	(111%)	(106%)	(109%)	(117%)	(115%)	(115%)	(118%)
Case 18	C3+C6	14.36	12.85	1.66	12.40	16.60	6.49	24.48	18.33	15.46	28.23	16.01	24.46	25.51
		(102%)	(101%)	(101%)	(108%)	(108%)	(103%)	(107%)	(102%)	(106%)	(113%)	(107%)	(108%)	(113%)
Case 19	C3+C7	14.19	12.64	1.61	12.13	16.50	6.46	24.20	18.26	15.13	28.03	15.68	24.31	25.39
		(101%)	(100%)	(98%)	(106%)	(107%)	(103%)	(106%)	(101%)	(104%)	(112%)	(105%)	(108%)	(113%)
Case 20	C3+C8	13.56	12.03	1.49	11.70	16.01	6.21	23.62	17.68	14.65	27.45	15.11	23.56	24.83
		(96%)	(95%)	(91%)	(102%)	(104%)	(99%)	(103%)	(98%)	(101%)	(110%)	(101%)	(104%)	(110%)
Case 21	C4+C5	18.46	16.34	2.45	16.04	22.11	8.49	30.80	22.27	19.13	36.97	21.21	32.55	33.16
		(131%)	(129%)	(149%)	(140%)	(144%)	(135%)	(134%)	(123%)	(132%)	(148%)	(142%)	(144%)	(147%)
Case 22	C4+C6	17.55	15.58	2.27	15.48	21.39	8.10	29.92	21.50	18.79	36.13	19.99	31.43	32.30
		(124%)	(123%)	(138%)	(135%)	(139%)	(129%)	(131%)	(119%)	(129%)	(145%)	(134%)	(139%)	(144%)
Case 23	C4+C7	17.44	15.47	2.20	15.34	21.28	8.06	29.79	21.44	18.56	36.02	19.90	31.17	32.16
		(124%)	(122%)	(134%)	(134%)	(139%)	(128%)	(130%)	(119%)	(128%)	(145%)	(133%)	(138%)	(143%)
Case 24	C4+C8	16.93	14.99	2.07	15.01	20.87	7.87	29.32	20.99	18.18	35.56	19.50	30.61	31.75
		(120%)	(118%)	(126%)	(131%)	(136%)	(125%)	(128%)	(116%)	(125%)	(143%)	(130%)	(136%)	(141%)

4.5. Conclusions

In this study, we proposed an improvement plan by modifying the louver opening area targeting typical Indonesian housing and adding proper insulation to the external wall, roof, and ceiling. The numerical software THERB with NAF was used, and the simulation accuracy was confirmed using field-measured data. A numerical analysis was conducted to examine the improved effect of the developed cases. Additionally, the annual cooling loads for 14 target cities in Indonesia were calculated. A summary of this study is as follows:

- Louver openings affect indoor conditions, where the larger the louver opening area, the higher the indoor temperature during daytime, and the lower the relative humidity. However, the situation was sharply reversed at night, where the temperature slightly decreased for a larger louver compared with the existing case.
- Proper insulation effectively reduced indoor temperature and controlled relative humidity. Compared to the existing model, level 4 of insulation could reduce the indoor temperature and relative humidity to 2.10 °C and 7 % at peak conditions.
- The combination cases improved between various louver openings and insulation could reduce the indoor temperature to 2.2 °C at peak conditions, and relative humidity stable at 60% and 78% during the day and at night.
- Daily cooling loads of the test house in the selected area present a significant decrease in energy consumption by applying the best-improved case of approximately 25.09% compared with the existing case.
- The annual cooling load of each city declined by over 3.33 GJ/year. Therefore, the total annual cooling employing the optimizing cases was 155.30 GJ/year, which could save the annual cooling load of 46.63 GJ/year (23.09%) compared with the existing case.

This study established a plan to improve indoor temperature and reduce the energy consumption of low-income households in tropical climates through a passive approach. This result can be used as a reference not only for Indonesia but also for researchers in tropical countries.

References

[1] BRR, "Monthly Report, Pusdatin BRR, Indonesia," 2008.

[2] L. H. Sari, I. Hasan, M. Irwansyah, and E. Meutia, "an Environmental Assessment of Vernacular Housing in Banda Aceh, Indonesia," Tesa Arsitektur, vol. 15, no. 1, p. 1, 2017.

[3] S. Tong, J. Wen, N. H. Wong, and E. Tan, "Impact of façade design on indoor air temperatures and cooling loads in residential buildings in the tropical climate," Energy Build, vol. 243, p. 110972, 2021.

[4] E. Prianto and P. Depecker, "Optimization of architectural design elements in tropical humid region with thermal comfort approach," Energy Build, vol. 35, no. 3, pp. 273–280, 2003.

[5] H. E. Beck, N. E. Zimmermann, T. R. McVicar, N. Vergopolan, A. Berg, and E. F. Wood, "Present and future köppen-geiger climate classification maps at 1-km resolution," Sci Data, vol. 5, pp. 1–12, 2018.

[6] I. D. G. A. Putra et al., "Development of climate zones for passive cooling techniques in the hot and humid climate of Indonesia," Build Environ, vol. 226, no. 2, p. 109698, 2022.

[7] Wikipedia, "Time in Indonesia." https://en.wikipedia.org/wiki/Time_in_Indonesia (accessed May 26, 2023).

[8] X. Gong, Y. Akashi, and D. Sumiyoshi, "Optimization of passive design measures for residential buildings in different Chinese areas," Build Environ, vol. 58, pp. 46–57, 2012.

[9] H. Huang et al., "Optimum insulation thicknesses and energy conservation of building thermal insulation materials in Chinese zone of humid subtropical climate," Sustain Cities Soc, vol. 52, no. May 2019, p. 101840, 2020.

[10] S. Sana, Abolfazl Hayati, and M. Salmanzadeh, "Optimization of Window-to-Wall Ratio for Buildings Located in," Energies (Basel), vol. 14, 2021.

[11] F. Ahmadi, S. Wilkinson, H. Rezazadeh, S. Keawsawasvong, Q. Najafi, and A. Masoumi, "Energy efficient glazing: A comparison of microalgae photobioreactor and Iranian Orosi window designs," Build Environ, vol. 233, no. October 2022, p. 109942, 2023.

[12] M. Ashouri, F. R. Astaraei, R. Ghasempour, M. H. Ahmadi, and M. Feidt, "Optimum insulation thickness determination of a building wall using exergetic life cycle assessment," Appl Therm Eng, vol. 106, pp. 307–315, 2016.

[13] A. Ozaki and T. Tsujimaru, "Prediction of hygrothermal environment of buildings based upon combined simulation of heat and moisture transfer and airflow," IBPSA 2005 - International Building Performance Simulation Association 2005, pp. 899–906, 2005.

[14] D. Etheridge, Natural Ventilation of Buildings: Theory, Measurement and Design. 2011.

[15] P. Heiselberg, K. Svidt, and P. V. Nielsen, “Characteristics of airflow from open windows,” Build Environ, vol. 36, no. 7, pp. 859–869, Aug. 2001.

[16] A. Iqbal, A. Afshari, H. Wigö, and P. Heiselberg, “Discharge coefficient of centre-pivot roof windows,” Build Environ, vol. 92, pp. 635–643, 2015, doi: 10.1016/j.buildenv.2015.05.034.

[17] AIJ, “AIJ Recommendations for Loads on Buildings (2015) Architectural Institute of Japan,” 2019, [Online]. Available: https://www.aij.or.jp/

[18] D. Cóstola, B. Blocken, and J. L. M. Hensen, “Overview of pressure coefficient data in building energy simulation and airflow network programs,” Build Environ, vol. 44, no. 10, pp. 2027–2036, 2009.

[19] E. et al Maruta, Wind pressure coefficient database for natural ventilation design, no. 189. Building Research Institute, National research and developmmet agency, Japan, 2018. [Online]. Available: https://www.kenken.go.jp/japanese/contents/publications/data/189/all.pdf

[20] ASHRAE 14, “Measurement of Energy, Demand, and Water Savings,” ASHRAE Guideline 14-2014, vol. 4, pp. 1–150, 2014, [Online].
Available: www.ashrae.org%0Awww.ashrae.org/technology.

[21] U.S. Department of Energy–Federal Energy Management Program, “M&V guidelines: measurement and verification for performance-based contracts -Version 4.0,” U.S. Department of Energy, vol. 3, no. November, pp. 1–108, 2015.

[22] Efficiency Valuation Organization, “International Performance Measurement & Verification Protocol,” Handbook of Financing Energy Projects, vol. I, no. January, p. 122, 2016.

[23] G. Mustafaraj, D. Marini, A. Costa, and M. Keane, “Model calibration for building energy efficiency simulation,” Appl Energy, vol. 130, pp. 72–85, 2014.

[24] M. Royapoor and T. Roskilly, “Building model calibration using energy and environmental data,” Energy Build, vol. 94, pp. 109–120, 2015.

Chapter 5. Summary and future work

5.1. Summary

The discharge coefficient and wind pressure coefficient are two important factors in naturally ventilated houses for optimizing ventilation rates and indoor thermal comfort. They are determined through laboratory measurements and CFD simulations. Passive design improvements for naturally ventilated houses in tropical climates, aimed at generating a comfortable indoor environment and increasing energy efficiency by controlling temperature and humidity through insulation and the louver openings ratio, have been proposed and analyzed. The performance of the proposed design was verified through field measurements and numerical simulations using THERB for HAM (Heat, Air, and Moisture) with NAF (Network Airflow) model applied to the tested house.

In chapter 1,

The existing conditions of indoor thermal comfort and naturally ventilated houses in tropical regions of Indonesia, which are related to temperature, humidity, and the thermal load of passive design, were investigated and described in this dissertation. The background of this dissertation and the purpose of the study were also described.

In chapter 2,

A survey and investigation of the indoor thermal comfort of occupants in naturally ventilated houses in tropical regions were conducted. This study represents an initial step in understanding the actual conditions of typical low-cost houses in Indonesia, which commonly rely on window openings to cool the indoor environment during occupancy. The occupants desire a cooler and more comfortable experience, particularly during the cool season, for both types of houses examined. Additionally, relying on window openings is the most preferred method of achieving adaptive comfort.

In Chapter 3

Fundamental studies were conducted on naturally ventilated houses to optimize the natural ventilation system, which can passively cool or remove heat from the indoor environment. To achieve optimal natural ventilation and ensure accurate airflow, a design strategy that maximizes the ventilation rate with an appropriate discharge coefficient is necessary. However, there is limited research on discharge coefficients for louver openings with sashes. The presence of sashes affects the discharge coefficient due to increased contraction and friction losses. This study aims to determine the discharge coefficient values for different sash angles and assess the impact of louvre geometry on the coefficient. The results indicate that the discharge coefficients for louver openings decrease as the sash

opening angle increases. In addition, the wind pressure coefficient, which describes the pressure distribution on the building surfaces, was determined through CFD simulation. A numerical simulation model of louver openings in naturally ventilated buildings was developed. These findings suggest that THERB for HAM with NAF has the ability to accurately predict indoor temperature and humidity.

In Chapter 4

The study focuses on enhancing naturally ventilated houses by considering the louver area and insulation. The research approach involves conducting on-site measurements in Lhokseumawe, an Indonesian city, to collect data such as indoor/outdoor temperature and relative humidity. These experimental data are then used to validate a numerical simulation model. Subsequently, the simulation model is employed to devise energy-efficient design solutions for houses in 14 different locations across Indonesia. The results indicate that changes in louver areas have a minimal effect on indoor air conditions, while combining improvements in louver areas and building envelope insulation levels can significantly reduce indoor air temperature and relative humidity. The proposed improvement plan leads to a considerable reduction in daily cooling demand and annual cooling loads for the simulated regions. As a result, the study serves as a potential starting point to achieve zero-energy housing and enhance thermal comfort for occupants in unconditioned and naturally ventilated houses in Indonesia.

5.2. Future work

There were some errors in the recorded temperature and relative humidity, which could be attributed to two potential reasons. Firstly, inaccuracies in the measurement of ventilation rate, with potential errors of up to 100 m^3/h, could impact the indoor environment. Secondly, the influence of neighbouring rooms, such as corridors and rooms occupied by individuals, could affect the indoor environment due to factors like air conditioner operation and the opening/closing of blinds. Therefore, it is necessary to enhance the accuracy of simulations by conducting field measurements of ventilation rates in real naturally ventilated houses in the tropical climate of Indonesia. Additionally, this study proposes a passive design that incorporates only the louver opening ratio and building envelope insulation. However, it is essential to consider a comprehensive passive design for naturally ventilated houses including shading devices, building/openings orientation, wall thickness, wall types, external wall insulation, window-to-wall ratio, and roof insulation. This comprehensive approach is crucial to achieve energy-efficient load servicing and create a more comfortable indoor environment.

Appendix

References to the numerical simulation used in this dissertation and questionnaire are provided in the appendix.

Appendix A contains a paper describing a simulation called THERB for HAM, which is capable of estimating the hygrothermal environment and heat load of an entire building using a physical model.

Appendix B consists of a questionnaire that was utilized for surveying and assessing the indoor thermal comfort in naturally ventilated houses in Indonesia in (English and Indonesia version).

.

SIMULATION SOFTWARE TO DESCRIBE THE HYGROTHERMAL ENVIRONMENT OF WHOLE BUILDINGS BASED ON DETAILED PHYSICAL MODELS

ABSTRACT

A Heat, Air and Moisture (HAM) simulation software called THERB for HAM has been developed for the purpose of estimating the hygrothermal environment within buildings. This software has complete HAM features including principles of moisture transfer within walls. Generally simulation software to predict temperature, humidity, heating and cooling load of building spaces does not take into account moisture transfer in wall assemblies. Humidity calculation in most software is simply affected by ventilation and focuses on just the building spaces. THERB was developed to simulate humidity conditions in both building spaces and wall assemblies in detail. The moisture transfer model using the water potential, which is defined as thermodynamic energy, is a progressive feature of THERB, which incorporates moisture transfer including moisture sorption and desorption of walls. Thus THERB can predict the hygrothermal environment of the whole building taking into consideration the complex relationship between heat and moisture transfer and air flow.

In this paper, the prominent features of the THERB are highlighted. Then the accuracy is verified through the comparison of calculation and monitoring results of a residential building. The difference of hygrothermal environment is clarified based whether or not moisture sorption and desorption of walls are taken into account. Furthermore, Sensitive analysis utilizing THERB is performed with a number of parameters, such as moisture conductivity, moisture capacity, area and thickness of interior materials and so on, that influence indoor humidity. Eleven parameters that especially affect indoor humidity are defined by the sensitive analysis.

1. INTRODUCTION

THERB for HAM is a dynamic simulation software which can estimate temperature, humidity, sensible temperature, and heating/cooling load for multiple zone buildings and wall assemblies. The heat and moisture transfer models used in THERB such as conduction, convection, radiation and ventilation (or air leakage) are based upon the detailed phenomena describing actual building physics, and can be applied to all forms of building design, structure or occupant schedules, etc. All the phenomena are calculated without simplification of the heat and moisture transfer principles of any building component or element. The paper explains prominent features of the models, and the accuracy of THERB and sensitive analysis on indoor humidity is also described.

2. THEORETICAL FEATURE OF THERB FOR HAM

The following outlines the algorithms for heat and moisture transfer used in THERB for HAM, which are derived from fundamental building physics principles.

2.1 Conductive Heat and Moisture Transfer

The finite difference method is applied to the model of one-dimensional transient thermal conduction of multi-layer walls. Regarding thermal conduction to the ground, the finite difference method of two or three dimensions is applied to the previous calculation of the ground temperature and then the results are used as the input excitation for conductive calculation of the earthen floor and basement walls.
Water Potential which is derived by applying the chemical potential of thermodynamics to moisture diffusion is used as the driving force of moisture transfer. This approach is proposed to be more accurate than other models based on physical properties such as vapour pressure. The model called P-model using water potential makes it possible to combine moisture transfer with heat transfer perfectly, and take into account internal energy and external forces such as gravity. Balance equations of heat and moisture transfer in material are obtained as follows.

- Heat Balance

$$\frac{\partial C\rho T}{\partial t} + c_{lw} j_{lw} \nabla T = \nabla \lambda \nabla T + r_v \nabla \lambda_g' \nabla \left(\mu_w + \mu_f \right) \tag{1}$$

- Moisture Balance

$$\rho_{lw} \frac{\partial \phi}{\partial \mu} \frac{\partial \mu}{\partial t} = \nabla \lambda_g' \nabla \left(\mu_w + \mu_f \right) + \nabla \lambda_l' \nabla \left(\mu + \mu_f \right) \tag{2}$$

where C and ρ are specific heat and specific weight of material containing water. c_{lw}, ρ_{lw} and j_{lw} are specific heat, specific weight and flux of liquid phase water. λ is thermal conductivity. λ_g' and λ_l' are gaseous and liquid phase water conductivity for μ_w and μ gradients. r_v is heat of sorption (= latent heat of evaporation).

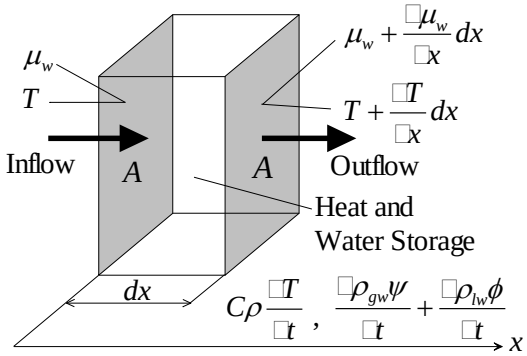

Figure 1 Conductive heat and moisture transfer

μ_w is the water potential and defined from the basic thermodynamic principles as Eqs.(3) to (5). The water potential is composed by saturated water potential μ_w^o and unsaturated water potential μ. μ_w^o expresses the thermodynamic energy of saturated vapour and μ expresses the difference of thermodynamic energy between saturated vapour and unsaturated vapour of moisten air.

$$\mu_w(p,T) = \mu_w^o(T) + \mu(p) \tag{3}$$
$$\mu_w^o(T) = 6.44243 \times 10^5 + c_{p,w_{kg}} (T - 273.15)$$

$$-Tc_{p,w_{kg}}\ln\frac{T}{273.15}+R_{w_{kg}}T\ln\frac{p_s}{1.01325\times10^5} \tag{4}$$

$$\mu(p)=R_{w_{kg}}T\ln\frac{p_w}{p_s} \tag{5}$$

where p_w is the vapor pressure of the humid air, and p_s is the saturated vapor pressure at temperature T. $c_{p,w_{kg}}$ is the specific heat which is expressed in units of [J/(kg K)] and $R_{w_{kg}}$ = 461.50 [J/(kg K)] which is calculated by dividing the gas constant R = 8.31441 [J/(mol K)] by the molecular weight of water 18.016x10^{-3} [kg/mol].

μ_f is the force water potential caused by internal energy and external forces. For instance, the force water potential which includes the influences of gravity and internal pressure is calculated by Eq.(6).

$$\mu_f = gz + p\overline{V}_w \tag{6}$$

where g is gravitational constant, z is height from reference position, $\overline{V}_w$ is the volume per unit weight of water and $p\overline{V}_w$ is equal to $R_{w_{kg}}T$.

2.2 Convective Heat and Moisture Transfer

By default, the convective heat transfer coefficients are recalculated at every time step on all surfaces of the exterior, interior and cavities of buildings using dimensionless equations as shown in Table 1 which are derived from either the profile method for boundary layer (based on the energy equation, the momentum equation and the fluid friction) or defined from the experimental findings according to natural or forced convection. Furthermore the natural convective heat transfer coefficients are classified into either vertical or horizontal surfaces. It is possible to use the functional equations of the wind direction and velocity for the exterior convective heat transfer coefficients and the functional equations of the temperature difference between surface and room for the interior convective heat transfer coefficients. It is also possible to set constant heat transfer coefficients all day long or modify the coefficients to take into consideration space conditioning time for every part of the building.

The convective moisture transfer coefficients on all surfaces of the exterior, interior and cavities of buildings are calculated from the dimensionless Sherwood number, which is derived on the basis of the analogy between heat and mass transfer. The Sherwood number can be calculated by replacing the Prandtle number with Schmidt number as shown in Table 1.

Thus the boundary conditions of heat and moisture balance equations are expressed as follows.

- Boundary conditions

$$-\lambda\frac{\partial T}{\partial n_v}-r_v\cdot\lambda'_g\frac{\partial\mu_w}{\partial n_v}=\alpha_c(T_a-T_s)+r_v\cdot\alpha'_\mu(\mu_{w,a}-\mu_{w,s})+q_s \tag{7}$$

$$-\lambda'_g\frac{\partial\mu_w}{\partial n_v}=\alpha'_\mu(\mu_{w,a}-\mu_{w,s}) \tag{8}$$

where n_v is normal line vector directed inward on a boundary surface, q_s is quantity of radiant heat. T_a, T_s, $\mu_{w,a}$ and $\mu_{w,s}$ are the temperature and water potential of the air and surface, respectively. α_c is convective heat transfer coefficient and α'_μ is convective moisture transfer coefficient for the water potential gradient. α'_μ can be calculated from general convective moisture transfer coefficient α'_p for the vapour pressure gradient on the basis of Eq.(3).

$$\alpha'_{\mu} = \alpha'_{p}\left(\frac{\partial p_w}{\partial \mu_w}\right) = \alpha'_{p}\frac{p_s}{R_{w_{kg}}T}e^{\mu/R_{w_{kg}}T} \tag{9}$$

Table 1 Convective Heat Transfer Coefficient

Part of Buildings	Dimensionless Number
Exterior	$Nu = 0.037\mathrm{Re}^{0.8}\,\mathrm{Pr}^{1/3}$
Interior (Vertical Plane)	$Nu = 0.241(Gr_i \cdot \mathrm{Pr})^{0.4}$ $Gr_i = g\beta\Delta T_a l^3/\upsilon^2$
Interior (Horizontal Plane)	$Nu = C \cdot Ra_f^m$ $Ra_f = Gr_i \cdot \mathrm{Pr}$ $f = (T_s + T_\infty)/2$
Upward	C=0.58, m=1/5
Downward	C=0.54, m=1/4 (Ra_f : 2E4 to 8E6) C=0.15, m=1/3 (Ra_f : 8E6 to 1E11)
Cavity (ventilated)	$Nu = 0.023\mathrm{Re}^{0.8}\,\mathrm{Pr}^{0.4}$
Cavity (closed)	$Nu = 0.035(Gr_c \cdot \mathrm{Pr})^{0.38}$ $Gr_c = g\Delta T_s l^3/T_m\upsilon^2$

Gr: Grashof number, *Nu*: Nusselt number, *Pr*: Prandtle number, *Ra*: Rayleigh number, *Re*: Reynolds number, T_m: mean temperature of surfaces, ΔT_a: temperature difference between surface and air, ΔT_s: temperature difference between surfaces, *g*: gravitational constant, *l*: length, β :expansion coefficient, υ : kinematic viscosity

2.3 Radiant Heat Transfer

On the exterior surfaces of the buildings, the standard method of using the radiant heat transfer coefficients and atmospheric radiation is applied in default. Interrelated radiation between both surfaces of building and the ground can be also calculated with temperature calculation of the ground. On the interior of buildings, instead of the general method (that is, the calculation of heat transfer between surface and indoor air and radiation between surfaces), the use of the long-wave absorption coefficient makes it possible to simulate a net absorption of radiant heat as a consequence of multiplex reflection among interior surfaces. Mutual radiation between the surfaces of cavities in walls and windows can be also calculated.

2.3.1 Multiplex reflection of long-wave radiation

The multiplex reflection of long-wave radiation between interior surfaces is simulated on the basis of Gebhart's absorption coefficient. The long-wave absorption coefficient $\beta_{l,j}$ is defined as the net ratio of absorbed radiant heat on surface *j* from the surface *l*.

$$\beta_{l,j} = F_{l,j}\varepsilon_j + \sum_{k=1}^{J} F_{l,k}(1-\varepsilon_k)\beta_{k,j} \tag{10}$$

where $F_{l,j}$ is the view factor from the surface l to the surface j and ε_j is emissivity of the surface j. Thus the net radiant heat emitted from the surface j (see Figure 2) is expressed by Eq.(11).

$$ELR_j = \varepsilon_j \sigma T_j^4 - \sum_{k=1}^{J} \beta_{k,j}\varepsilon_k \sigma T_k^4 \, S_k / S_j \tag{11}$$

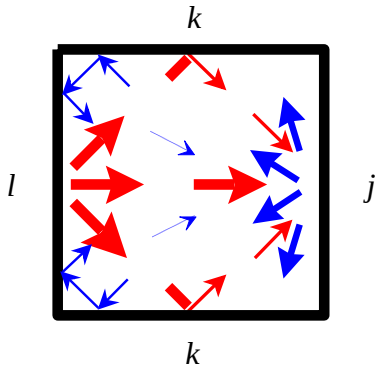

Figure 2 Multiple reflection of long-wave radiation

Eq.(11) can be re-arranged into Eq.(14) by using the principle of the conservation of energy and the reciprocal theorem expressed by Eqs.(12), (13).

$$\sum_{k=1}^{J} \beta_{j,k} = 1 \tag{12}$$

$$\varepsilon_k S_k \beta_{k,j} = \varepsilon_j S_j \beta_{j,k} \tag{13}$$

$$ELR_j = \varepsilon_j \sigma \sum_{k=1}^{J} \beta_{j,k}\left(T_j^4 - T_k^4\right) = \sum_{k=1}^{J} \beta_{j,k}\alpha_{r,jk}\left(T_j - T_k\right) \tag{14}$$

where S_j is the area of surface j. $\alpha_{r,jk}$ is the radiant heat transfer coefficient from surface j to surface k and can be approximated by Eq.(15).

$$\alpha_{r,jk} \equiv 4\varepsilon_j \sigma \left\{\left(T_j + T_k\right)/2\right\}^3 \tag{15}$$

2.4.2 Long-wave radiant heat emitted from lights and appliances

The long-wave absorption coefficient can be applied to long-wave radiant heat emitted from lights and appliances and human bodies, etc. If it is assumed that such radiant heat is equally emitted from the ceiling or floor, the absorption amount ALR_j on the surface j can be described by Eq.(16).

$$\begin{aligned} ALR_j &= \sum_{c=1}^{C} \beta_{c,j}\, LI_c S_c / S_j + \sum_{f=1}^{F} \beta_{f,j}\, LH_f S_f / S_j \\ &= \varepsilon_j \left(\sum_{c=1}^{C} \beta_{j,c}\, LI_c / \varepsilon_c + \sum_{f=1}^{F} \beta_{j,f}\, LH_f / \varepsilon_f \right) \end{aligned} \tag{16}$$

where LI_c and LH_f are the radiant heat from lights and appliances and human bodies, respectively. Thus the net radiant heat emitted from the surface j can be calculated by Eq.(17).

$$NLR_j = ELR_j - ALR_j \tag{17}$$

2.4 Incident Solar Radiation

Incident solar radiation on the exterior and into the interior of buildings is divided into direct and diffuse solar radiation and calculated for all parts of the building in all directions using accurate geometric calculations of shaded and unshaded portions of the building by considering the influence of overhangs and wings (see Figure 3). Isotropic model or anisotropic models can be chosen for diffuse solar radiation. Transmitted solar radiation is calculated by the multi-layer window model and considers multiplex reflection (depending on an incidence angle of solar radiation) between not only the glazing layers but also between the window and interior shade at every time step. The multiplex reflection of both direct and diffuse solar radiation among interior surfaces including re-transmission of solar radiation from the inside to the outside through the windows is calculated by using the short-wave absorption coefficient. In addition the absorption coefficients of short wave are applied to radiant heat emitted from lights and appliances.

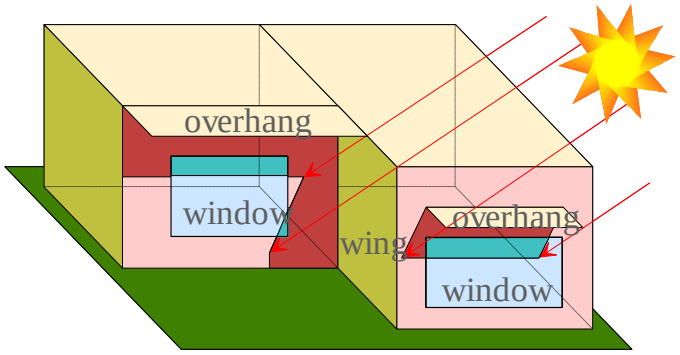

Figure 3 Geometric calculations of shaded and unshaded portions of the building

2.4.1 Multiplex Reflection of Short-Wave Radiation

Regarding direct solar radiation, when TDN_m is the transmitted direct solar radiation through the window striking a normal surface m, a_l and ρ_l are the solar absorptance and reflectance on the surface l, θ_l is incidence angle upon the interior surface l, and S_l is the insolation area of the surface l. The solar absorption and reflection on the surface l are expressed by $a_l \cdot TDN_m \cos\theta_l$ and $\rho_l \cdot TDN_m \cos\theta_l$, respectively. Solar absorption $ADT_{m,j}$ on the surface j based on TDN_m is expressed as Eq.(19) by using the short-wave absorption coefficient $\gamma_{l,j}$, which is defined as the net ratio on the surface j of absorbed solar radiation reflected from the surface l (see Figure 4).

$$\gamma_{l,j} = F_{l,j} a_j + \sum_{k=1}^{J} F_{l,k} \rho_k \gamma_{k,j} \tag{18}$$

$$ADT_{m,j} = TDN_m \sum_{l=1}^{L} \left(\delta_{j,l} a_l \cos\theta_l + \rho_l \gamma_{l,j} \cos\theta_l S_l / S_j \right) \tag{19}$$

$$(\delta_{j,l} = 1 \text{ when } j = l,\ \delta_{j,l} = 0 \text{ when } j \neq l)$$

Eq.(19) can be rearranged into Eq.(21) by the reciprocal theorem expressed by Eq.(20).

$$a_l S_l \gamma_{l,j} = a_j S_j \gamma_{j,l} \tag{20}$$

$$ADT_{m,j} = a_j \cdot TDN_m \sum_{l=1}^{L} \left(\delta_{j,l} + \rho_l \gamma_{j,l} / a_l \right) \cos\theta_l \tag{21}$$

When ADW_m is the direct absorption of direct solar radiation on window m, the solar absorption ADT_j on the interior surface j is obtained by Eq.(22).

$$ADT_j = \sum_{m=1}^{M} \left\{ \delta_{j,m} ADW_m + a_j \cdot TDN_m \cdot \sum_{l=1}^{L} \left(\delta_{j,l} + \rho_l \gamma_{j,l} / a_l \right) \cos\theta_l \right\} \tag{22}$$

Regarding sky diffuse solar radiation, when TSD_m is the transmitted sky diffuse solar radiation through the window m and ASW_m is the direct absorption of the sky diffuse solar radiation on window m, the solar absorption AST_j on the interior surface j is obtained by Eq.(23) if TSD_m is assumed to spread equally into the room (see Figure 5).

$$AST_j = \sum_{m=1}^{M} \left(\delta_{j,m} ASW_m + a_j \gamma_{j,m} TSD_m / a_m \right) \tag{23}$$

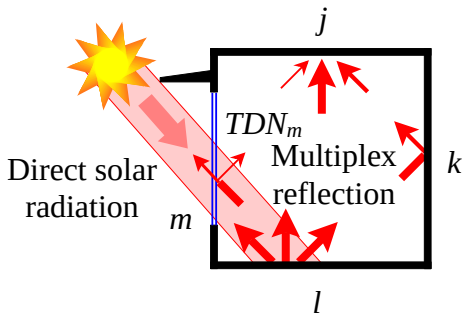

Figure 4 Multiplex reflection of transmitted direct solar radiation

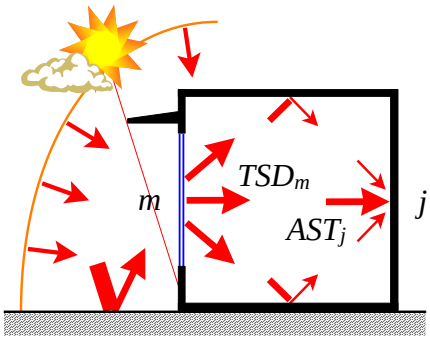

Figure 5 Multiplex reflection of transmitted sky diffuse solar radiation

2.4.2 Short-wave radiant heat emitted from lights and appliances

The short-wave absorption coefficient can be applied to short-wave radiant heat emitted from lights and appliances. If it is assumed that the radiant heat is equally emitted from some parts of ceiling, the absorption amount ASR_j on the surface j can be described by Eq.(24).

$$ASR_j = \sum_{c=1}^{C} \gamma_{c,j} SI_c S_c / S_j = a_j \sum_{c=1}^{C} \gamma_{j,c} SI_c / a_c \tag{24}$$

where SI_c is the short-wave radiant heat from lights and appliances. Thus the absorption amount NSR_j of the short-wave radiant heat on the surface j is expressed by Eq.(25)

$$NSR_j = ADT_j + AST_j + ASR_j \tag{25}$$

2.4.3 Multi-Layer Window Model

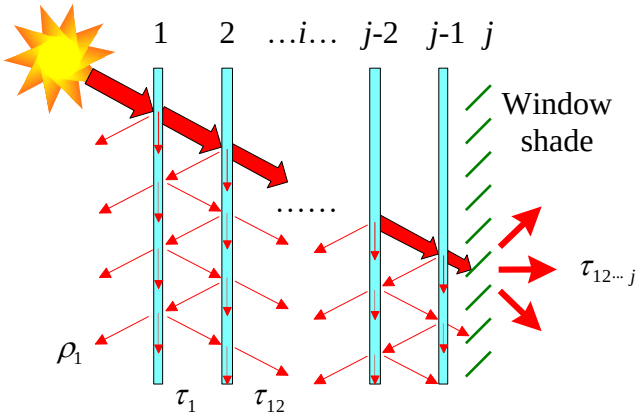

Figure 6 Multi-layer window model

When solar radiation transmits through double-glazing (through 1 to 2 as in Figure 6), the overall transmittance, absorptance and reflectance of the window caused by multiple reflections between the glazings can be described by the following infinite series.

$$\tau_{12} = \tau_1\tau_2 + \tau_1\tau_2\rho_1\rho_2 + \tau_1\tau_2\rho_1^2\rho_2^2 + \cdots = \frac{\tau_1\tau_2}{1-\rho_1\rho_2} \tag{26}$$

$$\alpha_{\bar{1}2} = \alpha_1\left(1 + \tau_1\rho_2 + \tau_1\rho_1\rho_2^2 + \cdots\right) = \alpha_1\left(1 + \frac{\tau_1\rho_2}{1-\rho_1\rho_2}\right) \tag{27}$$

$$\alpha_{1\bar{2}} = \alpha_2\tau_1\left(1 + \rho_1\rho_2 + \rho_1^2\rho_1^2 + \cdots\right) = \frac{\alpha_2\tau_1}{1-\rho_1\rho_2} \tag{28}$$

$$\rho_{12} = \rho_1 + \tau_1^2\rho_2 + \tau_1^2\rho_1\rho_2^2 + \cdots = \rho_1 + \frac{\tau_1^2\rho_2}{1-\rho_1\rho_2} \tag{29}$$

where α_1, ρ_1, τ_1 and α_2, ρ_2, τ_2 are the absorptance, reflectance and transmittance of the glazing layers 1 and 2. $\alpha_{\bar{1}2}$ and $\alpha_{1\bar{2}}$ are the overall absorptance of glazing 1 and 2, respectively. ρ_{12} is the overall reflectance on the side of glazing layer 1 of a double-glazed window.
If the overall transmittance, absorptance and reflectance of a double-glazed window are regarded as the properties of an imaginary single glazing, the equations for triple-glazing can be described as follows.

$$\tau_{123} = \frac{\tau_{12}\tau_3}{1-\rho_{21}\rho_3} \tag{30}$$

$$\alpha_{12\bar{3}} = \frac{\alpha_3\tau_{12}}{1-\rho_{21}\rho_3} \qquad \left(\rho_{21} = \rho_2 + \frac{\tau_2^2\rho_1}{1-\rho_1\rho_2}\right) \tag{31}$$

where $\rho_{21}\ (\neq \rho_{12})$ is the overall reflectance on the side of glazing layer 2 of the double-glazed window.

By regarding the glazing 2-3 of triple-glazing as an imaginary single glazing, the following equations are obtained.

$$\alpha_{\bar{1}23} = \alpha_1\left(1+\frac{\tau_1\rho_{23}}{1-\rho_1\rho_{23}}\right) \tag{32}$$

$$\alpha_{1\bar{2}3} = 1-\tau_{123}-\rho_{123}-\alpha_{\bar{1}23}-\alpha_{12\bar{3}} \tag{33}$$

or $$\alpha_{1\bar{2}3} = \alpha_{1\overline{23}}-\alpha_{12\bar{3}} \tag{34}$$

Thus the general equations of overall transmittance, absorptance and reflectance of multi-layer glazing including a window shade can be expressed as follows.

$$\tau_{12\cdots j} = \frac{\tau_{12\cdots j-1}\tau_j}{1-\rho_{j-1\cdots 21}\rho_j} \tag{35}$$

$$\alpha_{12\cdots\bar{j}} = \frac{\tau_{12\cdots j-1}\alpha_j}{1-\rho_{j-1\cdots 21}\rho_j} \qquad \left(\rho_{j\cdots 21} = \rho_j+\frac{\tau_j^2\rho_{j-1\cdots 21}}{1-\rho_j\rho_{j-1\cdots 21}}\right) \tag{36}$$

$$\alpha_{12\cdots\bar{i}\cdots j} = \alpha_{12\cdots\overline{i\cdots j}}-\alpha_{12\cdots\overline{i+1\cdots j}} \tag{37}$$

$$\alpha_{\bar{1}2\cdots j} = \alpha_1\left(1+\frac{\tau_1\rho_{23\cdots j}}{1-\rho_1\rho_{23\cdots j}}\right) \tag{38}$$

$$\left(\alpha_{12\cdots\overline{i\cdots j}} = \frac{\tau_{12\cdots i-1}\alpha_{i\cdots j}}{1-\rho_{i-1\cdots 21}\rho_{i\cdots j}},\quad \alpha_{i\cdots j} = 1-\tau_{i\cdots j}-\rho_{i\cdots j},\quad \rho_{i\cdots j} = \rho_i+\frac{\tau_i^2\rho_{i+1\cdots j}}{1-\rho_i\rho_{i+1\cdots j}}\right)$$

2.5 Ventilation

The network airflow model integrating a thermal model with a plant model estimates natural and forced ventilation quantities of each zone (rooms and cavities) caused by air leakage, infiltration and mechanical ventilation. As for independent cavities naturally ventilated in the walls, it is possible to estimate airflow quantities by hydrodynamic analysis as the solution to the equations of motion, energy and continuity. Constant ventilation quantities can be also set every hour for all zones.

2.5.1 Network Airflow Model

The network airflow model, which is based on the equations of continuity and airflow quantities for openings and cracks as shown in Eqs.(39) to (41), is solved (see Figure 7 and 8).

$$\sum_{i=1}^{I} Q_i = 0 \tag{39}$$

$$Q_i = \alpha_i A_i\sqrt{\frac{2g}{\gamma}|\Delta p_i|} \equiv 4\alpha_i A_i\sqrt{|\Delta p_i|} \tag{40}$$

$$Q_i = a_i l_i \Delta p_i^{1/n} \tag{41}$$

where A is the opening area, Q is the airflow quantity, a is crack constant, g is gravitational constant, l is the length of crack, $n \equiv 1.5$ (constant 1 to 2), Δp is the pressure difference, α is the flow factor and γ is the specific weight of air.

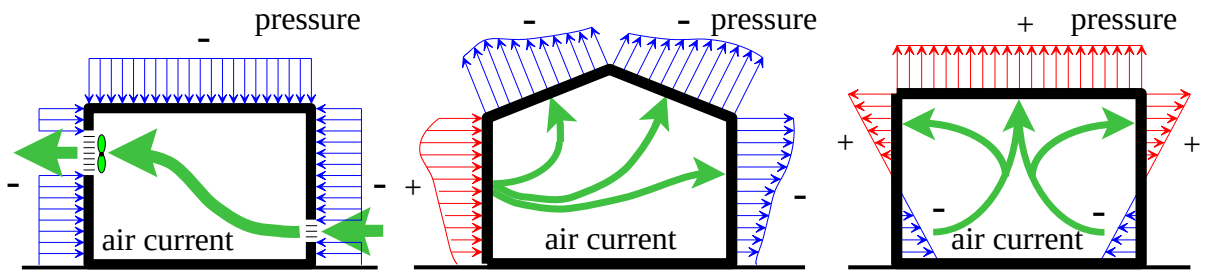

(a) Mechanical Ventilation (b) Wind forced ventilation (c) Buoyant ventilation

Figure 7 Mechanical or natural ventilation

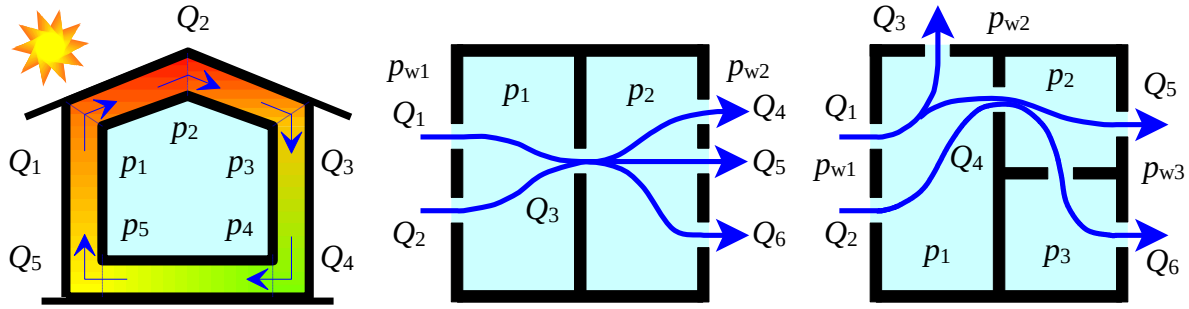

(a) Buoyant airflow (b) Natural or forced ventilation

Figure 8 Network airflow model based on the equations of continuity and airflow quantities

2.5.2 Dimensionless Buoyant Airflow Model in Cavity

Buoyant airflow quantity through a cavity sandwiched between a heating and adiabatic surface as in Figure 9 can be estimated by the equations of continuity, energy and motion described by Eqs.(42) to (44).

$$\frac{\partial u}{\partial x}+\frac{\partial v}{\partial y}=0 \tag{42}$$

$$\rho c_p u\frac{\partial T}{\partial x}+\rho c_p v\frac{\partial T}{\partial y}=\lambda\frac{\partial^2 T}{\partial y^2} \tag{43}$$

$$u\frac{\partial u}{\partial x}+v\frac{\partial u}{\partial y}=\upsilon\frac{\partial^2 u}{\partial y^2}-\frac{1}{\rho}\frac{\partial P_d}{\partial x}+\beta g\left(T-T_o\right) \tag{44}$$

$$\left(P_d=p-p_o,\ \ \beta=\frac{\rho_o-\rho}{\rho\left(T-T_o\right)}\right)$$

Eq.(45) expresses boundary conditions.

$$\left.\begin{aligned} &x=0,\ 0<y<b:\ u=\bar{u},\ v=0,\ T=T_o \\ &y=0,\ x\geq 0:\ u=0,\ v=0,\ T=T_w \\ &y=b,\ x\geq 0:\ u=0,\ v=0,\ \partial T/\partial y=0 \\ &x=0:\ P_d=0 \\ &x=l:\ P_d=0 \end{aligned}\right\} \tag{45}$$

Eqs.(42) to (45) can be rearranged into the dimensionless equations expressed by Eqs.(47) to (50) by applying the following dimensionless number.

$$\left.\begin{aligned} &U=\frac{bu}{\upsilon Gr},\ V=\frac{bv}{\upsilon},\ X=\frac{x}{bGr},\ Y=\frac{y}{b} \\ &P=\frac{P_d b^2}{\rho\upsilon^2 Gr^2},\ \Theta=\frac{T-T_o}{T_w-T_o},\ Gr=\frac{g\beta(T_w-T_o)b^3}{\upsilon^2},\ \mathrm{Pr}=\frac{\mu c_p}{\lambda} \end{aligned}\right\} \tag{46}$$

Equations of continuity, energy and motion are rewritten as follows:

$$\frac{\partial U}{\partial X}+\frac{\partial V}{\partial Y}=0 \tag{47}$$

$$U\frac{\partial \Theta}{\partial X}+V\frac{\partial \Theta}{\partial Y}=\frac{1}{\mathrm{Pr}}\frac{\partial^2 \Theta}{\partial Y^2} \tag{48}$$

$$U\frac{\partial U}{\partial X}+V\frac{\partial U}{\partial Y}=\frac{\partial^2 U}{\partial Y^2}-\frac{\partial P}{\partial X}+\Theta \tag{49}$$

Boundary conditions are represented as follows:

$$\left.\begin{aligned} &X=0,\ 0<Y<1:\ U=Q,\ V=0,\ \Theta=0 \\ &Y=0,\ X\geq 0:\ U=0,\ V=0,\ \Theta=1 \\ &Y=1,\ X\geq 0:\ U=0,\ V=0,\ \partial\Theta/\partial Y=0 \\ &X=0:\ P=0 \\ &X=L:\ P=0 \end{aligned}\right\} \tag{50}$$

where Q (dimensionless buoyant airflow quantity) and L (dimensionless height of a cavity) are defined by Eqs.(51), (52).

$$Q=\frac{b\bar{u}}{\upsilon Gr}=\int_0^1 U dY \tag{51}$$

$$L=\frac{l}{bGr} \tag{52}$$

In the case difference coordinates are used as in Figure 10, the value of Q can be calculated by Eq.(53) on the basis of Simpson's law.

$$Q=\frac{\Delta Y}{3}\left(4\sum_{j=1}^{(K-1)/2}U_{m+1,2j}+2\sum_{j=1}^{(K-3)/2}U_{m+1,2j+1}\right) \tag{53}$$

If Q and Pr are given as initial conditions, the distributions of pressure, velocity and temperature can be solved from Eqs.(47) to (49) for every height level by convergence calculation as a function of Q, which is obtained from Eq.(53), on the basis of the boundary conditions. When P becomes 0, the dimensionless height L is obtained and then the relationship of Pr/L (revised Rayleigh number) to Q is identified as in Figure 11.

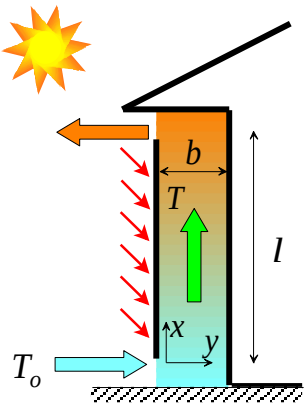

Figure 9 Buoyant airflow through a cavity

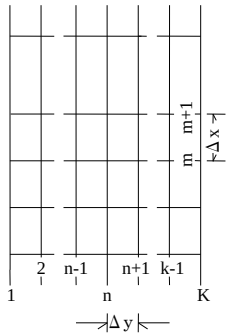

Figure 10 Difference coordinates

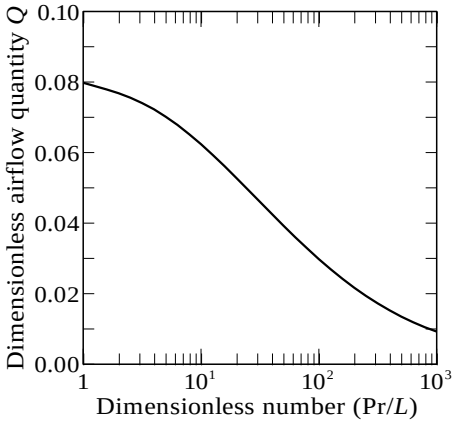

Figure 11 Correlation between Q and Pr/L

2.5 Space Conditioning

Indoor air temperature and humidity can be calculated from heat and moisture balance of a space based on convection, ventilation, internal generation of heat and moisture. By default, indoor humidity is interrelated with sorption and desorption of walls through the application of P-model. General humidity calculation that is just affected by ventilation is also available.
Sensible and latent heat load are obtained from the equations of heat and moisture balance, in which unknown quantities are space heating and cooling load, on condition that temperature and humidity are set at reference ones. Control methods for space conditioning are classified into three types: heating, cooling, and simultaneous heating and cooling. By default, humidity control and temperature control are linked. Temperature and humidity set-point and ranges can be optionally set every hour. Moreover the control of humidity is automatically performed in the case when the sensible temperature such as PMV is set as the set-point of space conditioning.

3. PREDICTION OF HYGROTHERMAL ENVIRONMENT WITHIN BUILDINGS

3.1 Outline of the Monitoring House

The figure 12 shows the first and second floor plan and the wall assembly of the monitoring house. This house was built in Fukuoka in December, 2004 with the traditional wet construction method that doesn't use heat insulating material. A family consisting of a husband, his wife and two children lives there and uses a heating system

3.2 Monitoring of the Hygrothermal Environment

The figure 13 shows the monitored values (December 4 - 6) of the temperature and humidity in the living room. During these three days, the room was heated in the morning (from around 6 for 2.5 hours on average) and in the afternoon (from 12 for 8 hours on average). The indoor temperature increases by heating while the indoor relative humidity decreases. The humidity decreased to 23% during heating in the afternoon on 5th and was in excessive dryness. On the

other hand, the indoor absolute humidity increased according to the temperature after heating started and decreased after heating stopped. The water vapour is adsorbed and desorbed according to the change of the indoor temperature and humidity.

3.3 Arithmetic Precision of THERB

The accuracy of THERB is verified by comparing the monitored and calculated values for the house describe in the previous section. The figure 13 shows the monitored and calculated values of the temperature and humidity in the living room (the detailed calculation and the simplified calculation allowing for moisture adsorption and desorption). The value of the detailed calculation almost agrees with the monitored value and the average absolute error for three days is only 2.5% for the relative humidity and 0.3g/kg' for the absolute humidity. For the simplified calculation based on zero moisture capacity, as the indoor absolute humidity follows the outdoor absolute humidity, the daily range of the relative humidity increases. Although the simplified calculation assuming the moisture capacity is 16.7 g/(m3 kg/kg') generally used almost captures the monitored value during heating, it generates a significant error due to little absolute fluctuating and indoor relative humidity rises extremely high during non-heating

4. SENSITIVE ANALYSIS ON VARIOUS FACTORS AFFECTING THE INDOOR HUMIDITY

Thermal insulation and airtight of recent buildings pays to save energy while it may cause excessive dryness during heating in winter. As the dry environment can cause health impairment such as rough dry skin and allergic disease, maintaining the proper indoor humidity is considered a new challenge. Thus humidity control is expected of the interior material using the natural adsorption and desorption of water vapour. However, as it is a complex phenomenon associated with the phase change of gaseous and liquid water combined with transfer of heat, moisture and air in the indoor space and the material and consists of many factors. The effect of moisture adsorption and desorption of materials is the level of qualitative explanation and is far from quantitative assessment level.

The hygrothermal environment of the whole building is predicted by numerical simulation and factors affecting the indoor humidity are analyzed focusing on the indoor excessive dryness during heating. A sensitive analysis and multiple linear regression analysis is performed with various factors (input values) as explanatory variables and the indoor relative humidity as object variables and the factors are examined that have an effect on improving the indoor excessive dryness.

4.1 Building Model and Calculation Condition

The figure 14 shows the first and second floor plan and the wall assembly of the building model used for calculation. The thermal performance (heat insulation and airtight) of the house shall be equivalent to the next generation energy conservation law. The table 2 shows the calculation condition and the table 3 shows the standard condition of various factors. The analysis condition shall be the time when the outdoor relative humidity is 60% or less and may easily cause the indoor excessive dryness during heating in winter (January to February). The living and dining

room shall be analyzed and the average of indoor relative humidity during heating shall be the object variable.

4.2 Influence of various factors on the indoor humidity

The indoor temperature and humidity are subject to various factors such as weather, materials and thermal performance of the building, space conditioning, ventilation and life style. Sensitive analysis is made based on the following factors (explanatory variables) affecting the indoor humidity; (A) material property of the moisture adsorption and desorption (moisture conductivity and moisture capacity of interior materials), (B) water vapour resistance of interior finish, (C) the area of the moisture adsorption and desorption materials per space volume, (D) thickness of the materials, (E) thermal loss coefficient of the building (except thermal loss by ventilation), (F) ventilation frequency, (G) heating time, (H) preset heating temperature, (I) indoor generated water vapour, (J) building angle of direction, (K) outdoor air temperature, (L) outdoor absolute humidity.
The figure 15 through 27 and the table 4 through 16 show the correlation between the average indoor relative humidity and each factor. "Moisture conductivity and capacity, area of the materials, thermal loss coefficient, indoor generated water vapour and the outdoor absolute humidity" have positive correlation against the indoor humidity, while "water vapour resistance, ventilation frequency, heating time, preset heating temperature and outdoor temperature" have negative correlation. The indoor generated moisture volume and the preset heating temperature have significant effect on the indoor humidity. On the other hand, the thickness of the material and the building angle of direction have little effect on it.

4.3 Multiple Linear Regression Analysis on the Indoor Humidity and Various Factors

Based on the sensitive analysis, the multiple linear regression analysis is made with 11 factors except low sensitive cases (D) and (J) as shown in the table 3 (the thickness of the moisture adsorption and desorption material and the building angle of direction) as the explanatory variable X and the average relative humidity Y [%] as the object variable (when the outdoor relative humidity is 60% or less and the indoor excessive dryness is significant).
The table 17 shows the result of multiple linear regression analysis. The multiple correlation coefficient is 0.984 and is fully reliable. The standardized partial regression coefficient is calculated to compare the degree of incidence of the explanatory variable on the object variable (the average indoor relative humidity during heating). The following factors have profound influence on the humidity in the order except weather conditions; (1) indoor generated water vapour, (2) preset heating temperature, (3) water vapour resistance of interior finish, (4) area of the moisture adsorption and desorption material and (5) moisture capacity of interior materials. The indoor excessive dryness in winter can be effectively improved by changing these factors that easily affect the indoor humidity

6. CONCLUSIONS

In this paper, the hygrothermal environment of houses is estimated by using the simulation software THERB which has been developed to include complete features on heat, moisture and air. Hygrothermal theories on conduction, convection, radiation and ventilation of THERB are

outlined, particularly algorithm on combined heat and moiture transfer using water potential (thermodynamic energy) is the progressive feature, which incorporates moisture transfer including moisture sorption and desorption of walls. Then, the hygrothermal environment during heating in winter and various factors affecting it is analyzed by monitoring and numerical simulation of the temperature and humidity of detached houses. The calculation precision of THERB allowing for the combination of heat and moisture transfer and airflow of whole buildings is also verified. The major results obtained are listed below.

1) The model called P-model using water potential as the driving force of moisture transfer, which is derived by applying the chemical potential of thermodynamics to moisture diffusion, makes it possible to combine moisture transfer with heat transfer perfectly, and can take into account internal energy and external forces such as gravity.
2) Dimensionless equations, which are derived from the profile method for boundary layer or defined from experimental findings according to natural or forced convection, are used to calculate convective heat and moisture transfer coefficients for every part of buildings.
3) The long-wave and short-wave absorption coefficients make it possible to simulate the net absorption of radiant heat and transmitted solar radiation as a consequence of multiplex reflection among interior surfaces of buildings. The absorption coefficients are applicable to radiant heat emitted from lights, appliances and human bodies, etc.
4) A multi-layer window model, which defines the overall transmittance, absorptance and reflectance of solar radiation as an infinite series, is proposed.
5) A network airflow model is used to calculate ventilation quantities in each zone where each zone is represented by nodes. Furthermore, the dimensionless buoyant airflow model derived from the equations of continuity, energy and motion is applicable to independent wall cavities naturally ventilated.
6) The indoor humidity becomes often 30% or less excessive dryness during heating. THERB can predict the indoor humidity in good precision by calculating the combination of heat and moisture transfer and airflow of whole buildings in detail.
7) The simplified calculation to approximate the influence of moisture adsorption and desorption by adding the moisture capacity of the walls to the room space produces a significant error.
8) As the indoor generated water vapour, the preset heating temperature, the water vapour resistance of interior finish, the area and moisture capacity of the moisture adsorption and desorption material have a significant influence on the indoor humidity, the indoor excessive dryness during heating can be effectively improved by changing those factors.

REFERENCES

Fujii W. and Imura H., 1972, Natural Convection Heat Transfer from a Plate with Arbitrary Inclination, *Int. J. Heat Mass Transfer*, Vol.15, p.755-767

Gebhart, B., 1959, A New Method for Calculating Radiant Exchanges, *ASHRAE Transactions*, Vol.65

Heinz R. Trechsel, 2001. Moisture Analysis and Condensation Control in Building Envelopes, *American Society for Testing and Materials*, MNL40

Ozaki A., Watanabe T., et al., 1990, Heat and Mass Transfer at Outside Surface of Buildings – Wind Tunnel Tests of Heat and Mass Transfer on Horizontal Surfaces, *Journal of Archi-*

tecture, Planning and Environmental Engineering, Architectural Institute of Japan, No.407, p.11-25

Ozaki A., Watanabe T., et al., 1997, Analysis of Draft Quantity through Ventilated Air Space, *Proc. of the 14th International Conference on Passive and Low Energy Architecture*, Vol.2, p.33-38

Ozaki A., Watanabe T., Hayashi T. and Ryu U., 2001, Systematic Analysis on Combined Heat and Water Transfer through Porous Materials Based on Thermodynamic Energy, *Journal of Energy and Buildings*, Vol.33, No.4, p.341-350

Ozaki A. and Tsujimaru T., 2005, Prediction of Hygrothermal Environment of Buildings Based upon Combined Simulation of Heat and Moisture Transfer and Airflow, *Proc. of Building Simulation 2005, The 9th International IBPSA Conference*, Vol.II, p.899-906

Perez R., et al., 1990, Modeling Daylight Availability and Irradiance Components from Direct and Global Irradiance, *Solar Energy*, Vol.44, No.5, p.271-289

九州大学
KYUSHU UNIVERSITY

DOCTORAL COURSE RESEARCH
GRADUATE OF HUMAN ENVIRONMENT STUDIES
THERMAL COMFORT SURVEY

House code : ……..…… Orientation : East-West / North-South / Northeast-Southwest / Northwest-Southeast Age : ……. year
Location : ……..……..… Floor Area : ……. M2 Height : ……. (m)
Date : ……..….. Ethnic : Aceh / Batak / Minang / Javanese / Sundanese / Other Weight : ……. (Kg)
Time : ……wib Electricity Consumption: …….. (kWh/Month) / (Rp./Month) Gender : Male / Female

Please respond to the following questions on your thermal comfort at present by circle the answer

1. How do you feel at this moment in the room?
   a. Hot
   b. Warm
   c. Slightly warm
   d. Neutral
   e. Slightly cool
   f. Cool
   g. Cold

2. Do you feel Comfortable in this room?
   a. Much too warm
   b. Too warm
   c. Comfortably warm
   d. Comfortable
   e. Comfortably cool
   f. Too cool
   g. Much too cool

3. How would you prefer the current environment to be?
   a. Warmer
   b. No Change
   c. Cooler

4. How do you feel about air freshness in the room now?
   a. Much too fresh
   b. Too fresh
   c. Slightly fresh
   d. Neutral
   e. Slightly stuffy
   f. Too stuffy
   g. Much too stuffy

5. How do you feel about the air humidity in this room now?
   a. Much too humid
   b. Too humid
   c. Slightly humid
   d. Just right
   e. Slightly dry
   f. Too dry
   g. Much too dry

6. How do you feel about airflow in this room now?
   a. Much too breezy
   b. Too breezy
   c. Slightly breezy
   d. Just right
   e. Slightly still
   f. Too still
   g. Much too still

7. Are you sweating now?
   a. No sweating
   b. Slightly
   c. Moderate
   d. Profusely

8. What do you do when you are sweating?
   a. Open the window : always / most likely / often / seldom / very unlikely
   b. Usage of fan : always / most likely / often / seldom / very unlikely
   c. Usage of AC : always / most likely / often / seldom / very unlikely
   d. Bath : always / most likely / often / seldom / very unlikely
   e. Drink : always / most likely / often / seldom / very unlikely
   f. Go out : always / most likely / often / seldom / very unlikely
   g. Clothing : always / most likely / often / seldom / very unlikely

9. If the air temperature is not suitable, choose your action and circle the timing? (you can choose more than one time by circle the answer)

✓ The usage of Air Conditioning: a. Morning (09.00-12.00 AM) b. Noon (12.01-03.00 PM) c. Evening (03.01-06.00 PM) d. Night (06.01 PM-06.00 AM)	✓ The usage of bedroom windows: a. Morning (09.00-12.00 AM) b. Noon (12.01-03.00 PM) c. Evening (03.01-06.00 PM) d. Night (06.01 PM-06.00 AM)
✓ The usage of Fan: a. Morning (09.00-12.00 AM) b. Noon (12.01-03.00 PM) c. Evening (03.01-06.00 PM) d. Night (06.01 PM-06.00 AM)	✓ Others: ……. a. Morning (09.00-12.00 AM) b. Noon (12.01-03.00 PM) c. Evening (03.01-06.00 PM) d. Night (06.01 PM-06.00 AM)

10. What is your activity before filling this questionnaire?
    a. Sleeping c. Seated/quiet e. Cooking
    b. Reclining d. Standing/relaxed f. Housecleaning

Please choose the answer according to the clothes that you are using right now, by putting a check mark (√) in the answer sheet below.

Clothing Type	Answer
Underwear	
Underwear	
Singlet / Tanktop / Lingerie	
Short-sleeved shirt without collar	
Shirt without a long-sleeved collar	
T-shirt pants	
T-Shirt, Shirt and Blouse	
T-shirt with a short sleeve collar	
Shirt with a long sleeve collar	
Short sleeves shirt	
Long-sleeved shirt	
Flannel shirt (thicker material)	
Sleepwear / short sleeve pajamas	
Sleepwear / long sleeve pajamas	
Blouse	
Vests, Suits, Sweaters and Jackets	
Vest / cardigan / outer	
Suit / blazer	
Sweater	
Jacket	
A dress or a robe	
Skirt	
Long robe and long sleeves	
Short dress / negligee / tunic	
Pants and Socks	
Thin long pants (cotton, etc.)	
Thick trousers (jeans)	
Jumpsuit	
Stocking	
Half hose	
Long socks	
Shorts	
Sports / training pants	
Koko or Gamis	
Short koko shirt and short sleeve	
Short koko shirt and long sleeve	
Short-sleeve male robe	
Long sleeve male robe	
Sarong	

Thank you for your cooperation – Muhammad Iqbal

九州大学
KYUSHU UNIVERSITY

DOCTORAL COURSE RESEARCH
GRADUATE OF HUMAN ENVIRONMENT STUDIES
SURVEI KENYAMANAN THERMAL

Kode rumah : ……..... Orientasi : Utara/Timur Laut/Timur/Tenggara/Selatan/Barat Daya/Barat/Barat Laut Usia : ……. Tahun
Lokasi : ……..…… Luas Rumah : ……..… M2 Tinggi : ……. M
Tanggal : ……..…… Etnik : Aceh / Batak / Minang / Jawa / Sunda / Lainnya Berat : ……. Kg
Waktu : ……..… Wib Konsumsi Listrik : ……(kWh/bln) / (Rp./bln) Jenis kelamin: Laki-laki / Perempuan

Mohon tanggapan anda tentang pertanyaan kenyamanan termal pada saat ini dengan melingkari jawabannya.

1. Bagaimana perasaan anda di ruangan ini sekarang?
   a. Panas
   b. Hangat
   c. Sedikit hangat
   d. Netral
   e. Sedikit sejuk
   f. Sejuk
   g. Dingin

2. Apakah anda merasakan nyaman di ruangan ini?
   a. Panas
   b. Terlalu hangat
   c. Hangat nyaman
   d. Nyaman
   e. Hangat sejuk
   f. Terlalu sejuk
   g. Dingin

3. Lingkungan yang bagaimana yang diinginkan saat ini?
   a. Lebih hangat
   b. Tidak ada perubahan
   c. Lebih dingin

4. Bagaimana perasaan anda tentang kesegaran udara di ruangan ini?
   a. Sangat segar
   b. Segar
   c. Sedikit segar
   d. Netral
   e. Sedikit pengap
   f. Pengap
   g. Sangat Pengap

5. Bagaimana perasaan anda tentang kelembaban udara di ruangan ini sekarang?
   a. Sangat lembap
   b. Lembap
   c. Sedikit lembap
   d. Tepat
   e. Sedikit kering
   f. Kering
   g. Sangat kering

6. Bagaimana perasaan anda tentang aliran udara di ruangan ini sekarang?
   a. Sangat berangin
   b. Berangin
   c. Sedikit berangin
   d. Tepat
   e. Sedikit hampa
   f. Hampa
   g. Sangat hampa

7. Apakah anda berkeringat sekarang?
   a. Tidak
   b. Sedikit
   c. Banyak
   d. Sangat banyak

8. Apa yang anda lakukan ketika berkeringat?
   a. Membuka jendela : selalu / paling sering / sering / jarang / sangat jarang
   b. Menggunakan kipas : selalu / paling sering / sering / jarang / sangat jarang
   c. Menggunakan AC : selalu / paling sering / sering / jarang / sangat jarang
   d. Mandi : selalu / paling sering / sering / jarang / sangat jarang
   e. Minum : selalu / paling sering / sering / jarang / sangat jarang
   f. Keluar rumah : selalu / paling sering / sering / jarang / sangat jarang
   g. Buka/ganti baju : selalu / paling sering / sering / jarang / sangat jarang

9. Jika suhu udara panas, pilih sikap anda dan lingkari waktu nya?
   (anda dapat memilih lebih dari satu dengan melingkari jawabannya)

✓ Menggunakan AC: a. Pagi (09.00-12.00 AM) b. Siang (12.01-03.00 PM) c. Sore (03.01-06.00 PM) d. Malam (06.01 PM-06.00 AM)	✓ Menggunakan/buka jendela kamar: a. Pagi (09.00-12.00 AM) b. Siang (12.01-03.00 PM) c. Sore (03.01-06.00 PM) d. Malam (06.01 PM-06.00 AM)
✓ Menggunakan kipas angin: a. Pagi (09.00-12.00 AM) b. Siang (12.01-03.00 PM) c. Sore (03.01-06.00 PM) d. Malam (06.01 PM-06.00 AM)	✓ Lainnya; …….. a. Pagi (09.00-12.00 AM) b. Siang (12.01-03.00 PM) c. Sore (03.01-06.00 PM) d. Malam (06.01 PM-06.00 AM)

10. Apakah kegiatan anda sebelum mengisi kuisioner ini?
    a. Tidur c. Duduk/diam e. Memasak
    b. Berbaring d. Berdiri/rilek f. Membersihkan rumah

11. Silahkan pilih jawaban di bawah ini menurut pakaian yang anda gunakan saat ini dengan mencontreng tanda (√) pada kertas jawaban.

Jenis Pakaian	Jawaban
Pakaian Dalam	
Pakaian dalam	
Singlet / *Tanktop* / *Lingerie*	
Kaos tanpa kerah lengan pendek	
Kaos tanpa kerah lengan panjang	
Celana kaos (*legging*)	
Baju Kaos atau Kemeja dan Blouse	
Kaos dengan kerah lengan pendek	
Kaos dengan kerah lengan panjang	
Kemeja lengan pendek	
Kemeja lengan panjang	
Kemeja *flannel* (bahan lebih tebal)	
Baju tidur / *piyama* lengan pendek	
Baju tidur / *piyama* lengan panjang	
Blouse	
Rompi, Jas, Sweater dan Jaket	
Rompi / *cardigan* / *outer*	
Jas / *blazer*	
Sweater	
Jaket	
Gaun atau Gamis	
Rok	
Gamis panjang lengan panjang	
Gaun pendek / daster / *tunic*	
Celana dan Kaos Kaki	
Celana panjang tipis (katun, dll)	
Celana panjang tebal (*jeans*)	
Celana 1 set baju (*jumpsuit*)	
Stocking	
Kaos kaki pendek	
Kaos kaki panjang	
Celana pendek	
Celana olahraga / *training*	
Baju Koko atau Gamis	
Baju koko pendek dan lengan pendek	
Baju koko pendek dan lengan panjang	
Gamis laki-laki lengan pendek	
Gamis laki-laki lengan panjang	
Sarung	

Terima kasih atas kerjasama nya -Muhammad Iqbal-

Acknowledgments

I would like to express my heartfelt gratitude to all those who have provided guidance and advice throughout my research and thesis writing. The completion of this dissertation would not have been possible without the support and encouragement of numerous individuals.

First and foremost, I am deeply grateful to Professor Akihito Ozaki for his invaluable guidance and mentorship. Despite his busy schedule, he has consistently shown me politeness and courtesy. I am thankful for his unwavering support, encouragement, and for providing me with the opportunity to undertake this dissertation. I would also like to extend my gratitude to Associate Professor Younhee Choi and Assistant Professor Yusuke Arima for their valuable advice and insights, which have greatly contributed to shaping the direction of my research.

Furthermore, I want to express my appreciation to the graduate and undergraduate students of Ozaki Laboratory and Sumiyoshi Laboratory, as well as the Student Support Centre at the Graduate School of Human-Environment Studies, Kyushu University. Your contributions, feedback, and collaboration have been immensely valuable.

Lastly, I would like to acknowledge the tremendous support of my wife, Delvi Sardi, during my PhD studies in Japan. Her unwavering assistance and support at home have been invaluable and have enabled me to focus on my research. I am also grateful to all my children, as well as my mother and father, who have remained supportive and understanding throughout my journey in Indonesia and Japan. Thank you all once again for your guidance, encouragement, and support. I am truly grateful for the opportunity to have worked with such wonderful individuals.

Fukuoka, June 2023

Muhammad Iqbal